Parametric analysis of mechanical fastener disbond arrest features in bonded joints

N.A. van ’t Hof

Delft University of Technology

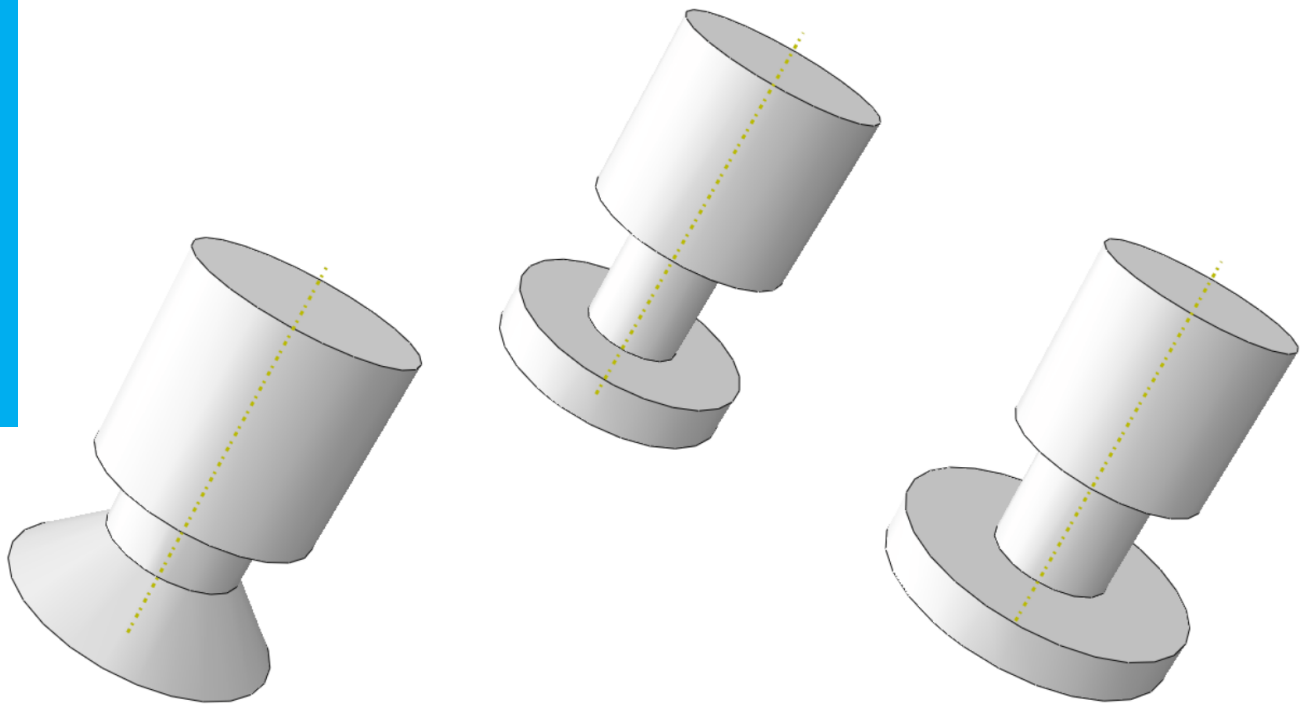

TU Delft

This page is intentionally left blank.

Parametric analysis of mechanical fastener disbond arrest features in bonded joints

by

N.A. van ’t Hof

to obtain the degree of Master of Science
at the Delft University of Technology,
to be defended publicly on Wednesday April 7, 2021 at 3:00 PM.

Student number:	4444469	
Project duration:	November 18, 2019 – April 7, 2021	
Thesis committee:	Prof. dr. C. Rans,	TU Delft, supervisor
	Dr.ing. S. Castro,	TU Delft
	Dr.ir. J.A. Pascoe,	TU Delft
	Dr. S.T. de Freitas,	TU Delft

An electronic version of this thesis is available at http://repository.tudelft.nl/.

TU Delft

Abstract

The aerospace industry is continuously striving toward ever lighter aircraft to improve aircraft efficiency. In order to reduce weight, composite materials are becoming increasingly important in the design of aircraft. Unfortunately, current joining techniques are not well suited for these materials resulting in thick structures with relatively poor fatigue performance.

The solution to this is to use bonded rather than mechanically fastened joints. These joints circumvent the issues that plague the traditional joints. Unfortunately, bonded joints cannot readily be certified as they may disbond under fatigue loading. Disbond arrest features are required to prevent this. The most promising of which are mechanical fasteners which reduce the driving force limiting the disbond growth.

The objective of this investigation is to analyse the effect fastener design has on the disbond growth. To this end, a finite element model has been developed which was verified and validated. Subsequently a sensitivity study was conducted in which the effect of altering the fastener shaft radius, head radius, material stiffness and head geometry were compared.

The model corresponds to those from previous research and experimental results. Shortcomings and approximations are also addressed. Finally, the sensitivity study shows the fastener shaft radius, head radius and material stiffness have relatively little effect on the disbond growth behaviour. The fastener head geometry has a measurable effect on the disbond growth rate.

Acknowledgements

Without a doubt writing this Master's thesis has been the most challenging thing I have ever done in my academic career. I realise that I would not have been able to successfully complete it without the help of colleagues, friends and family. I would like to acknowledge the help and support I have received over the last year.

Of course I would like to thank my supervisor Dr. Calvin Rans without whom I would never have started nor finished this project. The same goes for ir. Eva Smeets who has been able to help me along more times than I can count.

I would also like to thank my parents, friends and family for their everlasting support. I know 2020 has been a rough year for everyone, and the same goes for me, but I am certain it would have undo-able without you there.

Lastly I would like to thank the AE faculty staff. Their hard work and dedication has made my time at Delft as exciting and instructive as it was. Without them I would not have been able to complete my Bachelor's let alone my master's and for that I am forever grateful.

N.A. van 't Hof
Rijswijk, March 2021

Contents

List of Tables

List of Figures

List of Symbols

χ	Crack length correction parameter [-]
δ	Displacement [mm]
Γ	Transverse modulus correction parameter [-]
σ	Stress [Pa]
σ_{max}	Maximum stress [Pa]
A	Disbond area [mm^2]
a	Disbond length [mm]
a, b, n	Constants in Huth formula for flexural stiffness dependent on joint type [-]
a_0	Initial disbond length [mm]
A_{avg}	Average area per node [mm^2]
C	Lever length of the MMB loader [mm]
C_f	Flexural flexibility [$\frac{m}{N}$]
c_{burger}	Constant multiplier in the Paris' relation as suggested by Bürger, function of [m]
$c_{corrected}$	Constant multiplier used in Paris' relation, function of [mm]
d	Shaft diameter [m]
E_1	Young's modulus of the first plate [Pa]
E_2	Young's modulus of the second plate [Pa]
$G_{II_{max}}$	Maximum mode II SERR [J/m^2]
$G_{II_{min}}$	Minimum mode II SERR [J/m^2]
$i_{bondstate}$	Bond state of node i [-]
i_{serr}	Strain Energy Release Rate of node i [N/mm]
L	Half-span length of the MMB specimen [mm]
n	Exponent in the Paris' relation
n_{across}	Average number of nodes across the specimen [-]
P	Applied load [N]
R	Load ratio of the minimum and maximum load
$SERR_{avg}$	Average Strain Energy Release Rate [J/m^2]
t_1	Thickness of the first plate [m]
t_2	Thickness of the second plate [m]
W	Specimen width [mm]
w	Element width [m]

List of Acronyms

ASTM American Society for Testing and Materials

BOPACS Boltless Assembling of Primary Aerospace Structures

CLT Classical Lamination Theory

CoJAC Composite Joints with Inherent Disbond Arrest Capability

CTE Crack Tip Elements

CZM Cohesive Zone Modelling

DAF Disbond Arrest Feature

DIC Digital Image Correlation

FAA Federal Aviation Administration

FEM Finite Element Method

Glare Glass Laminate Aluminium Reinforced Epoxy

MMB Mixed Mode Bending

SERR Strain Energy Release Rate

SLS Single Lap Shear

TSL Traction Separation Law

VCCT Virtual Crack Closure Technique

WSLS Wide Single Lap Shear

XFEM Extended Finite Element Method

2D Two Dimensional

3D Three Dimensional

1

Introduction

Composite materials are becoming more commonplace in aircraft in a continuous push for lighter, more durable aircraft[26]. The current joining methods consistent of mechanical fasteners are not suitable for these new materials and lead to heavier joints requiring expensive manufacturing[20, 27]. As such a need arises for more appropriate joining methods.

One such method would be to use bonding to join components. This method of joining is attractive due to the lack of holes and points of load introduction[20]. These joints could allow for lighter structures with improved fatigue performance and appear to be the preferred joining method[28].

Unfortunately, problems arise with certification. Effectively the only way these joints can be brought to widespread use is through Disbond Arrest Feature (DAF) preventing disbonds to grow beyond a specific point. In recent years investigations conducted by the Boltless Assembling of Primary Aerospace Structures (BOPACS) project has shown the best way to do so is to use fasteners as DAFs[29].

Subsequent research has focused on joint design and is moving towards a further understanding of the problems and solutions concerning joints using mechanical fasteners as disbond arrest features. One point that has been paid relatively little attention is the fastener design. In this thesis the effect of fastener design is analysed through means of a sensitivity study conducted using a numerical model in Abaqus.

A more in depth description of the problem background as well as a description of available modelling techniques can be found in chapter 2. The following chapter outlines the methodology on which the research is based. Example results from the experiments can be found in chapter 4, with the most important results shown and discussed in chapter 5. Lastly, conclusions and recommendations are outlined in chapters 6 and 7 respectively.

Some information was not included in the report for the sake of readability. Curious readers are encouraged to find this in the appendices. Appendix A contains an in-depth explanation of the choice of modelling technique. Appendix B contains a number of useful remarks concerning the modelling of disbond behaviour in Abaqus. Finally, all data and models can be retrieved from[30].

2

Background

As new materials are developed, suitable joining methods are required. One such joining method is bonding, but faces problems concerning certification. A more detailed explanation on this can be found in section 2.1. DAFs are one way of solving these problems, and a number of prominent DAFs are discussed in section 2.2. The most promising of these, using mechanical fasteners as DAFs, is discussed separately in more detail in section 2.3. The analysis of these joints in this research is done through Finite Element Method (FEM), more details of which can be found in section 2.4. Lastly, a knowledge gap is identified and research goals are outlined in section 2.5.

2.1. Problem Description

Over the past half century the aerospace industry has aimed to reduce operational and maintenance cost. In order to do so a push has been made to design lighter, more damage resistant aircraft[26]. This has resulted in an increase in the usage of composite materials as seen in figure 2.1, a trend that has continued in recent years[11].

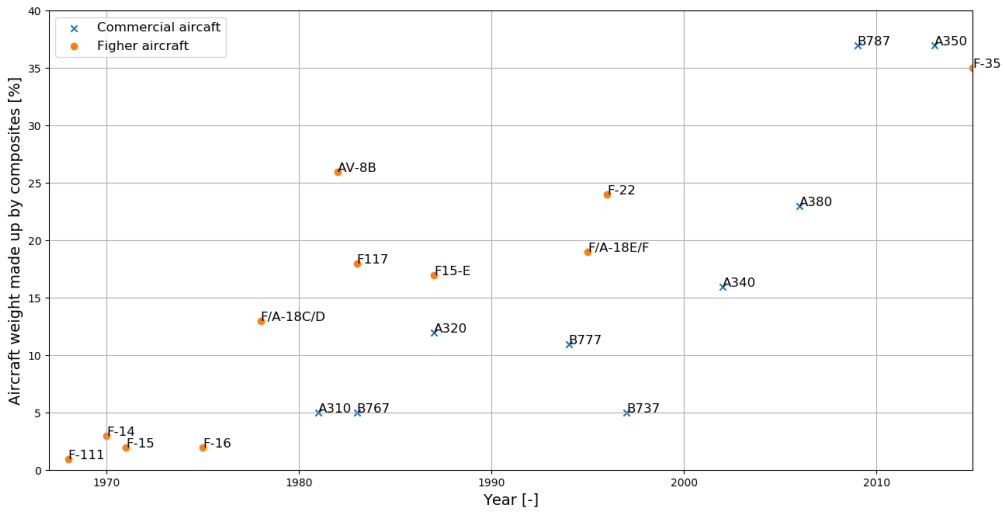

Figure 2.1: *Percentage of aircraft mass made up out of composite materials, adjusted from[11, 12]*

In much the same way the first metal bridges were built using mortise and tenon joints and dovetails[31], techniques more suitable for wood work, current joining techniques are not optimal for composite materials. In what is very much a legacy to metal joining, composites are often joined using rivets which result in heavy joints with poor fatigue performance[27]. As such there is incentive to develop better suited techniques to allow for improved performance.

One promising joining method is adhesive bonding in joints. These joints have as main advantage that it removes the discrete load transfer that is inherent to bolted joints. Furthermore, it removes the need for drilling holes, which is expensive and creates damage exactly at the points of highest stress[20]. One example of the effectiveness of bonded joints can be found in the increase of the usage of bonded joints in lightweight structures in recent years[28].

One drawback of bonded joints is that the connection is established through a chemical process which is less robust than mechanical fastening. Requirements have been formulated to ensure the reliability of such joints. Specifically § 23.573(a)(5) specified in the Advisory Circular AC 20-107B by the Federal Aviation Administration (FAA)[32] is of importance:

> (a) For any bonded joint, § 23.573(a)(5) states in part:
>
> "the failure of which would result in catastrophic loss of the airplane, the limit load capacity must be substantiated by one of the following methods—
> (i) The maximum disbonds of each bonded joint consistent with the capability to withstand the loads in paragraph (a)(3) of this section must be determined by analysis, tests, or both. Disbonds of each bonded joint greater than this must be prevented by design features; or
> (ii) Proof testing must be conducted on each production article that will apply the critical limit design load to each critical bonded joint; or
> (iii) Repeatable and reliable non-destructive inspection techniques must be established that ensure the strength of each joint."

As of yet no reliable non-destructive inspection techniques exist that can establish the strength of each joint[14, 33], this means option (iii) is out of the question. Similarly it is not economically feasible to test every component as would be required for option (ii)[14, 33]. As such, research has focused on option (i) to develop methods to prevent disbond growth.

2.2. Disbond arrest features

DAFs can be included in the design of primary structures to prevent disbond growth past a specified point in order to meet requirement § 23.573(a)(5). These features should result in a reduction of the disbond driving force resulting in a reduction of the disbond growth rate. This can be done through suppression of one or a combination of multiple opening modes. These modes are illustrated in figure 2.2. When considering Single Lap Shear (SLS) joints, the most common type of adhesive joint geometry[16], two main forces are at work. Most important is the load transfer which causes Mode II loading. Mode I loading is caused due to the geometric eccentricity of the joint which introduce secondary bending, as illustrated in figure 2.3. Generally very little Mode III loading is present.

In 2012 the BOPACS project was started with the goal to "reduce the weight and costs of primary aerospace structures by developing bolt free adhesive bonded joints that comply with the airworthiness requirements."[29]. Some of the most promising DAFs are discussed here.

2.2.1. Mechanical fastening

One option is to use mechanical fasteners as DAFs, which covers the usage of bolts, rivets and Hi-Lok fasteners. The driving aspect in reducing disbond growth is the reduction of the Mode I loading through clamping of the fastener, as shown in figure 2.4a. Mode II reduction may also be necessary to achieve complete disbond arrest[20, 34]. The Mode II suppression is achieved through two

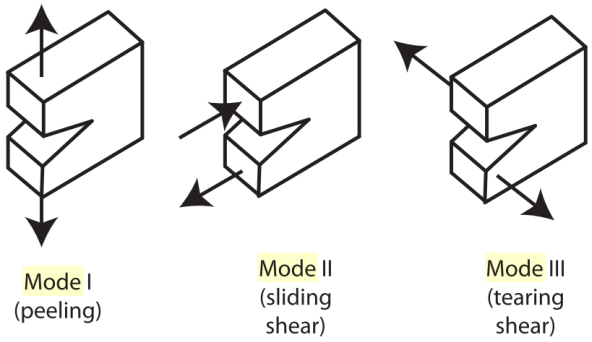

Figure 2.2: *Crack opening modes[2]*

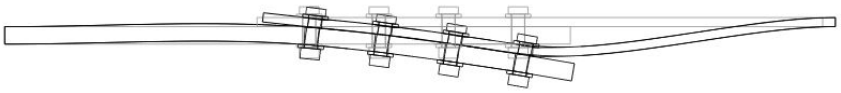

Figure 2.3: *Secondary bending in single lap joints, taken from[13]*

mechanisms[34, 35]: crack-face friction and fastener shear engagement. These are illustrated in figures 2.4b and 2.4c respectively.

Multiple research groups have looked into using fasteners as DAFs. This includes the BOPACS project[14, 36–40], Washington University[21, 24, 33–35, 41–46] and the Technical University of Delft[20, 22]. All three groups found that fasteners could be used effectively as DAFs. BOPACS concluded that generally the through thickness features such as bolts perform best[29]. The effectiveness of fasteners as DAFs is illustrated by figure 2.5 which shows a number of different configurations all of which greatly reduce the disbond growth rate behind the DAF.

An added benefit of such methods is that historically they have been widely used and can readily be put into manufacturing[33]. As such these can be more quickly introduced than other lesser known techniques, making them especially viable.

2.2.2. Bond-line toughening

Another approach to arrest the disbond growth comes from modifying the adhesive to increase the fracture toughness, greatly reducing the disbond growth rate. Approaches for this include micro particle reinforcement, creating a hybrid bondline and using adherend fibres as bondline reinforcement.

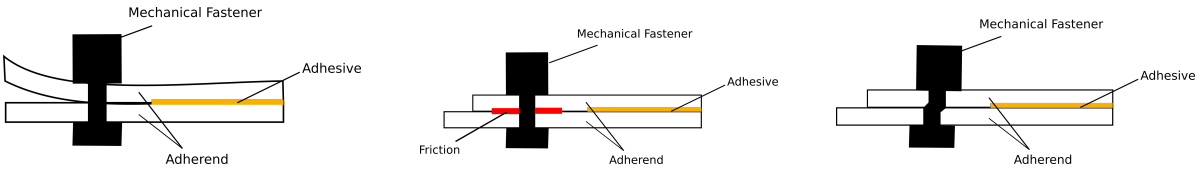

(a) *Mode I reduction is achieved through clamping by the fastener*

(b) *Mode II reduction is partially attributed to crack-face friction*

(c) *Mode II reduction is partially attributed to fastener shear engagement*

Figure 2.4: *Different disbond arresting mechanisms for mechanical fasteners*

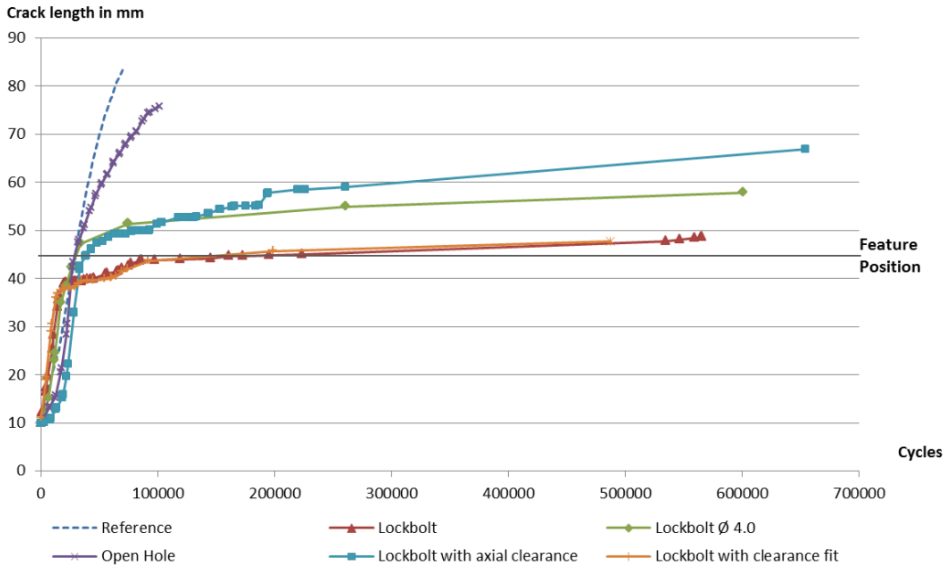

Figure 2.5: *Comparison of fatigue performance for different joints[14]*

One strategy for modifying the bondline is to locally increase its fracture toughness through the addition of toughening particles. The addition of carbon nanotubes to a bondline has been observed to increase its fracture toughness by as much as 40-50% in Mode I and 140% Mode II[47, 48]. Even greater increases in fracture toughness are believed to be possible if greater control of the alignment of the long nanotubes perpendicular to the crack plane could be achieved[49]. While promising, carbon nanotubes have their drawbacks in terms of their high cost[22], difficulties in effectively dispersing the particles in the adhesive[49, 50], worse performance at high impact velocities[51] as well as health and safety issues[52, 53]. Alternative reinforcing particles such as glass micro spheres[54], clay nanoparticles[55, 56], and silica nanoparticles[57] can overcome many of these drawbacks, however, they generally have a lower potential for toughening due to their lower particle aspect ratio.

Rather than locally toughening the adhesive to create a DAF, Lobel[58] suggests locally using a different adhesive with a higher toughness, creating a hybrid bondline with two adhesives. By applying a change through adhesives it is suggested to create a physical barrier. This was later researched by BOPACS, concluding that it improved the resistance to crack propagation[59].

Another approach investigated within the BOPACS project was the use of the adherends as bondline reinforcement[14]. This was achieved by removing the surface resin layer of the adherend through a laser ablation process. This process exposes the fibres on the surface of the adherend, which then penetrate into the adhesive bondline as is illulstrated in figure 2.6. This creates a more direct bond between the load carrying fibres of the adherend resulting in a tougher crack path for the disbond.

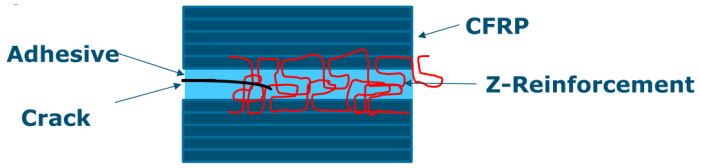

Figure 2.6: *Principle of adherend used as a z-reinforcement[14]*

2.2.3. Z-Pinning

Z-pinning, also called through thickness reinforcements, has also been considered[60, 61]. These methods use arrays of pins such as the ones shown in figure 2.7 as DAFs. The rigid rods are inserted into the uncured plies. After these have been inserted using an ultrasonic machine the ends are cut off[62]. The final result is a reinforcement similar to nails used in woodworking.

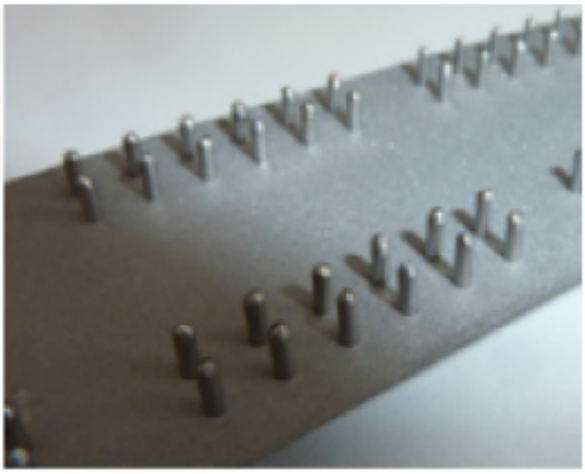

Figure 2.7: *Array of pins used for z-pinning[15]*

Using such pins has the benefit of not requiring drilling of holes or cutting of fibres and result in improved strength of the joint[15]. It has also been shown to improve delamination resistance and fracture toughness[63]. These approaches do face manufacturing issues and require components to be co-cured[22]. Currently the Composite Joints with Inherent Disbond Arrest Capability (CoJAC) program is conducting further research into using this DAF[64].

2.2.4. Joint design modification

Another option is to change how joints are designed to transfer loads to reduce stress concentrations. While these solutions may be effective and seem promising they are often expensive because they require new manufacturing techniques to be implemented[22].

Temiz et al.[16] suggest to bend the leading edges of the joints, as shown in figure 2.8. During bonding, pressure is added to flatten the adherends. After the pressure is removed the elastic spring-back causes the edges to bend back, causing a compressive force which reduces peel stresses. Experiments showed this caused the failure load to increase by 40 - 55 % depending on adherend thickness. Unfortunately this method relies on spring back, meaning it is only applicable to joints with metal adherends.

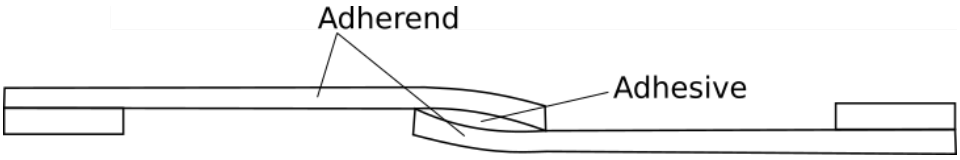

Figure 2.8: *Bending the adherends allows for reduced peel stresses, adjusted from[16]*

Another approach that could be applied to composite materials is to zigzag the entire inter-

face, as shown in figure 2.9. This adds the benefit of mechanical interlocking causing compressive stresses on the bondline increasing fatigue properties[17]. Using this method improvements of up to 40% in static strength have been recorded with larger, more frequent zigzag patterns resulting in a higher benefit[65].

Figure 2.9: *Mechanical interlocking is achieved through creating a wavy adherent, adjusted from[17]*

Fibre bridging is a method which interleaves continuous fibres across the entire thickness of the bondline, as shown in figure 2.10. Using this as a DAF results in a five fold increase of the fracture toughness at the location of the DAF[18], perhaps allowing for full disbond arrest[22].

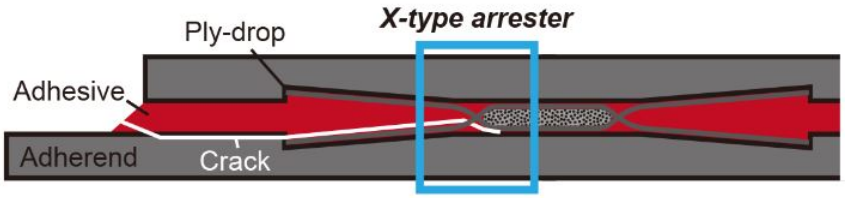

Figure 2.10: *An example of fibre bridging[18]*

Turaga and Sun[19] suggest to improve the SLS design by adding different load paths, as shown in figure 2.11. Similarly to the other joint design modifications the attachments are designed to introduce compressive stresses at the disbond front, reducing peel stresses[66]. Using this method it has been shown strength improvements of up to 60% are possible and the design can be used for both composite and metallic joints.

Figure 2.11: *Attachments that allow for more efficient load paths[19]*

2.3. Hybrid and Bonded-Fastened Joints

While the idea of using mechanical fasteners as DAFs is relatively new, the thought of combining the two joining types is not. Hart-Smith[67–69] published research regarding these hybrid joints as early as 1973. Originally these joints were mostly of interest as a fail safe design, which limited the spread of damage. Lately hybrid joints have been of interest because of their improved fatigue properties compared to their conventional counterparts[70–74].

Whilst the design philosophy of these hybrid joints is different to the joints which use mechanical fasteners as a DAF, they still behave in much the same way. Following is a description of the current understanding of the behaviour of these joints and the effect design choices have on their

performance.

2.3.1. Adhesive and adherend properties

Possibly the most important aspect in the design of hybrid joints are the adhesive and adherend properties. By making the adherend stiffer and the adhesive more ductile the fastener will carry a larger fraction of the total load. Similar effects also occur when increasing the adherend and adhesive thickness. Lastly, decreasing the overlap length will also increase the fraction of the load caried by the fastener[75, 76].

An important feature in hybrid joints is load sharing. The goal of load sharing is for both the fastener and the bondline to carry part of the shear loads, resulting in stronger total loads. If little or no load sharing is present typically the bondline will fail first after which the joint fails as if it were a bolted joint[70, 75, 77–80].

The design philosophy for bonded joints with DAFs does not share this focus on load sharing. The goal of the DAF is not to carry the load but only to limit the disbond growth rate after the bond has started to fail. This also means the joint designs can be very different.

2.3.2. Fastener pre-load

One of the more commonly analysed features is the fastener pre-load. It is commonly thought to improve fatigue performance. Samaei et al.[73] for instance found fatigue life could be improved up to 79% by increasing the clamping torque. Similar results in performance have been recorded by numerous researchers[72, 81–83].

Research in DAFs has led to similar conclusion. First and foremost, the Mode I reduction is increased, improving fatigue properties. Furthermore, the pre-load also increases the friction reducing Mode II loading, further improving the fatigue properties[21].

In contrast, van Teeseling reported an increase in Mode II Strain Energy Release Rate (SERR) behind the fastener at increased loads and higher clamping pressures suggesting there is an optimum clamping pressure[20]. These results were based on a Two Dimensional (2D) FEM model which analysed a clamped DAF. In his experiments he varied the clamping pressure to analyse the effect this had on the SERR, the results of which are shown in figure 2.12. He concludes the Mode II SERR is overestimated when the disbond front reaches the clamp due to the misalignment of the clamping forces causing the adherends to slip. The most important observation is that at higher clamping pressures the Mode I SERR is greatly reduced over a short distance.

2.3.3. Fastener shaft

One of the driving components behind the reduction in Mode II loading is the fastener joint stiffness[21, 34]. This suggests stiffer fasteners would perform better in reducing the Mode II driving force.

One measure for the stiffness of a fastener is the flexural flexibility. This measure quantifies the expected displacements for a fastener based on the applied loading, as shown in figure 2.13. The fastener flexibility can be estimated using equation 2.1 and table 2.1 developed by Huth[1] who fit experimental data to find a semi empirical relation.

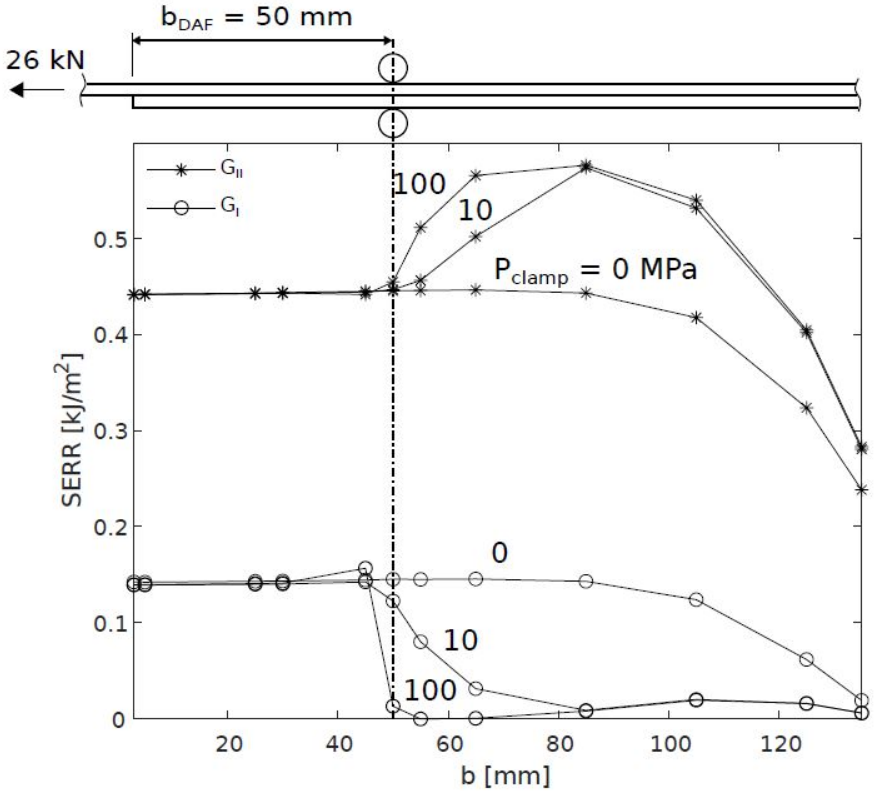

Figure 2.12: *Results reported by van Teeseling[20], comparing the SERR for different pressures of the clamp*

$$C_f = \left(\frac{t_1+t_2}{2d}\right)^a \frac{b}{n}\left(\frac{1}{t_1E_1}+\frac{1}{nt_2E_2}+\frac{1}{nt_1E_3}+\frac{1}{2nt_2E_3}\right) \tag{2.1}$$

This equation computes the fastener flexural flexibilities based on joint design. In this equation n=1 for single lap joints, and 2 for double lap joints, a and b are joint dependant constants and can be found in table 2.1. Finally, t_1, t_2, E_1 and E_2 are the thickness and Young's moduli of the adherends.

As mentioned previously, the reduction of mode II loading is strongly dependent on the flexural stiffness of the fastener. Equation 2.1 might give a rough indication how large of an effect changing certain fastener design parameters might make.

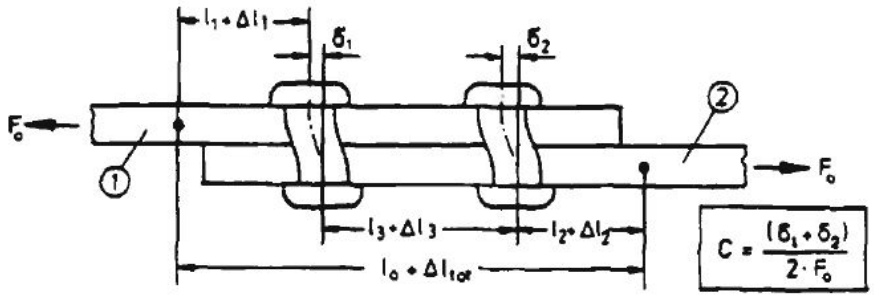

Figure 2.13: *The flexural flexibility quantifies the displacements of the fastener as a function of applied load[1]*

Table 2.1: *Constants used to estimate flexural flexibility[1]*

Joint type	a	b
Bolted metallic joints	2/3	3.0
Riveted metallic joints	2/5	2.2
Bolted graphite epoxy joints	2/3	4.2

2.3.4. Fastener head

Huth[1] also analysed parameters such as the fastener head type, but did not include them in the flexural stiffness formula. This suggests these parameters have little effect on the flexural stiffness and the strength of the joint.

This is in strong contrast to other experiments which showed protruding fasteners result in 15% stiffer joints compared to otherwise similar countersunk fasteners[84]. Furthermore, the maximum stress for a given load is higher in hybrid joints using countersunk fasteners[84]. Countersunk fasteners also result in weaker joints[85]. This is thought to be caused by the fastener area in the countersunk region not being considered "active". The reduced loads transferred by the countersunk fastener can cause the adherends to crack less quickly. In his experiments Zavatta[23] reports countersunk fasteners resulted in a longer fatigue life compared to the protruding counterparts as a result of this.

In addition to changing the fastener head geometry, washers can also be introduced. Fu and Mallick[86] analysed the effects of using such washers and concluded they have a positive effect on the static and fatigue strength in hybrid joints. This effect was strongest when the washer covered the entire bonded section, and a FEM analysis showed this was due to a reduction in peel stresses.

2.3.5. Fastener clearance

The consensus is that a tight fit allows for improved fastener shear engagement, improving the fatigue strength of the joint[35]. This is in agreement with previous research which concluded the clearance resulted in extra crack propagation up to 250 times the clearance dimension itself[34]. It was also found that too much clearance could completely prevent a crack from being arrested as was recorded in multiple samples[24].

Experiments also show the quasi static strength reduces by as much as 50% as a result of increased clearance[24]. Similarly, Caputo et al.[84] analysed the effect of clearance using Three Dimensional (3D) FEM analysis. Based on this analysis it was found that a clearance of 180 μm, or 3% of the hole diameter, resulted in a 14% drop in stiffness. This is the direct result of the fastener carrying more of the shear loads and reducing Mode II loading of the bond.

Raju et al.[77] investigated the effects of applying an interference fit. At low values of interference fit this resulted in an increase of the load carried by the fastener and reduction of the disbond driving force. At higher interference fit values the strength decreases due to complete yielding of the adhesive. Emami Geiglou and Chakherlou[87] analysed the effects of cold expansion processing and found that the fatigue strength increases with an increase in cold expansion processing. This effect was especially strong at lower load levels.

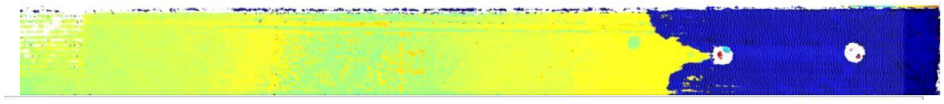

Figure 2.14: *Debonding of a 1 x 2 fastener array, blue has debonded[21]*

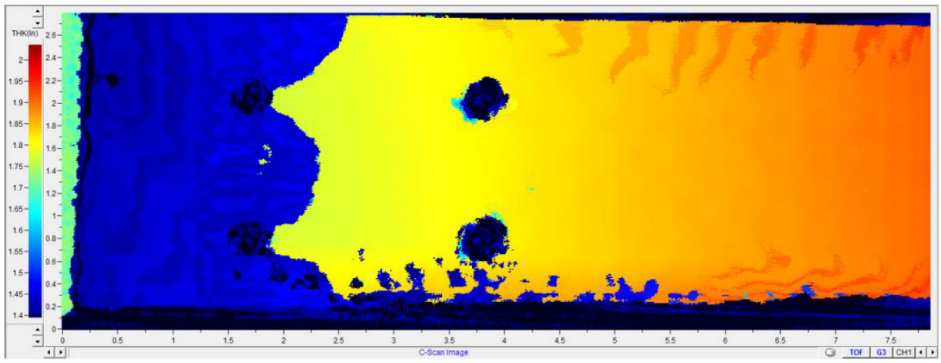

Figure 2.15: *Debonding of a 2 x 2 fastener array, blue has debonded[21]*

2.3.6. Fastener arrays

While a single fastener is highly effective in crack retardation[41], it is not enough to consistently arrest disbond growth[88]. Lin et al.[35] showed two fasteners in series can be used for effective arrest. The same conclusion was also drawn in other reports[21, 24].

It was also shown that the samples with a single row had a similar disbond front to those with two rows[21], see figures 2.14 and 2.15. This suggests that conclusion drawn based one experiments with a single row can be extrapolated to larger specimen.

Further analysis has shown the pitch distance, or distance between rows, can be increased beyond what is required for the fasteners to function as a second loadpath at limit load[37]. Reducing the fastener pitch does improve the crack stopping abilities[35]. Not only does reducing fastener pitch come at the expense of an increased number of fasteners, it can also shift the failure mode from bearing to net section failure[75].

2.4. Modelling

Two modelling techniques are commonly available to model disbond fatigue using FEM: Virtual Crack Closure Technique (VCCT) and Cohesive Zone Modelling (CZM)[22, 89]. These will be discussed in subsections 2.4.1, 2.4.2 respectively. An extension of these methods exists in the form of Extended Finite Element Method (XFEM), discussed in subsection 2.4.3.

Crack Tip Elements (CTE) will not be discussed even though Richard[90] also suggests this method may be used. CTE does not seem to be commonly used in the modelling of hybrid joints. This may be due to the re-meshing required when modelling disbond growth which makes this a computationally expensive method[90].

2.4.1. VCCT

One widely used method to model the disbond growth in hybrid joints is VCCT[21, 24, 35, 42, 91]. It was first developed by G.R. Irwin[92] in 1957.

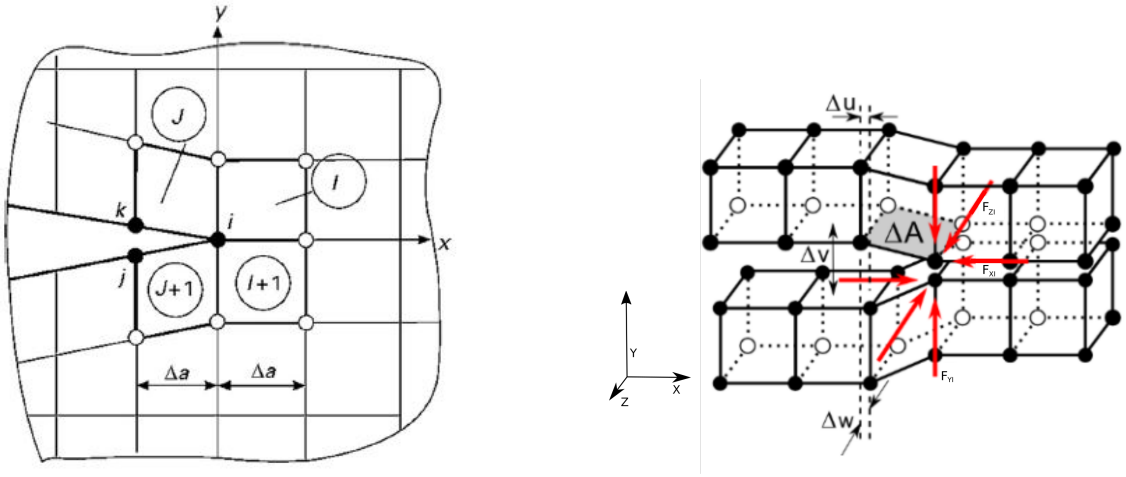

(a) *2D sketch of the workings of VCCT[94]*

(b) *3D sketch of the workings of VCCT, adjusted from[95]*

Figure 2.16: *The displacements used in the VCCT to compute the SERR*

VCCT is based on linear elastic fracture mechanics and assumes the energy required to open it, SERR, is the same as that required to close it[93]. In the 2D case the Mode I SERR is computed with equation 2.2 and Mode II with equation 2.4[94], with $\Delta v_{k,j}$ and $\Delta u_{k,j}$ as defined in equations 2.3 and 2.5. The displacements are illustrated in figure 2.16a. For the 3D case Mode III loading is included as well, as shown in figure 2.16b, with corresponding SERR as shown in equation 2.6.

$$G_I = \frac{F_{Yi} \cdot \Delta v_{k,j}}{2 \cdot \Delta a} \tag{2.2}$$

$$\Delta v_{k,j} = v_k - v_j \tag{2.3}$$

$$G_{II} = \frac{F_{Xi} \cdot \Delta u_{k,j}}{2 \cdot \Delta a} \tag{2.4}$$

$$\Delta u_{k,j} = u_k - u_j \tag{2.5}$$

$$G_{III} = \frac{F_{Zi} \cdot \Delta w_{k,j}}{2 \cdot \Delta a} \tag{2.6}$$

The different SERRs have to be combined to a single value in order to compute the disbond growth rate. There are a number of ways to do this but conventionally this is done using the Benzeggagh-Kenane mixed mode fracture criterion, also commonly referred to as the "B-K law". This adds the different SERRs as shown in equation 2.7 and 2.8[10].

$$G_{equivC} = G_{IC} + (G_{IIC} - G_{IC}) \left(\frac{G_{II} + G_{III}}{G_I + G_{II} + G_{III}} \right)^{\eta} \tag{2.7}$$

$$G_{equiv} = G_I + G_{II} + G_{III} \tag{2.8}$$

If the SERR is in the Paris regime, shown in figure 2.17, the disbond growth rate can be computed using the equivalent SERR and Paris relation, shown in equation 2.9[96–98]. In this relation ΔG is the difference in SERR between the minimum and maximum applied load, and c and n are material dependent parameters found experimentally. This simplicity of VCCT is often considered its main

strength[99].

$$\frac{da}{dN} = c \cdot \Delta G^n \tag{2.9}$$

This method has already been implemented in Abaqus[100]. In addition to this behaviour outside of the Paris regime is modelled as well. If the SERR is below the lower limit the disbond is assumed not to grow, if it is above the critical limit as defined in equation 2.7, the disbond will increase with one element per cycle[10].

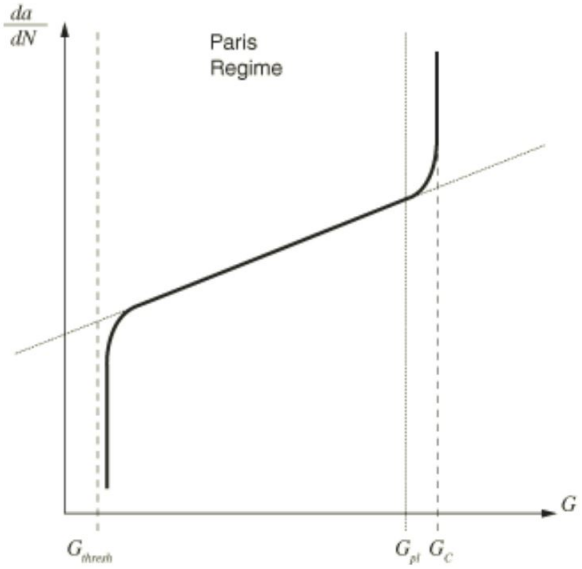

Figure 2.17: *The disbond growth prediction is split into multiple sections, depending on SERR[10]*

There does not seem to be a consensus regarding mesh sensitivity. According to some VCCT works very well even with large elements[101] and is not very mesh sensitive[99]. Others state that VCCT is mesh dependant[89, 90]. It is also mentioned that the mesh should confirm to the mesh front[91] and the mesh should have the same dimensions in front of and behind the crack tip[33, 102].

Similarly there is no clear consensus about how computationally expensive VCCT is compared to other methods. By some it is described as the fastest method to compute disbond growth[90, 99] and by others as a method that is up to 15 times slower than CZM[103]. It should be noted the final paper compared the methods based on disbond length versus number of cycles in a specimen where the SERR was strongly dependant on crack length. This comparison inherently favours CZM as VCCT does not allow for softening, and a more suitable method would be comparing the models based on SERR versus disbond length.

Furthermore, VCCT cannot be used to compute the onset of delamination growth[99]. Abaqus has implemented a method to do this based on an adjusted Paris relation[10], but this does not appear to be widely used.

2.4.2. CZM

CZM models the disbond behaviour using cohesive cracks. A Traction Separation Law (TSL) is used to define the response of these elements[103, 104]. This TSL can be defined in a number of ways, as

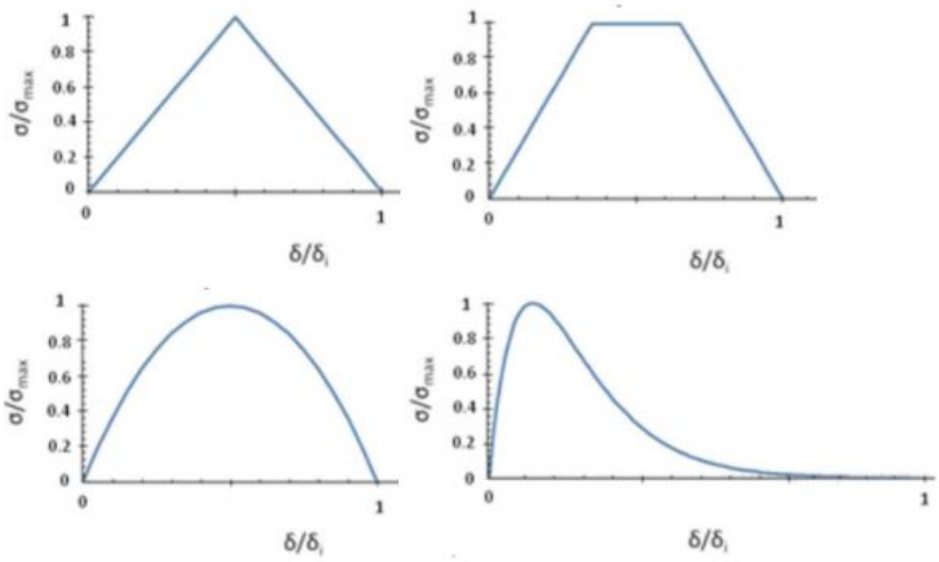

Figure 2.18: *Examples of different TSLs[22]*

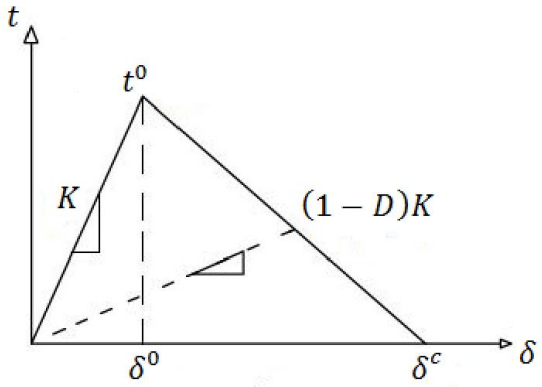

Figure 2.19: *The bi-linear TSL[23]*

long as the integral of the curve is equal to the SERR[22], as illustrated in figure 2.18.

The most widely used TSL is the Bi-linear TSL[103–105], which was developed by Turon et al.[106]. It is shown in figure 2.19 and is entirely defined by the maximum traction, the displacement at maximum traction, and the critical SERR[23].

Different from VCCT, CZM can be used to compute the number of cycles to nucleation[99]. CZM also allows for softening of the material. This means problems that are strongly dependant on disbond length such as those using in Mixed Mode Bending (MMB) tests can be more accurately modelled with courser meshes[103].

CZM does have a number of drawbacks. For instance, it is not possible to find the SERR for different opening modes. Furthermore, when modelling high-cycle fatigue this method becomes computationally expensive. For these cases a modified TSL has been developed[107–111], and has been put to use in practice[27, 39, 104]. Furthermore CZM is described to be mesh sensitive[99]. This in part because the number of elements in the processing zone need to be about 3 to 5[104].

2.4.3. XFEM

Originally proposed by Belytschko and Black[112] in 1999 XFEM represents one of the latest developments in modelling crack growth[22, 113]. In more recent years the method has been adapted to also allow for simulating fatigue loading[113].

XFEM is an extension on existing FEMs, allowing for crack propagation within an element[22, 89]. It does this by using enrichment functions to allow for discontinuities within elements[89, 113]. Because of the usage of these enrichment functions, it may be considerably more computationally expensive[22]. As such it is only applicable in cases when the crack growth path is not known a priori.

2.5. Knowledge gap

The current understanding is that DAFs will be required to certify bonded joints in primary structures. So far research has focused on a number of features in SLS joints such as the fastener pre-load and the spacing of these fasteners. Relatively little effort has been made to understand the effects of fastener design.

Based on this observed knowledge gap, research objectives and questions are formulated in subsections 2.5.1 and 2.5.2 respectively. Expected outcomes are discussed in subsection 2.5.3.

2.5.1. Research objectives

The objective of this research is to further the understanding on the design of bonded joints with mechanical fasteners used as DAFs. More specifically the objective is:

> "To achieve an improved understanding of what features and properties of a fastener are of interest in designing a fastener purpose-designed as a disbond arrest feature by means of a sensitivity study in a 3D finite element model".

2.5.2. Research question

The main research question to be answered is:

> What features are desirable in a purpose-designed mechanically fastened DAF?

More specifically, the question is what the effect is of:

- fastener material stiffness
- fastener shaft radius
- fastener head radius
- countersunk versus protruding fastener head

This will be limited to the use of DAFs in SLS joints as these are the most common type of bonded joint[16]. Furthermore it will only focus on the disbond behaviour of the adhesive: analysing the cracking of the adherends is outside the research scope.

2.5.3. Hypotheses

The expectation is that fasteners with a higher flexural stiffness will be better able to reduce Mode II loading. The size of this effect is expected to be dependent on the stiffness of the adherends as in thin, flexible adherends the fastener may be considered rigid.

Other expectations are that fasteners with a stiffer shaft will exert more clamping and thus will be better able to reduce Mode I loading. As such stiffer materials and a wider fastener shaft should reduce the crack growth rate the most. The size of these effects is expected to be extremely dependent on the adherends for the same reasons.

It is expected that countersunk fasteners will perform similarly to the protruding heads as the head type is not taken into consideration by Huth[1] in estimating flexural stiffness. For the Mode I loading, some differences may be measured as the fastener-hole interaction is known to be less effective.

3

Methodology

In chapter 2 the design problems and solutions regarding bonded joints have been outlined. Based on this, the question is raised: what features are desirable in a purpose-designed mechanically fastened DAF? In this chapter the research methodology used to answer this question is described.

3.1. Research Setup

To answer the research question regarding the effect of fastener design on its disbond arresting capabilities a sensitivity study is conducted. Firstly, a suitable specimen is chosen to model. In order to evaluate the validity of the analysis verification and validation is done. The methodology of which is described in subsections 3.1.2 and 3.1.3 respectively. Finally the sensitivity study setup can be found in subsection 3.1.4.

3.1.1. Specimen

In order for the results to be useful and the experiments to be feasible a number of aspects have to be taken into consideration in the specimen choice.

Most importantly the results should be applicable for answering the research question and for future research. This means it should be a hybrid bonded-bolted joint. It would also be preferable to model an SLS joint, which is the most common joint type in aircraft composite structures[16].

Furthermore, the model has to be validated. This means extensive experimental data should be available to allow for validation. This includes experiments analysing the fatigue response of the joints, as well as experimental data regarding the material properties of the adherend and adhesive as well as the fastener.

Furthermore the experimental data should clearly show the effect of the fastener. It is expected that joints which show a large effect of the DAF will also show large differences between different fasteners. This would allow for clearer results and more reliable conclusions.

Lastly, the specimen is preferred to be simple rather than complex. Not only does this make modelling mistakes less likely, it should also allow for a smaller number of elements, reducing the run time for each sample. As a result of this a larger number of experiments may be conducted, again increasing the reliability of the sensitivity study.

The experiments conducted by I. van Teeseling[20] on hybrid bonded-bolted SLS specimen tested under fatigue loading meet these requirements. He reports results for several different DAFs ensuring extensive validation is possible. Furthermore, material data is available for both the adherend and adhesive[2–5, 114]. The specimen is relatively small, especially compared to similar experiments conducted with Wide Single Lap Shear (WSLS) which would be considerable more computationally expensive to model. As such it was decided to use the experiments using FM94

adhesive[20] as a basis for the sensitivity study.

3.1.2. Verification

The model verification is done in four steps. The first of which is to do a convergence study regarding the time step settings and the mesh size. Using the results of this convergence study the model settings are found that will be used during the rest of the testing.

The next step is to conduct a number of sanity checks. This will be done by visual inspection and probing values. The goal of these checks is to ensure no gross modelling errors are overlooked. The following checks are done:

- stresses are of the correct order of magnitude
- the SERR ratio between Mode I and Mode II is about 1:3[20]
- the stresses in the adherends during the static step increase linearly with the fastener pre-load
- the displacements of fastener and adherends are the order of single [mm]
- the fastener does not clip through the adherends
- the adherends do not clip through each other
- the adherends do not rotate about the clamped edges

The third step is to check if the model responds as expected to changing the simulation settings. These experiments are listed in table 3.1. Experiment V_1 and V_{1a-d} differ based on the region that is modelled as bonded, which will be described in more depth in section 3.2. Especially experiment V_3 is of interest as it is unclear how large of an error caused by neglecting friction is.

Table 3.1: *Description of experiments done for verification*

Specimen ID	Change	Expected result
Base	-	-
V_1	Pre-load is halved to 3884 [N]	little effect as friction is not modelled
V_{1a}	Pre-load is reduced to 0 [N] for a fully bonded specimen	
V_{1b}	Pre-load is reduced to 1162 [N] for a fully bonded specimen	
V_{1c}	Pre-load is reduced to 2325 [N] for a fully bonded specimen	
V_{1d}	Pre-load is halved to 4649 [N] for a fully bonded specimen	
V_2	Doubling η to 2 in the VCCT fracture criterion	no effect as the critical SERR is never reached
V_3	Including a friction parameter	reduce the Mode II SERR

The final verification step is to compare the results to those recorded in previous research. There are three pieces of research that appear applicable: van Teeseling[20], Zavatta[23] and Luke et al.[24] all did experiments with FEM analysing the behaviour of hybrid SLS joints.

Firstly, results can be compared to those reported by van Teeseling[20] who modelled the clamped specimen using an 2D FEM model.

Zavatta[23] modelled specimen very similar to those conducted by van Teeseling[20] with only small differences in adherend dimensions. Zavatta conducted three experiments in which the SERR

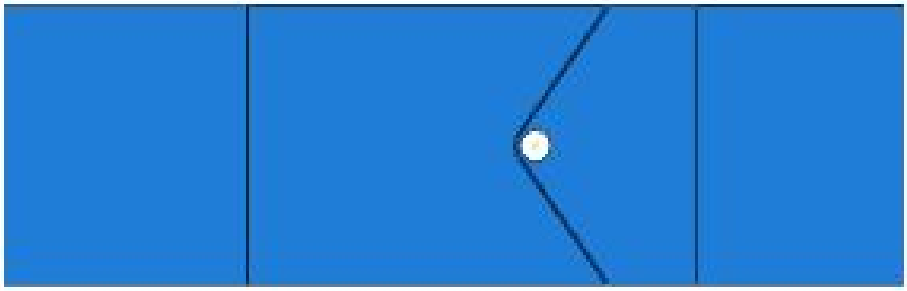

Figure 3.1: *One of the three crack fronts used to find the distribution of the SERR along the crack front, as a function of the position of the crack front[23]*

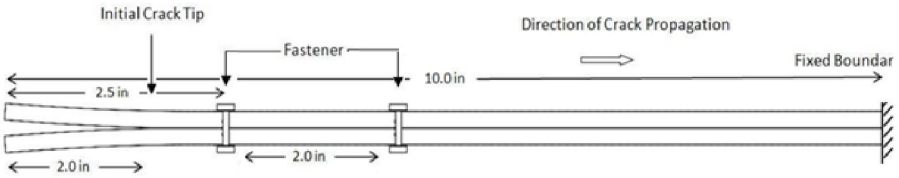

Figure 3.2: *Richard and Lin[24] used two fasteners as DAFs*

was measured over the disbond front. He analysed the effect of the fastener by varying the distance between the crack front and the fastener the effect of the fastener on the SERR. One of these crack fronts is shown in figure 3.1.

This method of analysing the SERR circumvents some of the issues encountered with modelling the disbond growth using VCCT. For instance, it is well known that VCCT will follow the mesh which generally results in a straight disbond front. By comparing results some assessment of these effects on the analysis may be made.

Lastly, a comparison is made with the results reported by Luke et al.[24]. These experiments are not directly comparable for a number of reasons. The most important difference between their specimen and the one used by van Teeseling[20] is the adherend thickness and Young's modulus. The adherends are almost twice as thick. Because of this the Mode II reduction will be less effective than that reported by van Teeseling.

Another difference is that they used a 2D model under quasi-static loading. This means the applied load was increased throughout the experiment. To compare these results to the ones in this thesis a normalised SERR is computed by dividing the reported SERR by the load squared.

A last difference is the number of fasteners, as they used two fasteners rather than one, as shown in figure 3.2. This was because earlier research had shown one fastener was not sufficient to consistently arrest a disbond.

3.1.3. Validation

In the experiments conducted by van Teeseling[20], different hybrid SLS specimen are tested. These include experiments 2_11 with no DAF, 2_09 with a clamp as a DAF and 2_12 with a Hi-Lok as a DAF.

All three experiments are compared for validation purposes, the experiments for which can be

Table 3.2: *Description of experiments done for validation*

Specimen ID	Corresponding experiment code	DAF
Va_1	2_11	-
Va_2	2_09	Clamp
Base	2_12	Hi-Lok

found in table 3.2. These are compared by a disbond growth rate versus crack length rather than a disbond length vs number of cycles. By doing so effects early on do not give the illusion of differences. It also makes it easier to compare the remaining differences.

The first comparison is done for the specimen with no DAF and the clamped DAF. These comparisons should allow to assess the errors caused by inaccuracies in for instance the material properties and the experimental setup. Lastly the results from the experiments using a fastener as a DAF are compared. This should allow for the correctness of the fastener definition and interactions to be validated.

3.1.4. Sensitivity study

In the sensitivity analysis each fastener geometry property is changed independently. This covers four properties: head radius, shaft radius, material stiffness and head shape. One last sensitivity analysis is included to check the effects of friction, used to confirm the validity of the results.

The sensitivity analysis of the fastener head radius, fastener shaft radius and material stiffness is done with six experiments listed in table 3.3.

Table 3.3: *Description of experiments done in the sensitivity study*

Specimen ID	Description radius [mm]	Fastener head radius [mm]	Fastener shaft stiffness [GPa]	Faster shaft and head stiffness [GPa]	Collar
Base	-	4.64	2.4	113.8	73.1
S_1	Head radius 120%	5.568	2.4	113.8	73.1
S_2	Head radius 80%	3.72	2.4	113.8	73.1
S_3	Shaft radius 80%	4.64	1.92	113.8	73.1
S_4	Stiffness 80%	4.64	2.4	91	58.5
S_5	Stiffness 50%	4.64	2.4	56.9	36.6

The sensitivity analysis of the fastener head style included four geometries, illustrated in figure 3.3. With each of which one experiments is conducted, outlined in table 3.4.

3.2. Model definitions

The first step in analysing the effect of fastener design is developing the FEM model that will be used. A number of assumptions and design choices were made at the start, these can be found in subsection 3.2.1. Using these assumptions three models were designed to replicate the experiments conducted by van Teeseling, described in subsections 3.2.2, 3.2.3 and 3.2.4. A more extensive description of the model definition and difficulties encountered in the development of the model can be found in appendix B, and a .cae file with all the models used can be retrieved from[30].

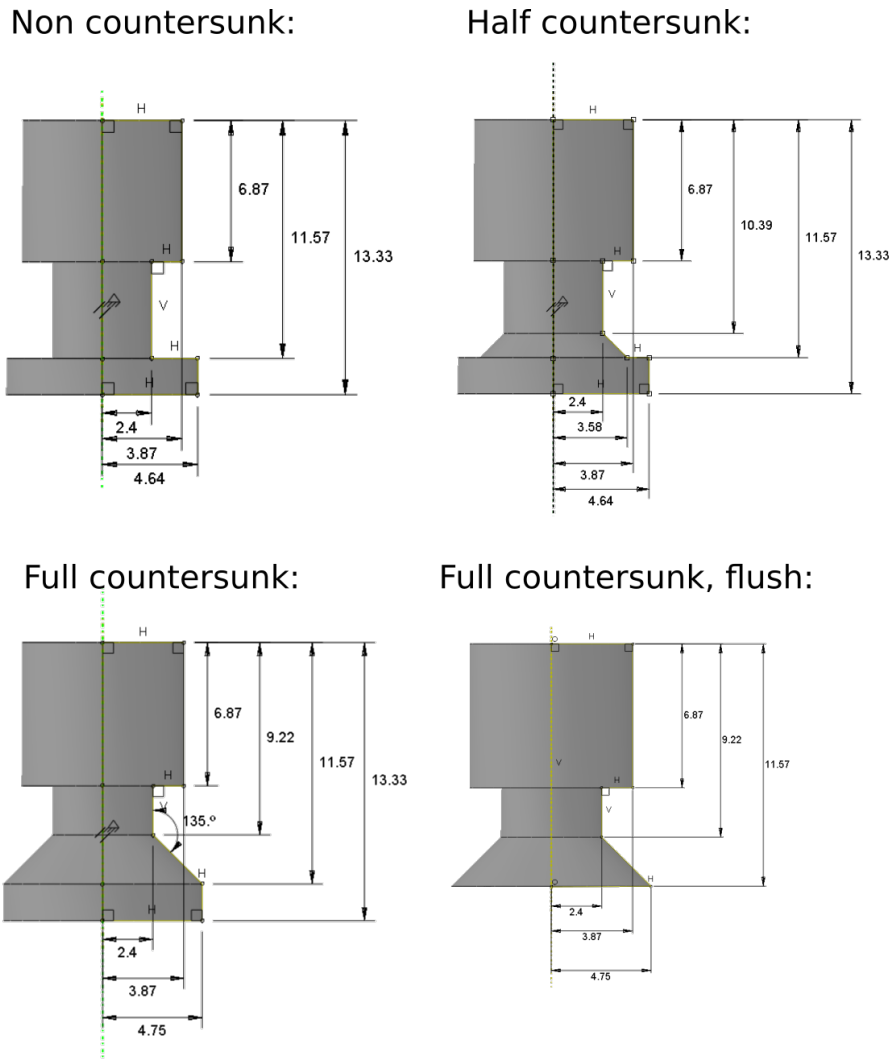

Figure 3.3: *The different fastener heads used*

Table 3.4: *Experiments for the fastener head style sensitivity*

Speceimen ID	Head style
Base	Non countersunk
Fcp	Full countersunk, protruding
Fcf	Full countersunk, flush
Hc	Half countersunk

3.2.1. Analysis assumptions

In designing the model for the analysis of the hybrid joint a number of assumptions and design choices are made. These choices are either made to reduce the complexity of the model or to improve the usefulness of the results.

The first design choice is that friction will be neglected. The reasoning behind this is that friction coefficients can be highly variable and in the aerospace industry joints are not designed to transmit loads through friction. It is expected that this will result in conservative estimations of the SERR as friction reduces the Mode II disbond driving force. This assumed effect will be confirmed during verification.

Furthermore, it is assumed the critical SERR is never reached. This assumption reduces the number of material parameters required, some of which might not be available. An effect of this is that the disbond growth rate will be underestimated if the peak SERR does exceed a critical value. Even if this is the case, these peak SERR would only occur in a very small area about the fastener, causing a relatively small error in the total disbond growth behaviour.

Based on previous work of Zavatta[23] the adhesive is assumed infinitesimally thin. This reduces the number of nodes and further limits the material data required.

Fatigue of the adherends is also ignored. This is done to limit the research scope to the effect of fastener design on the disbond driving forces. The cracking of the adherend is known to effect the disbond growth rate, but will not be covered and can be analysed separately in the future.

In his experiments van Teeseling[20] used a triangulated disbond front such as the one shown in figure 3.4. As this is not necessary for the numerical simulations this was neglected. Instead a straight disbond front was applied in order to create a structured mesh.

Figure 3.4: *Triangular disbond front, adjusted from[20]*

A last difference between the experiments and numerical analysis is the load regimen. In the experiments a starting load of 28 [kN] was used to start the disbond growth after which it was reduced to a load of 26 [kN]. This allowed for a closer match between different matches and made interpretation of the differences in SERR easier.

3.2.2. No disbond arrest feature

The most basic of all three experiments has no DAF. As shown in figure 3.5 this is a hybrid bonded-bolted SLS joint with two parts: the lap and strap.

Both of these two are created using a deformable 3D solid extrusion, with dimensions as shown in figures 3.6 and 3.7. A composite layup is assigned to these parts corresponding to Glass Laminate Aluminium Reinforced Epoxy (Glare) 2A-4/3-0.4, the properties of which are defined in table 3.5. The parts are split into sections using datum planes. This ensures that the interaction definitions

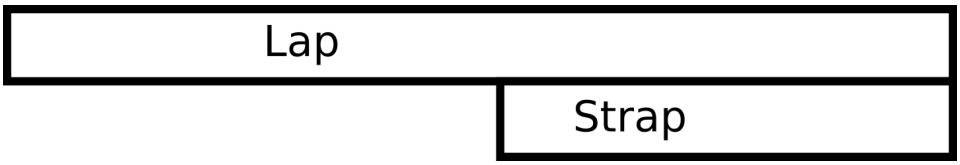

Figure 3.5: *The positioning of the lap and strap adherends*

Table 3.5: *Properties of Glare 2A-4/3-0.4*
The Glass fibre plies in the original experiments had a thickness of 1.33 [mm], but were stacked in layers of two, for clarity these are combined into one single layer

Property	Aluminium plies taken from[114][20]	Glass fibre plies taken from[114][20]	Glare, computed using CLT
Thickness [mm]	0.4	0.266	2.35
Orientation [deg]	-	0	0
Layers	1, 3, 5, 7	2, 4, 6	-
Young's Modulus L [GPa]	72.4	48.9	64.6
Young's Modulus LT [GPa]	72.4	5.5	51.2
Shear Modulus [GPa]	27.6	5.55	20.3
Poisson ratio ν_{xy} [-]	0.33	0.33	0.33
Poisson ratio ν_{yx} [-]	0.33	0.0371	0.26

are applied to the correct locations. It also results in the mesh being aligned between the two components and makes adjusting positions easier. The mesh is of structured type and made up out of 8-node linear bricks with reduced integration disabled.

The loads are applied in two steps: a static and a direct cyclic step. The static step is used to allow for the crack definition as a crack cannot directly be defined in a direct cyclic step. The direct cyclic step models a single loading cycle and extrapolates the damage until the cycle where at least one element fails.

The settings for the direct cyclic step are found through a convergence study, the method of which is described later in subsection 3.1.2. The exact settings used are listed in table 3.6.

The debonding of the adhesive is modelled using an interaction with VCCT fracture criterion, the reason for choosing a VCCT criterion over an CZM are discussed in appendix A. The critical SERRs for VCCT criterion do not matter, as long as they are significantly higher than necessary to

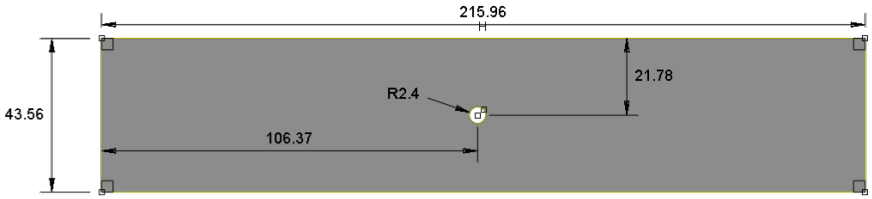

Figure 3.6: *Dimensions for the lap, in [mm]. The lap is modelled 3 [mm] longer than the real length, to allow for boundary conditions to be applied as described in B*

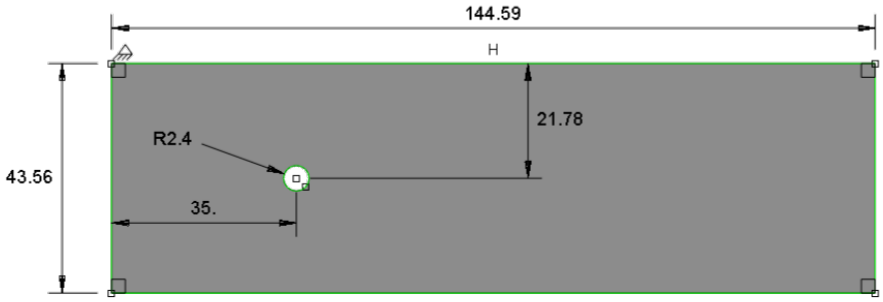

Figure 3.7: *Dimensions for the strap, in [mm]*

Table 3.6: *Settings used for the direct cyclic step*

Cyclic time period	1
Incrementation type	fixed
Maximum number of increments	200 (has no influence)
Increment size	0.05
Maximum number of iterations	2
Initial number of Fourier terms	1
Maximum number of Fourier terms	1
Increment number of Fourier terms	1
Include low-cycle fatigue	Enabled
Maximum number of cycles	151500
Damage extrapolation tolerance	1

Table 3.7: *Paris constants for FM94, dA/dN is in [mm/cycle], calculated based on values from[2]*

c	$7.2 \cdot 10^{-4}$
n	3.85

Table 3.8: *Amplitude definition*

Property	Amplitude 1	Amplitude 2
Circular frequency	6.28	6.28
Starting time	0	-0.5
Initial amplitude	1	0.55
A	0	0.45
B	0	0

prevent debonding to occur during the static loading step. The fatigue damage is defined separately in the keywords.

The properties for the FM94 adhesive are found from experimental data supplied by Bürger[2]. The constants for the Paris' relation are taken from table 3.2 for the case where mode II makes up 75% of the total SERR, as this most closely resembles the expected loading[20]. Bürger used an adjusted value for the total SERR. Furthermore, Bürgers constant are related to [m] and the model is drawn in [mm]. Equation 3.1 was used to find the adjusted constants. This resulted in constants as shown in table 3.7.

$$c_{corrected} = c_{burger} \cdot (1 - R)^{2 \cdot n} \cdot 1000^{n+1} \tag{3.1}$$

The adhesive itself is assumed infinitesimally thin and is not modelled. Instead, a separate normal interaction is used to define the interaction between the two adherends. This is done using a linear contact stiffness with a contact stiffness of $1E+11$. The interaction uses surface to surface discretization, with small sliding allowed.

The specimen is loaded longitudinally. Both of the edges are clamped against rotations and translations. The lap only edge is free to move longitudinally and a coupling constraint is used to ensure the entire face moves in unison. A load of 26 [kN] is then applied to a reference point which is tied to this surface. For a more detailed description of how the boundary conditions are applied see section B.3.

Finally, the direct cyclic step requires all loads and boundary conditions to have an amplitude. Two amplitudes are defined, the properties of which are listed in table 3.8. Amplitude 1, which has an R-ratio 0.1, is used for boundary constraints as these are constant throughout the analysis. Amplitude 2 is used to define the cyclic load. With these settings a load ratio R of 0.1 is achieved with the peak halfway through the step. This also means the field output requests can be limited to only measuring every 10^{th} increment to measure the peak SERR.

3.2.3. Clamped disbond arrest feature

The clamped specimen is largely the same as the specimen with no DAF. The only difference is that a clamp has been added at 35 [mm] from the leading edge of the strap. This clamp adds a pressure

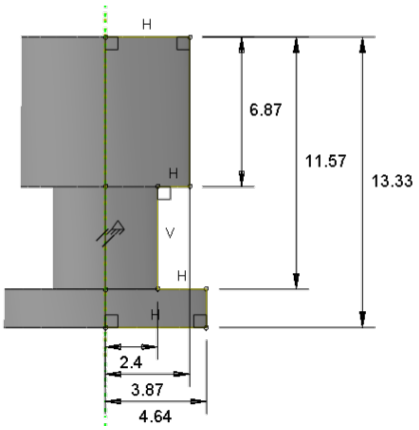

Figure 3.8: *Dimensions for the fastener, in [mm]*

Table 3.9: *Properties fastener material, taken from[3–9]*

Property	Titanium 6Al-4V	Aluminium 2024-T4
Young's Modulus [GPa]	113.8	73.1
Poisson's ratio [-]	0.342	0.33

of 100 [MPa] and is 0.4 [mm] wide. This is simulated using traction forces, applied to 0.4 [mm] wide surface defined using datum planes. Amplitude 1 is used to simulate constant loading.

3.2.4. Fastened disbond arrest feature

The final model includes a fastener. This part is generated using a deformable solid 3D revolution. The dimensions for the base fastener are shown in figure 3.8.

The fastener is partitioned into three parts to allow for meshing: head, shaft and collar. Here the shaft is said to stop completely as soon as the collar is reached. These sections are also used to apply the materials, with the shaft and head being made from Titanium 6Al-4V and the collar from Aluminium 2024-T4[115], properties of which can be found in table 3.9.

Similar to the lap and strap, the fastener is also made up from 8-node linear bricks with reduced integration disabled. The elements have dimensions of 0.4 x 0.4 x 0.4 [mm].

A fastener preload is defined using a "bolt load" with a load of 7767 [N]. This preload is defined with amplitude 1 as the load is constant throughout the cycle.

The same normal interaction used for the interaction between the two adherends is also used for the interaction between the fastener and adherends. Instead of using a surface to surface discretization, a node to surface dicretization is used to aid convergence.

The region about the fastener hole was meshed using tetrahedral elements without reduced integration enabled, as shown in figure 3.9. This was required in order to mesh the adherend in case of modelling a countersunk fastener and corresponding countersunk hole.

This region about the hole is not included in the VCCT fracture criterion. This was done for a number of reasons. Firstly, the interaction does not appear to be possible when using different el-

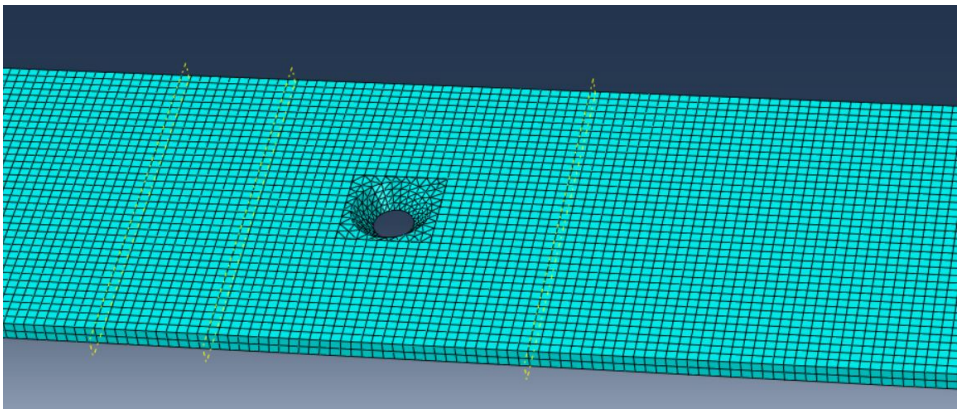

Figure 3.9: *Meshing for the countersunk hole*

ement types. Furthermore, models using the tetrahedral elements in combination with the VCCT fracture criterion did not seem to show mesh convergence. Lastly, models which modelled the adhesive right up to the hole had numerous problems regarding convergence, especially at higher preloads. These effects could be circumvented by not incorporating this region in the interaction.

Modelling part of the adherend using tetrahedral elements required another change in the model. Tetrahedral elements do not support composite layups. To prevent differences in stiffness between different sections of the adherend to cause unexpected behaviour it was decided to use an anisotropic material to model the adherend response. The properties of the material used for this were derived using Classical Lamination Theory (CLT).

When modelling countersunk fasteners the hole had to be sloped. This was implemented by adding chamfer to the hole.

The verification process required two variations to be made to this model: one with friction enabled and one with the VCCT fracture criterion applied to the entire surface.

For the first variation friction was added defining a tangential behaviour with a Lagrange multiplier of 0.05. This friction interaction was only applied in the non-bonded region as the friction and VCCT interactions cause some undefined behaviour.

Lastly, the case when the VCCT fracture criterion extends up to the hole. In this model the entire adherend is modelled using a 8 node linear bricks. The pre-load is reduced to 1294 [N] to aid convergence when the disbond front reaches the fastener hole.

3.3. Data Analysis

During the analysis a number of parameters are measured: the number of cycles, the bond state, the SERR and displacements. The data processing steps applied to these results are described here.

Firstly, the disbond area is calculated by taking the sum of the bond state values and multiplying this by an average area per node, as shown in equation 3.2[1]. This only introduces a small error as the elements are all very similar in size. The average disbond length is then computed by dividing the disbond area by the specimen width and adding the initial crack length, as shown in equation 3.3. This introduces an error in the crack length which is slightly overestimated before reaching the

[1]The disbond time was not used as this feature is not supported in the direct cyclic step

Figure 3.10: *Example disbond front, the green area is bonded and the red area has failed*

region about the hole.

$$A = \sum i_{bondstate} \cdot A_{avg} \tag{3.2}$$

$$a = \frac{\sum i_{bondstate} \cdot A_{avg}}{W} + a_0 \tag{3.3}$$

An average SERR is calculated as well as shown in equation 3.4. The reason for using the number of nodes across rather than the number of nodes on the disbond front is that a number of nodes will not be "activated". Figure 3.10 illustrates this: the nodes marked with the blue circle will increase the number of nodes on the disbond front, but will only marginally increase the average SERR. By dividing only by the number of elements across the specimen the final result will be more consistent. This measure is used because it allows to summarise an entire iteration with one value for each opening mode. As a side effect of this manipulation information regarding concentration of the SERR is lost.

$$SERR_{avg} = \frac{\sum i_{serr}}{n_{across}} \tag{3.4}$$

Finally the SERR can be normalised in order to compare different specimen and illustrate the effect of the DAF more clearly. This is done by dividing the experimental SERR by the expected SERR for the same specimen without a DAF. The analytical model for SLS specimen[116] was developed by van Teeseling[20]. First the deflections and moments are computed based on the work from Lei et al.[117], using which the SERR could be computed with the equations derived by Fernlund and Spelt[118].

To compare the validation data to the FEM results, disbond growth rate versus disbond length is compared. This is done to prevent errors early in the analysis causing an offset later on. The disbond growth rate was calculated using two steps. First, a sample of the data is taken from the original data set, one measurement for every 1000 cycles, as shown with the blue x's in figure 3.11. This is done to remove numerical noise. The second step is to calculate the disbond growth rate using the American Society for Testing and Materials (ASTM) standards[119]. This method finds the best fit of a quadratic polynomial through seven points to find the derivative. The code for this can be retrieved at[30].

The numerical noise mentioned previously concerns the original data which shows a "wave" pattern. This is due to the bond state switching from 1 to 0 without an intermediate value. As a result of this the disbond growth rate spikes when the crack front advances and not all the cells fail at exactly the same time. To filter this out the disbond length is interpolated every 2500 cycles from which the disbond growth rate is calculated, as shown in figure 3.11.

Lastly, the maximum rotation per cycle of the fastener head, fastener collar and adherend is measured. This is done by measuring the position of three points on each face. First the original

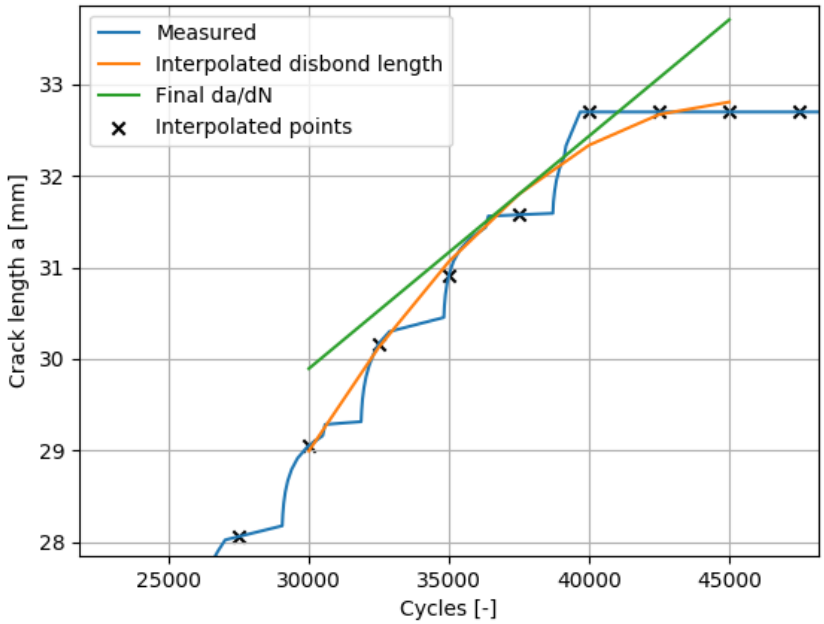

Figure 3.11: *Visual representation of the interpolation method used to calculate the disbond growth rate*

position is recorded for each of the points after which the displacements are added for each time step. Two vectors are constructed with these three points. Computing the cross product of these two vectors allows for the construction of a vector normal to the surface. Using equation 3.5 the angle with the axis perpendicular to the non deformed plane can then be computed.

$$\theta = \arccos\left(\frac{v_1 \cdot v_2}{\|v_1\|\|v_2\|}\right) \tag{3.5}$$

In cases when the fastener has a thin head the measurement points may need to be taken closer to the center. This would be done to prevent bending of the head from introducing measurement errors. In thin fastener head the edges tend to curl up due to pre-loading, causing the resulting fastener head to be non-flat.

4

Results

Chapter 3 outlined the research setup and model definitions. Conducting these experiments resulted in a large amount of data which was processed according to the methods described in section 3.3. The methodology outlined four distinct parts: a convergence study, verification, validation and a sensitivity study. The convergence study and verification showed the model behaved as expected, more detail can be found in the Appendices C and D. The validation results are included in this chapter.

4.1. Representative results

The results of the model the data produced by the experiments are analysed. In order to show how and why the data is manipulated a number of representative results are showcased in this section.

Firstly, one of the most important data is the SERR. When the disbond front is entirely straight the SERR is relatively smooth, as shown in figure 4.1. When the disbond front is spread out over multiple rows the SERR is much more jagged.

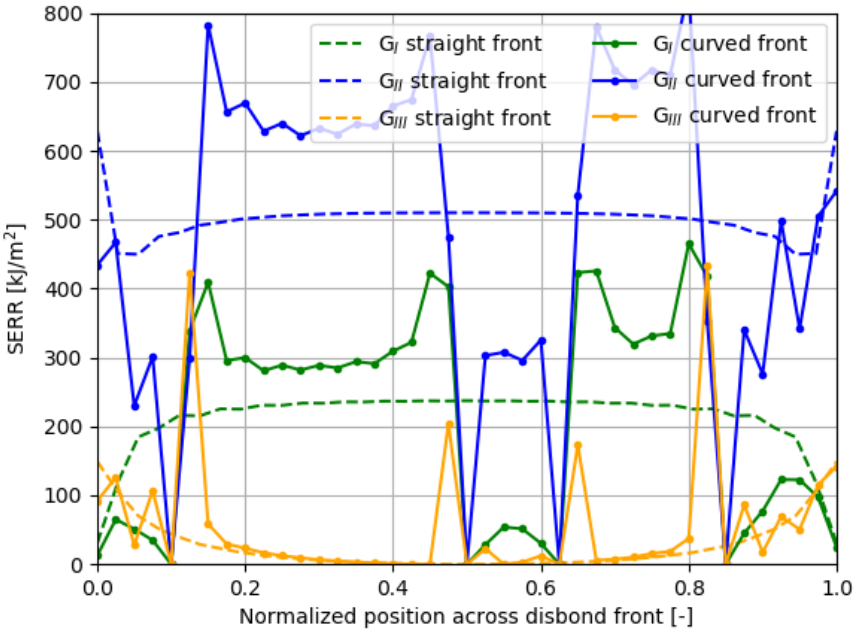

Figure 4.1: *Comparing the SERR for different disbond front shapes*

This concentration of SERR has multiple effects. Firstly, because the section towards the front has a larger SERR the disbond front remains relatively straight. Another effect is that the SERR is

concentrated in a few nodes, increasing the disbond growth rate. Using equation 4.1 to compute the disbond growth rate it is clear the curved crack front in this example has an increased disbond growth rate of almost 150% larger than the straight disbond front.

$$\frac{dA}{dN} = \Sigma c \cdot (\Delta G_I + \Delta G_{II} + \Delta G_{III})^n \cdot w \tag{4.1}$$

By calculating an average SERR over the disbond front the graphs from figure 4.1 can be reduced to a single number for each opening mode. This operation has two main benefits. Firstly, it is a more constant value as seen in figure 4.2. Secondly, this single number can be more easily compared between different disbond front positions and different specimen.

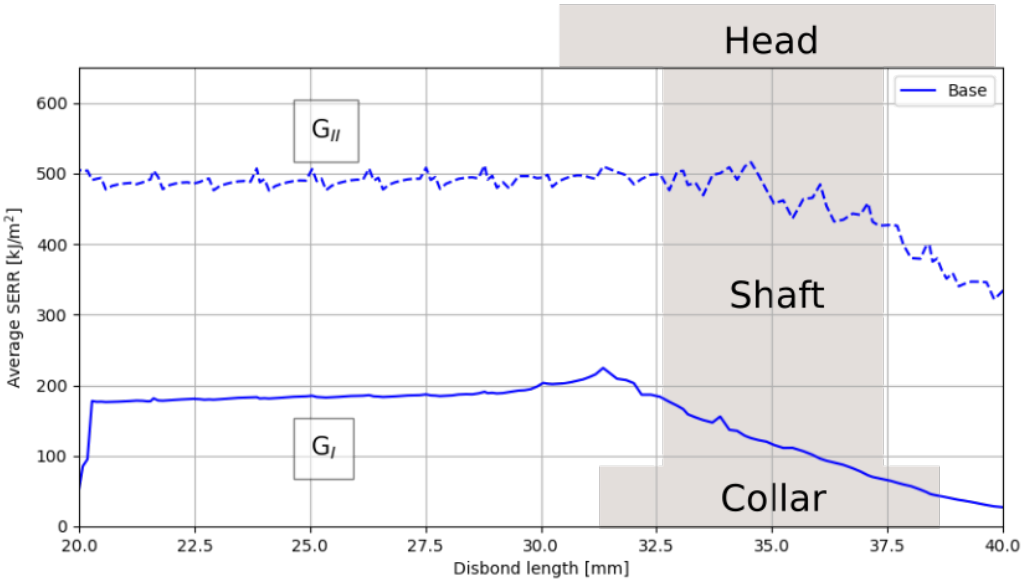

Figure 4.2: *Example average SERR, the gray area represent the position of the fastener shaft, head and collar*

Another measured parameter is the bond state. Each element has a state of either 1, bonded, or 0, failed. All the elements together define the bond state and crack front shape, as shown in figure 4.3.

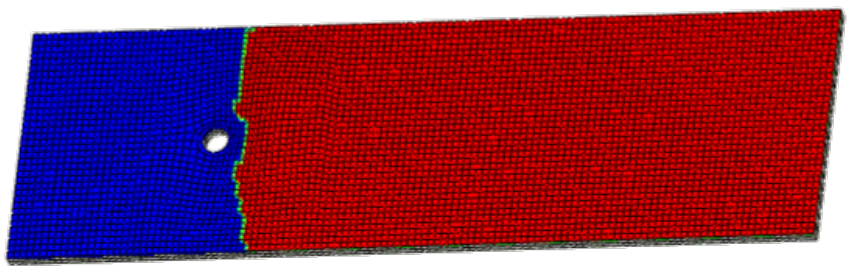

Figure 4.3: *Example of the disbond state, in red are the bonded elements, in blue the failed elements*

The disbond area is computed by subtracting the number of bonded elements from the total number of elements in the originally bonded region. In order to make these more easily comparable to other data an average disbond length is computed. This is a linear mapping and does not alter the nature of the graph, as can be seen in figure 4.4 which has the disbond area and disbond

length plotted side by side. This mapping is not entirely accurate as the region about the hole is not bonded, this however only introduces a relatively small error.

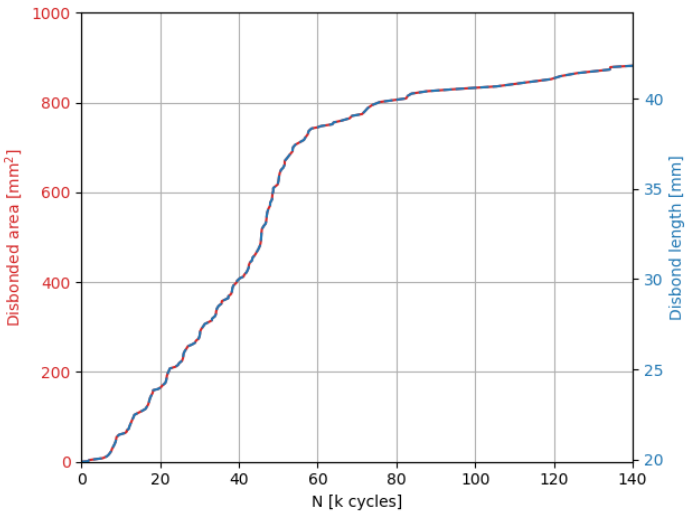

Figure 4.4: *The disbond length is computed with a linear mapping from the disbond area*

Finally, the disbond growth rate is computed from the average disbond length. An example of this is shown in figure 4.5. It is important to notice the increase in disbond growth rate is not caused by an increase in average SERR. This increase is caused by the disbond front being narrower at this location, causing the SERR to be spread out over a smaller area resulting in a higher disbond growth rate.

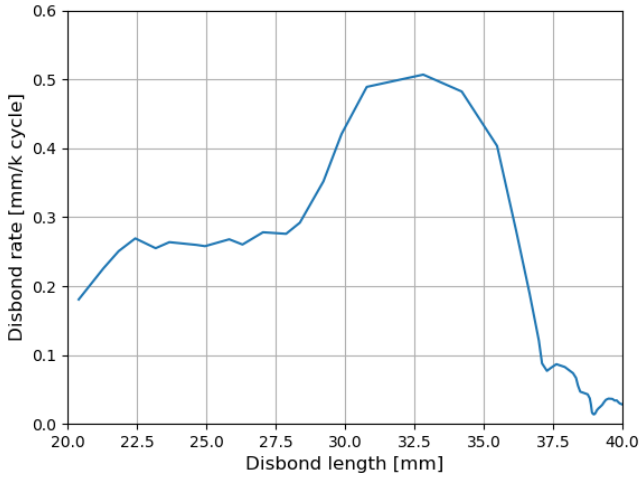

Figure 4.5: *An example of the disbond growth rate versus the crack length*

One last measurement that was conducted was the rotation of the fastener head, collar and the adherend. The computation of which is done by calculating a cross product of two vectors parallel to the surface. The resulting vector of which is perpendicular to this surface, using which the rotation angle is computed, as show in figure 4.6. Plotting the rotation angle for different disbond lengths results in graphs such as the one shown in figure 4.7.

The rotation at the same point of specimen 2_11, which has no DAF, is also included to show the effect of the fastener. It appears this rotation is slightly larger than that of the other specimen. This seems to be caused by the presence of the fastener locally stiffens the joint reducing the rotations. It also shows a divergence between 2_11 and the Base experiments starts to occur at about 27 [mm]; almost 8 [mm] ahead of the fastener location.

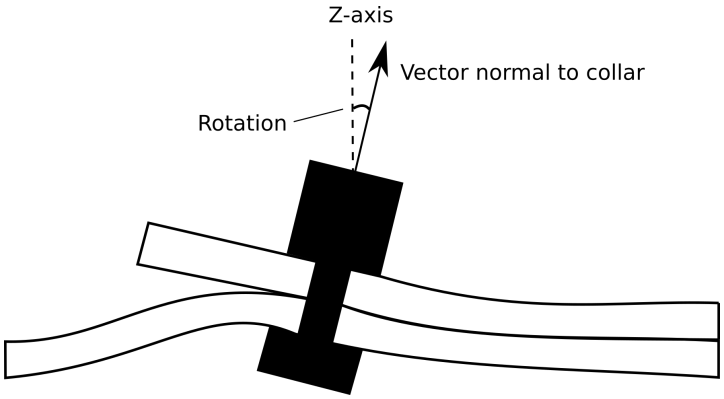

Figure 4.6: *The rotation of the fastener is measured relative to the z-axis*

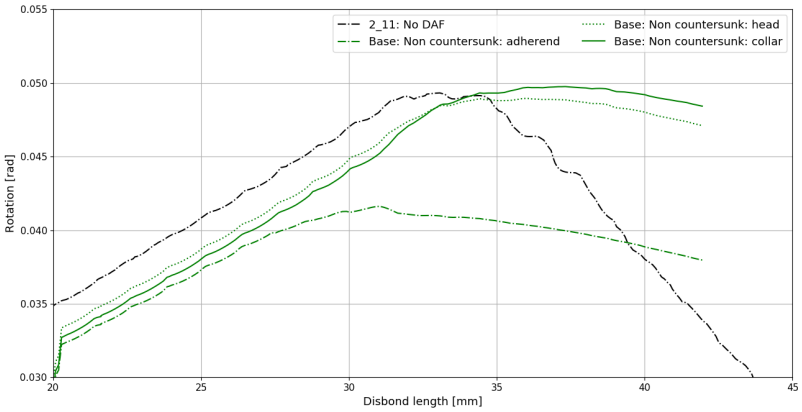

Figure 4.7: *An example of the rotations measured as a function of the disbond length*

4.2. Validation results

Three experiments conducted by van Teeseling[20] are used for validation data: no DAF, a clamped DAF and a bolted DAF. These results are discussed in subsections 4.2.1, 4.2.2 and 4.2.3 respectively.

4.2.1. No DAF

The first model to be addressed did not have a DAF. Results are shown in figure 4.8 which includes three sets of measurements, two of which are experimental and taken from van Teeselings work[20] and are used as validation data.

The disbond growth rate was measured using two methods. Firstly the disbond growth was monitored using visual inspection. The disbond growth rate was computed from this data using

the ASTM standards as discussed earlier in subsection 3.3. The disbond growth was also monitored using Digital Image Correlation (DIC) measurements. This included an algorithm that computed a likely disbond front using the available displacement data. The resulting disbond area was converted to an average disbond length after which the disbond growth rate was computed.

The numerical results from the FEM are also included. Comparing the disbond growth rate between the experimental and numerical results shows the numerical results slightly overestimate the crack growth rate. Nevertheless it is a relatively close match, especially given the fact that no calibration was done as all parameters were based on material data.

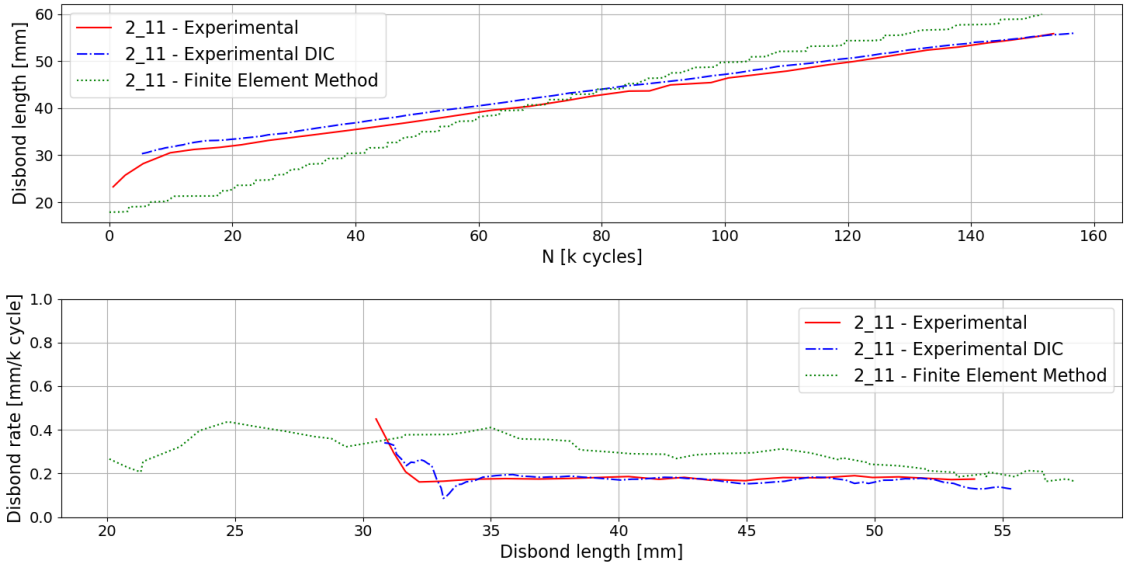

Figure 4.8: *Comparison between experimental and FEM results for the specimen with no DAF*

The initial heightened disbond growth rate is caused by two features of the experimental setup. Firstly, an increased load was used to allow for crack initiation to occur. Secondly, a teflon foil was used to create a triangular disbond front as shown in figure 3.4. This was done to allow the disbond front to grown evenly across the the entire width of the specimen. It also meant the SERR was concentrated at the tips of the triangles, causing an increase in the disbond growth rate.

Another contributing factor to the difference in disbond growth rates is the concentration of SERR as described in section 4.1. The model has the tendency to concentrate the SERR in the "corners" of the disbond front, combining this with the Paris' relation results in increased disbond growth rates.

In his experiments van Teeseling also measured the "Aspect Ratio" of the disbond. This is a measure for the warpedness of the disbond front. For the specimen with no DAF the aspect ratio stayed close to 1 throughout the entire experiment which was also the case for the numerical results. The hybrid joints show a strong bending behaviour once the disbond moves beyond the fastener. This is not captured by VCCT as this technique is well known to result in relatively straight disbond fronts.

4.2.2. Clamped DAF

This experiment used a clamp as a DAF at 35 [mm] from the edge. Shown in figure 4.9 are the experimental and numerical results. Comparing these results, it is clear that in both cases the disbond is completely arrested at the clamp. As mentioned previously, the heightened disbond growth rate at the start is caused by the experimental setup as well as the VCCT concentration effect. Once the disbond has reached beyond the triangular region, about 1-5 [mm] ahead of the clamp, the disbond growth rates appear to match closely.

The region 0-1 [mm] ahead of the clamp shows a significant difference. The experimental results show a reduction of the disbond growth rate in this region which the numerical do not match. This seems to be caused by the step stiffness employed by VCCT which causes the entire row of elements to fail at once, allowing the disbond to skip this section.

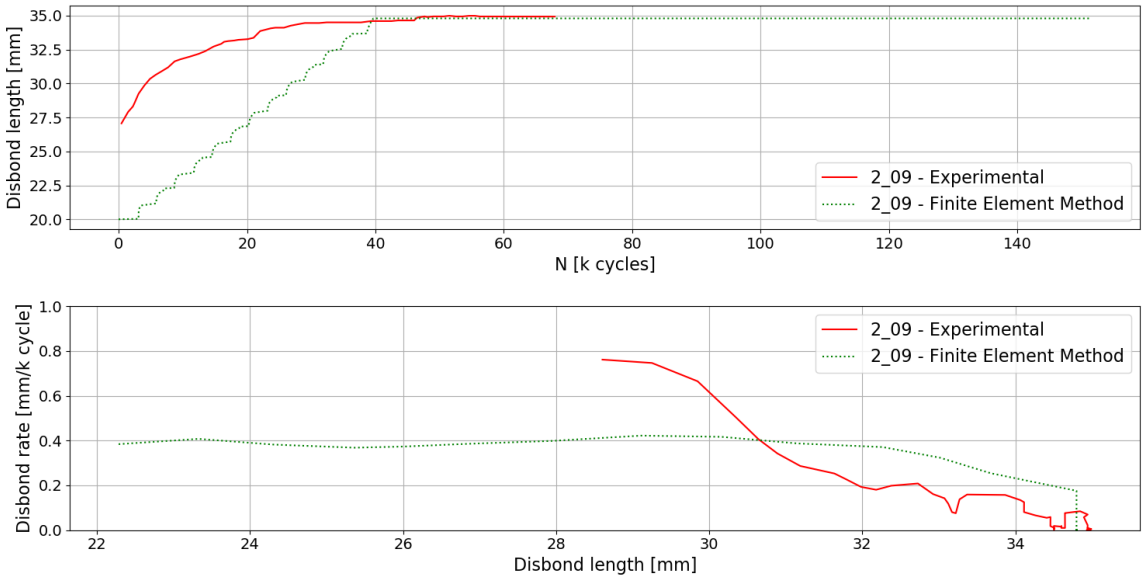

Figure 4.9: *Comparison between experimental and FEM results for the clamped experiment*

4.2.3. Mechanical fastener as a DAF

This experiment used a mechanical fastener as a DAF at 35 [mm] from the front edge. The results are shown in figure 4.10. The experimental results are cut short as the original experiment was halted due to failure of the adherends.

The difference in the disbond growth recorded using DIC and the visual inspection is caused by the warping of the disbond front. The crack grew faster towards the edges causing the visual inspection to overestimate the location of the disbond front. As expected, the numerical results did not show this warping behaviour. Nevertheless the numerical and experimental results show a similar reduction in the disbond growth rate after reaching the fastener.

The numerical results also show a significant increase in the disbond growth rate around the location of the fastener. This is caused by the bonded area being narrower in this region as required for modelling as discussed previously, which causes the SERR to be spread out over a narrower region. This results in an increased disbond growth rate due to the nature of the Paris' relation.

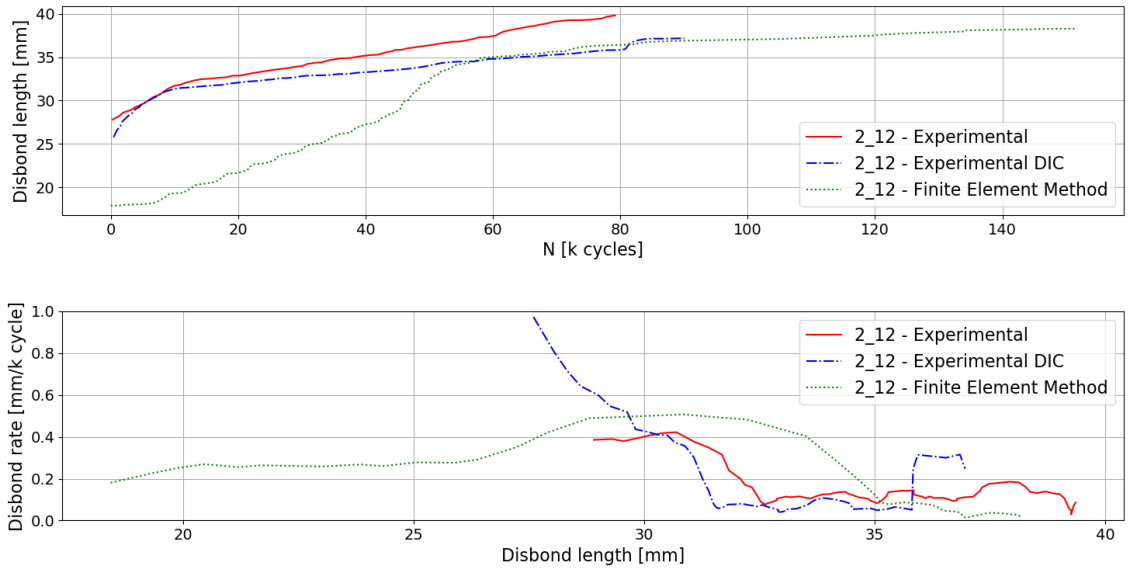

Figure 4.10: *Comparison between experimental and FEM results for the experiment with a fastener as DAF*

In summary, the numerical results seem to match the experimental results to an acceptable degree. Some differences remain but these are mostly caused by the limitations of using VCCT. Based on this the model may be deemed adequate for the intended purposes.

5

Discussion

The goal of this research has been to answer the question what features are desirable in a purpose-designed fastener DAF. To answer this, a sensitivity study has been conducted on an SLS specimen regarding fastener material stiffness, shaft radius, head radius and head shape. The results from this sensitivity study are discussed in sections 5.4, 5.6, 5.5 and 5.7 respectively. Before that, modelling challenges and limitations of using VCCT to model disbond growth are described in sections 5.1 and 5.2 and the validity of the model is described in section 5.3.

5.1. Challenges in modelling process

The model sometimes behaved in an unexpected fashion. A number types of this behaviour were recognised. More detailed descriptions, possible causes and solutions are discussed below. In general when an issue could not be resolved the results were excluded from the discussion in favour of a similar experiment that did not exhibit this behaviour.

Firstly, the adherends sometimes showed large displacements at the clamped edge. This is shown in figure 5.1. While several steps were taken to remove this effect, including changing the way the boundary conditions are applied, the exact cause of this remains unclear. Reduced integration was already disabled and was therefore not the cause of the problem either.

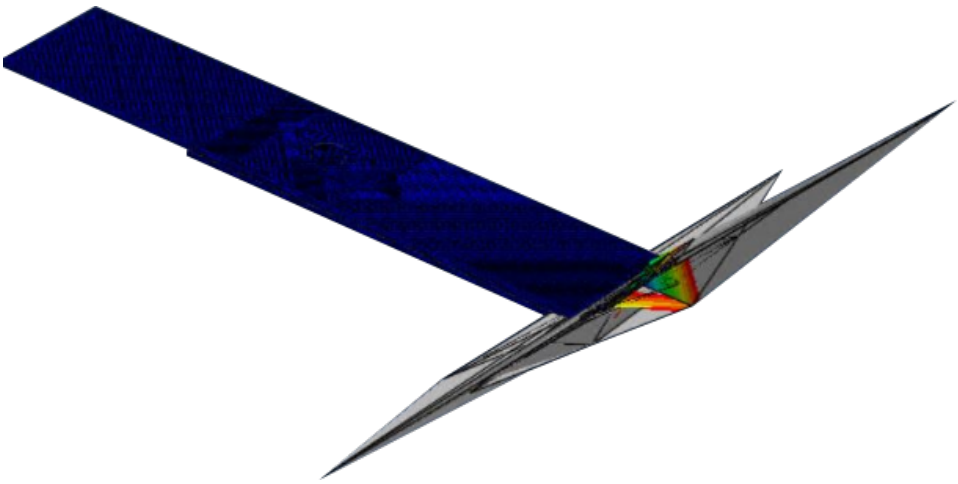

Figure 5.1: *Large displacements were recorded at the root*

In similar fashion in some cases the fastener would become extremely elongated when applying the fastener pre-load. This is shown in figure 5.2. No cause for this was found either. The solution was to re-mesh the fastener.The fastener also sometimes clipped through the adherends. This occurred especially often when modelling the countersunk Hi-Loks or when the disbond reached significantly far beyond the DAF. This was usually solved by changing the time step settings. For

instance reducing the time increment size sometimes fixed the problem.

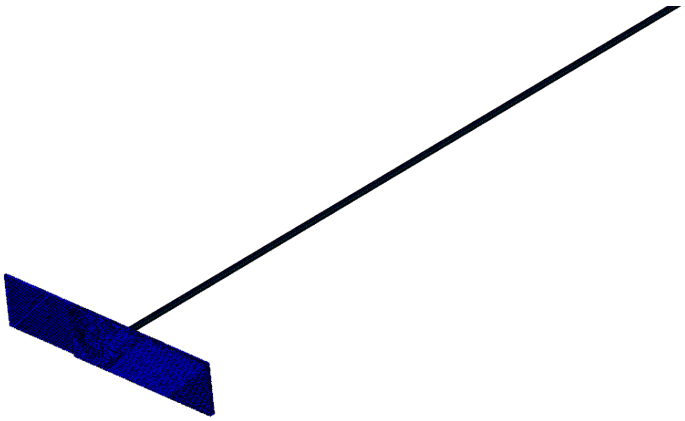

Figure 5.2: *Large displacements recorded in the fastener*

Another prominent aspect of the model is the concentration of SERR along the disbond front as described in section 4.1. When the disbond front is spread out over multiple rows the SERR is concentrated in the nodes at the corners. As a result of this concentration the disbond growth rate can also be significantly increased making the prediction of disbond growth rates inaccurate.

Lastly, sometimes the disbond growth spiked. This can for instance be seen in the results from the full countersunk, flush heads. It appears this might be due to a combination of afformentioned concentration of SERR and how the disbond growth is extrapolated, although it is not entirely clear how this works. It is thought the same issue might be the cause of the fully bonded model failing at higher pre-loads. The average SERR was unaffected by this and so in these cases some of the results can still be used.

Not so much an error, but an unexpected behaviour is that the model was quite sensitive. Small changes in the mesh could cause the model to completely fail to converge past the static loading step. This was solved by changing the mesh until it did converge.

5.2. Limitations of VCCT for studying DAFs

When choosing the modelling method the choice was between CZM and VCCT. The reasoning for choosing VCCT originally can be found in appendix A. Two known limitations VCCT faces are the lack of crack initiation criteria and the tendency to follow the mesh front. In doing the experiments three other limitations were encountered: the damage extrapolation near the hole was prone to errors, the disbond growth rate was consistently over estimated and the combination of friction and VCCT was problematic.

The sensitivity tests did not model the area around the fastener hole as bonded. This was for two reasons: modelling the area up to the edge of the hole resulted in incorrect results at higher pre-loads and it allowed for tetrahedral elements which do not support the VCCT fracture criterion, which was necessary to model the countersunk fasteners. The effect of this is that the disbond growth rate is overestimated as the disbond reaches the position of the hole. It also means all conclusions are only applicable several [mm] away from the hole.

Friction was ignored as joints cannot be certified based on their friction properties as these are too variable depending on circumstances. Furthermore, combining VCCT fracture criteria with friction interactions proved more complex than anticipated. One test was done to check the effects of this, showing little to no difference, this could be caused by the bond line not being modelled close to the fastener hole as especially near the fastener it is expected that friction would play a large roll.

5.3. Model validity

In order to assess the validity of the model, verification and validation analyses were done. The results regarding mesh sensitivity, step sensitivity as well as further verification and validation data show that the model meets the requirements for the sensitivity study.

Firstly, the model shows good convergence for both the mesh and step settings. These results match those from previous experiments conducted with an MMB specimen described in appendix A.

The verification confirmed that the model was consistent with expectations and previous experiments. Some differences remain, the causes for which are mostly understood and have been described extensively in appendix D. The model can be considered to be consistent with previous findings.

Lastly, all the numerical results mirror the validation data from the experiments. One large difference is the shape of the disbond front. As shown in figure 5.3 the experimental setup showed large warping of the disbond front which was not replicated by the FEM model as a result of the usage of VCCT.

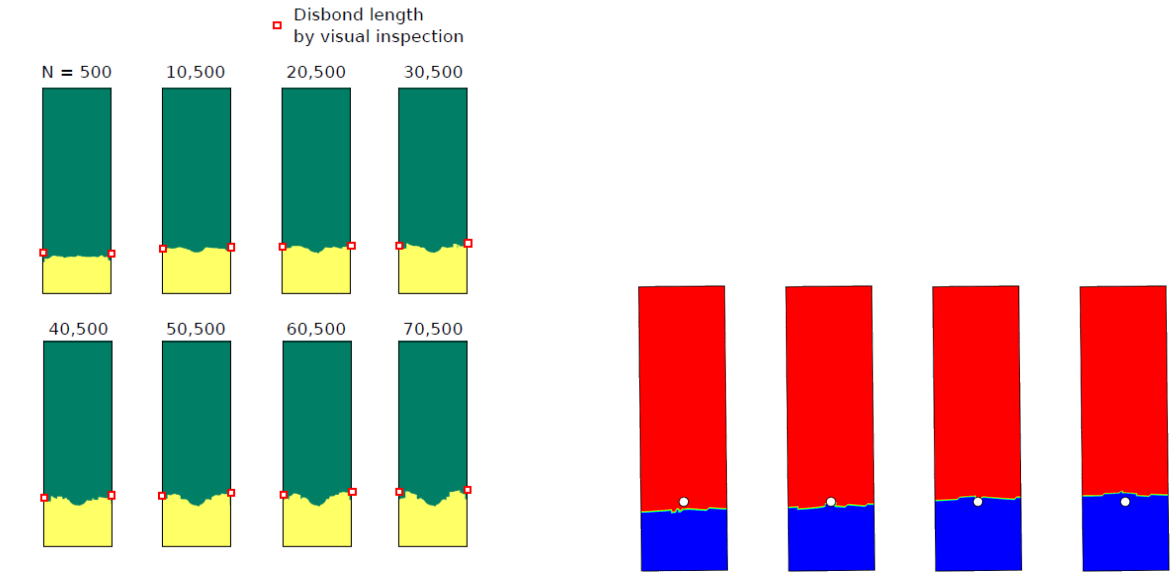

(a) *An example of the disbond growth as reported by van Teeseling[20]*

(b) *The disbond growth as predicted by the model*

Figure 5.3: *The experimental and FEM results showed large differences in the shape of the disbond front*

The straight disbond front also affects the SERR distribution across the disbond front. This is

very clearly visible when comparing the SERRs to those reported by Zavatta[23]. Figure 5.4 shows some these results for the Mode I SERR. When the disbond front reaches the fastener Zavatta showed the Mode I SERR to be largely suppressed. This is different from the results from the model as the disbond had not yet moved further beyond the fastener at the edges.

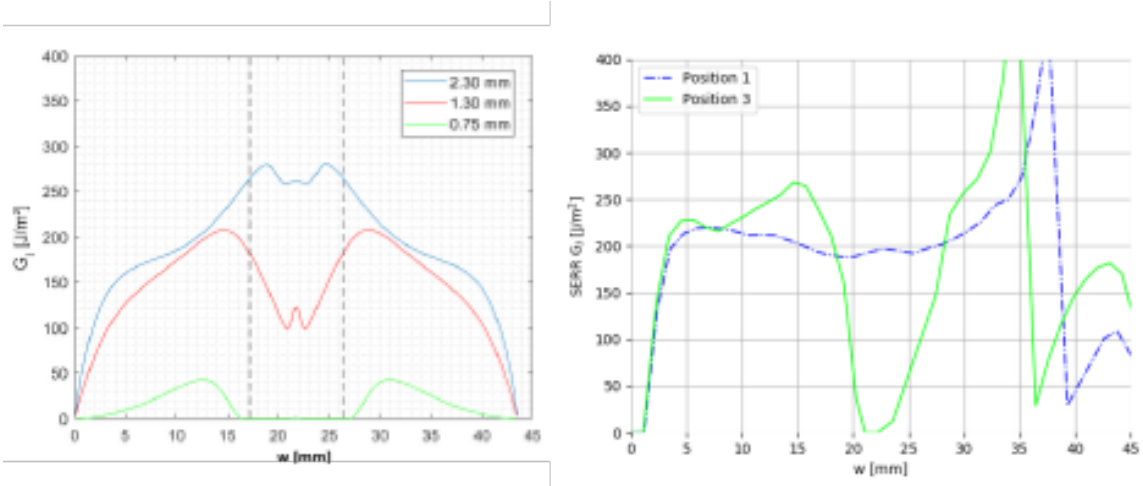

Figure 5.4: *Distribution of the Mode I SERR along the specimen width, on the left the results from Zavatta[23], on the right the comparison*

This discrepancy between the disbond front shapes is a systematic error. This still allows the model to be used for a sensitivity study as this focuses on the differences between different fasteners, and systematic errors will largely cancel out. It also means the model is not as suitable for prediction fatigue life behaviour.

Summarising, the model is consistent and good enough to allow for a comparison between different tests. Issues remain, especially regarding the disbond crack front geometry. This was expected and does not invalidate the sensitivity results. It does make the model unsuitable for the prediction of disbond growth.

5.4. Influence of fastener material stiffness

Three experiments were done with different fastener material stiffnessess. Here both the shaft, head and collar are adjusted to 50%, 80% and 100% of the original stiffness. The results are shown in figure 5.5. While the difference seem negligible they do follow the expected behaviour as a more ductile fastener will perform slightly worse in the reduction of Mode II loading. The lack of difference makes sense as the flexural flexibility only changes about 30% from 16 to 21 $[\frac{mm}{MN}]$.

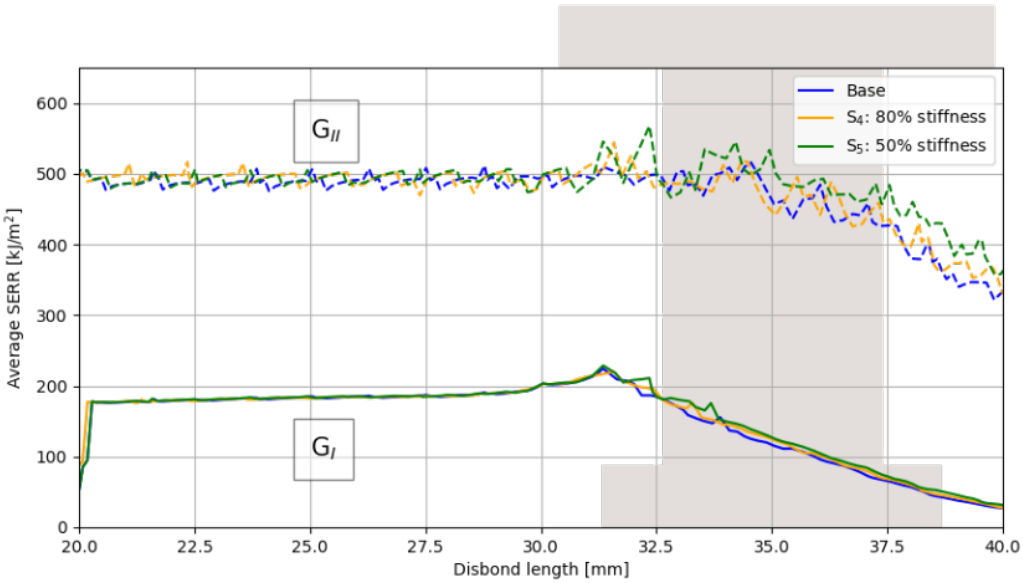

Figure 5.5: *Average SERR versus crack length for different fastener stiffnessess*

The Mode I behaviour is exactly the same for all three experiments. This is because the loads associated with the Mode I opening are so small compared to the stiffness of the fastener it may be considered rigid. This same behaviour is seen throughout all the other experiments as well supporting this observation.

Because the SERR reduces as the disbond grows past the DAF, the disbond growth also slows down allowing different specimen to reach roughly the same final disbond position. Logically as a result of this the position of the disbond lengths differ even less, which is shown in figure 5.6. This means small differences in the SERR behaviour result in even smaller differences in the disbond growth rates.

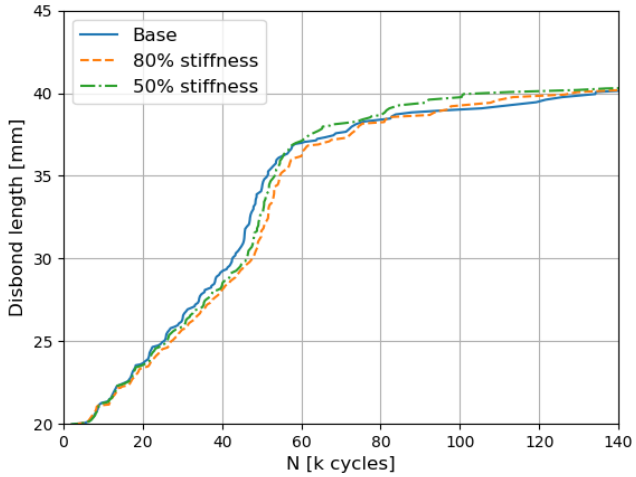

Figure 5.6: *Disbond length versus number of cycles for different fastener material stiffnessess*

5.5. Influence of fastener shaft radius

Similarly to the fastener material stiffness, the fastener shaft radius has relatively little influence on the SERR. The comparison between the base experiment and experiment S_3, as seen in figure 5.7, shows the behaviour is very similar especially for the Mode I SERR.

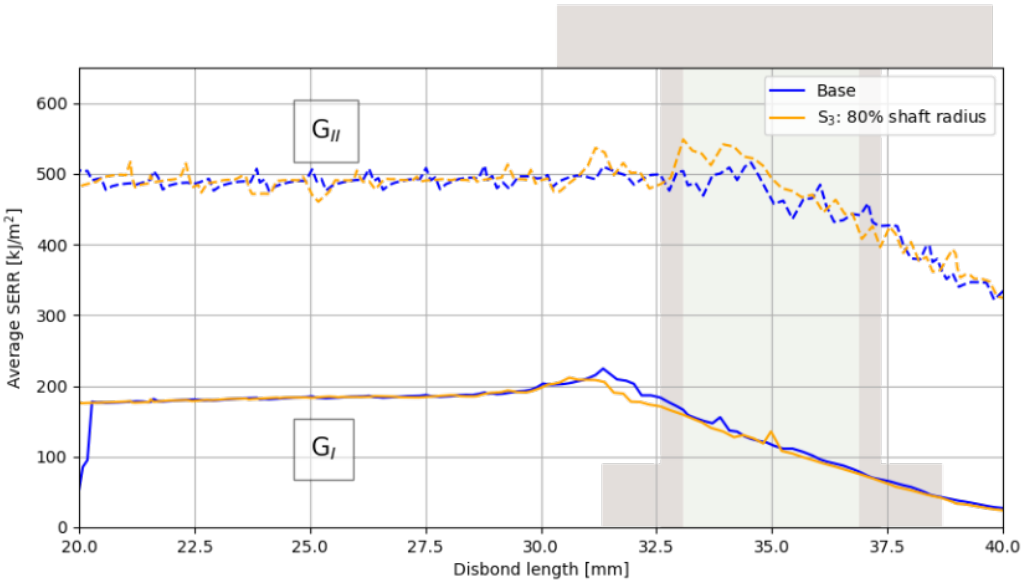

Figure 5.7: *The SERR versus crack length for different shaft radii*

While the Mode II SERR is less constant it does follow the same trajectory in both cases and differences can likely be considered numerical noise. This is surprising as the fastener flexibility increases about 16% by reducing the shaft radius by 20%, which might be expected to result in a lesser reduction of the Mode II driving force. This shows that while the fastener flexural flexibility does play a definite role in the Mode II suppression, large changes are required to result in measurable differences in thin specimen like the one analysed here.

5.6. Influence of fastener head radius

The fastener head radius is expected to have no effect on the disbond growth as it does not change the flexural flexibility. This hypothesis is partially confirmed by the results shown in figure 5.8 which shows the average SERR for three fasteners with different head sizes.

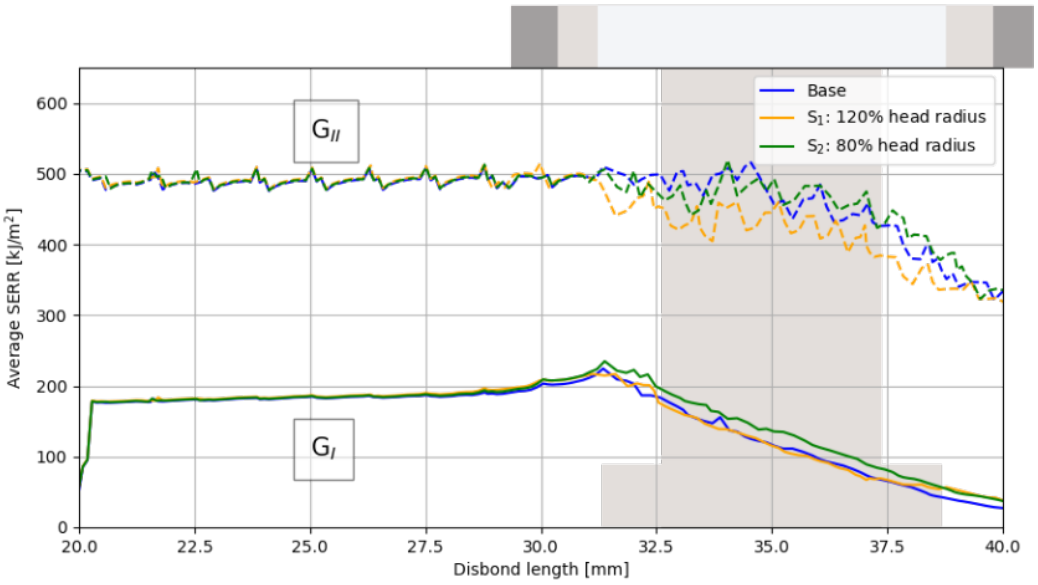

Figure 5.8: *Comparing the SERR versus crack length for different head radii*

As mentioned previously, the Mode I SERR shows little difference between the three experiments. It appears slightly larger for the smallest head radius when reaching the fastener. This could be a measurement error as it aligns with the results for experiment S_2 only slightly further. It could also be indicative the smaller head size is less apt at limiting the Mode I driving force, which could be due to the head radius only being 0.7 [mm] larger than the shaft radius. It is unlikely that this would large effect though as the collar is a similar size. Either way the effect is small enough to be considered negligible.

The Mode II SERR reduction seems to occur slightly earlier for the fastener with the larger head. This is likely the result of the head introducing the clamping effect at an earlier point, causing the mode II reduction to occur sooner. As a result of this the disbond front may be arrested at an earlier point, changing the disbond front shape. This would further alter the SERR. Unfortunately this could not be analysed due to the known limitations of VCCT.

5.7. Influence of fastener head style

Different head shapes ranging from non countersunk to a flush full countersunk head were compared. The crack length versus the number of cycles is shown in figure 5.9a, and shows a number of clear differences.
Firstly, at about 52 kilo cycles the analysis of the flush head failed. This behaviour was recorded throughout the experiments and seems to be related to the fastener-hole interactions.

Secondly, the region with increased disbond growth rate is significantly larger for the countersunk fasteners compared to the non-countersunk. This can be seen especially clearly in figure 5.9. This is due to the countersunk fasteners having a slightly wider and longer region without the VCCT criterion applied about the hole, required to be able to mesh the entire hole. This does not explain the differences between the different countersunk fasteners as they all have the exact same non-bonded area. This suggests the head shape does play a significant role in the disbond arrest.

The disbond arrest of the full countersunk fasteners appear to occur later. This might be due to

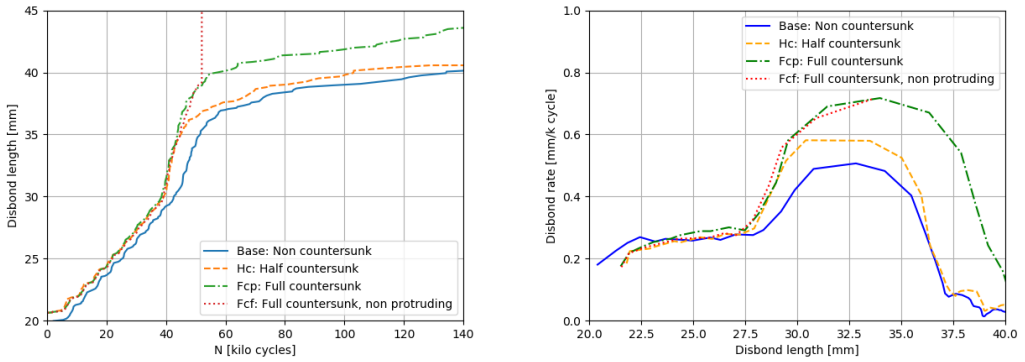

(a) *Disbond length versus number of cycles for different fastener head shapes*

(b) *Disbond growth rate versus disbond length for different head shapes*

Figure 5.9: *Results for the disbond growth for different head shapes*

the limited reduction of the Mode II SERR, as seen in figure 5.10. At a crack length of 40 [mm] the average SERR due to Mode II loading of the full countersunk fastener is 30% larger than that of the non countersunk fastener, the half countersunk fastener has marginally larger SERR. It is also clear that the head shape has little to no influence on the Mode I suppression. This may be due to the lesser effectiveness of load transfer for the slanted area. As reported throughout literature, the angled part of the hole is ineffective in transmitting load[120]. Interestingly this does not necessarily translate to the joint performing significantly better, as Zavatta[23] found the flush Hi-Loks resulted in a longer fatigue life caused by a reduction of fatigue damage in the adherends.

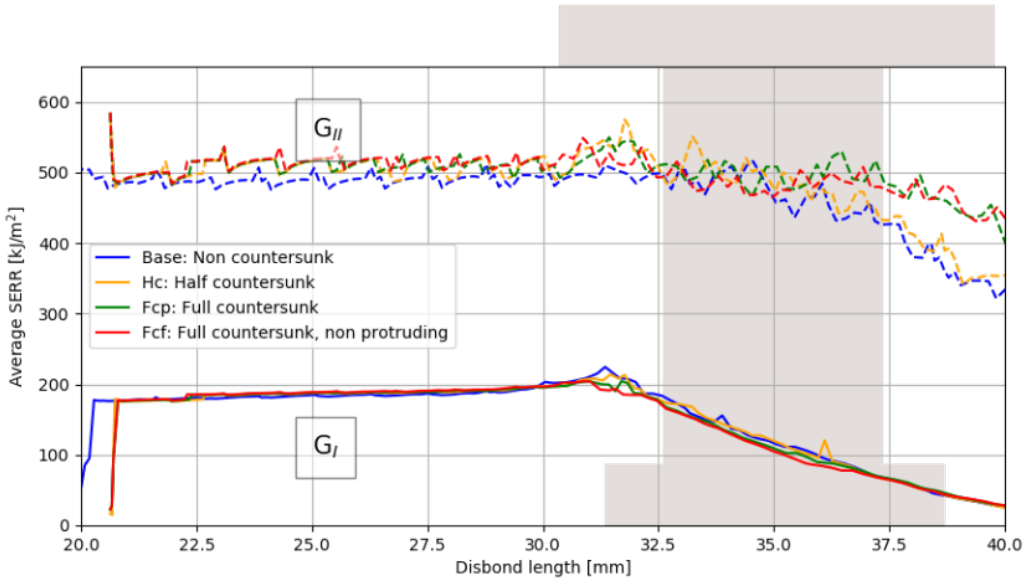

Figure 5.10: *Average SERR versus crack length for different head geometries*

Finally the rotations of the Hi-Lok head, collar and the adherend rotations are also compared to further understand the differences. The results, shown in figures 5.11 and 5.12, show there is a difference between the adherend rotation for the full countersunk fasteners. In figure 5.11 the rotation tapers off at a disbond length of about 27 [mm] and peaks at a crack length of 30 [mm] after which it stays nearly constant. Comparing this to the full countersunk fasteners in figure 5.12, the slope does

reduce somewhat at 30 [mm] but the peak occurs much later at a crack length of 35 [mm]. This suggests some clamping effect is already present as much as 8 to 5 [mm] ahead of the fastener. It also suggests the full countersunk fasteners only start transferring load at a much later point compared to the non-countersunk specimen.

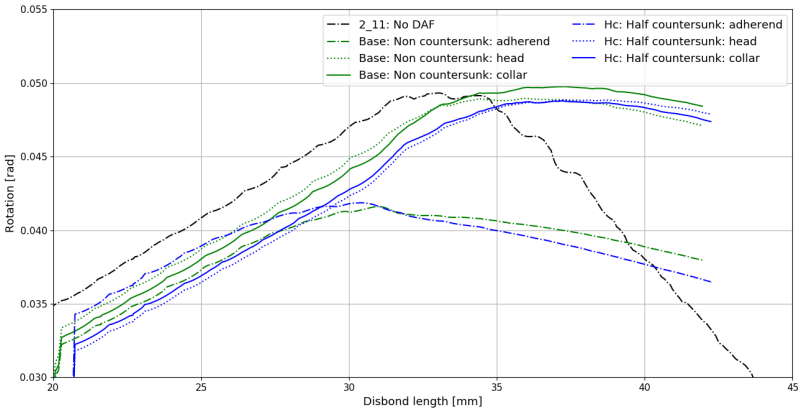

Figure 5.11: *Rotations for the non countersunk and half countersunk fasteners*

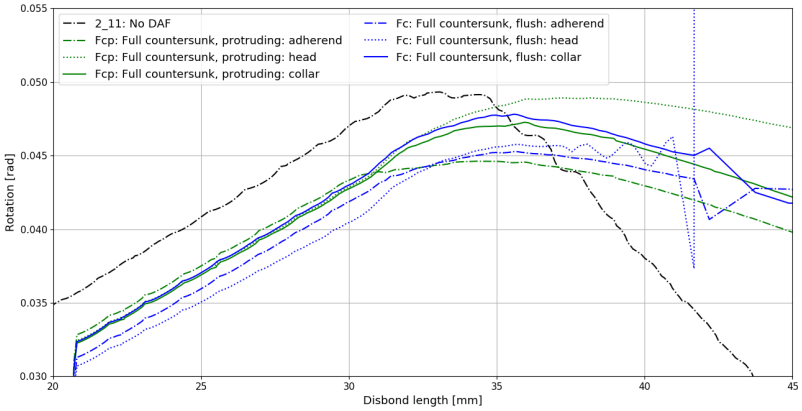

Figure 5.12: *Rotations for the full countersunk and full countersunk flush fasteners*

Another point of interest is the difference between collar and head. For the non and half countersunk fasteners these surfaces remain nearly parallel throughout the analysis. The full countersunk fastener shows a difference of almost 10% between the collar and head at a crack length of 40 [mm]. The cause of this is thought to be the diagonal shaft redirecting some of the force to push the head "up and out", as illustrated in figure 5.13. This leads to a less effective load transfer between the adherent and fastener and explains the reduced effectiveness of the Mode II suppression for the countersunk fasteners.

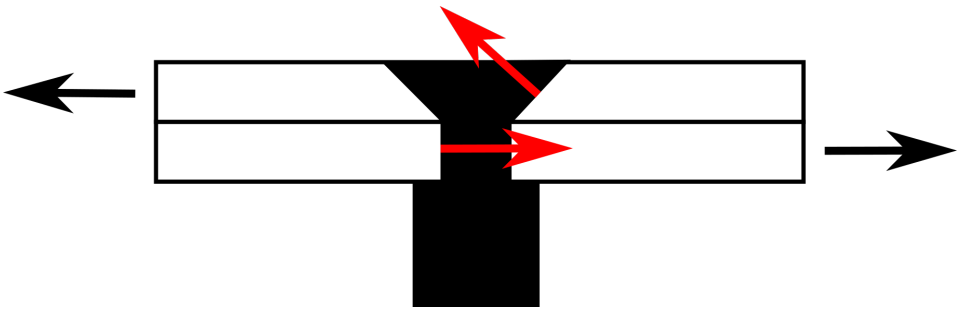

Figure 5.13: *The applied load (in black) is transferred through the diagonal section of the fastener head. The diagonal section redirects the load transfer (in red), causing the fastener head to rotate*

6

Conclusions

The research objective of this thesis is to achieve an improved understanding of what features and properties of a mechanical fastener are of interest in designing a fastener purpose-designed as a disbond arrest feature. This was done by means of a sensitivity study in a 3D FEM model. Such a model has been developed, verified and validated, the conclusions are found in section 6.1. Following this, a sensitivity study has been conducted, allowing for an improved understanding of what features of a fastener are of interest, the conclusions of which can be found in section 6.2.

6.1. Model accuracy

The model has been shown to be accurate enough for the intended purposes. When no obvious errors occurred, such as those described in section 5.1, the results were consistent and insensitive to mesh or time step settings. Some systematic errors were present and were taken into consideration in the sensitivity study when necessary.

Tests were also done to verify that the model did not grossly misrepresent reality and to confirm the assumptions made did not invalidate the results. Furthermore, the results corresponded to observations made in other research. The biggest difference was the disbond front shape which had previously been observed to warp around the fastener, a behaviour that was not observed in the experiments of this thesis. In other ways the model did mirror experimental results. Especially considering how sensitive the specimen is and how many factors influenced the results results were considered appropriately accurate.

Lastly, the question may be asked if the direct cyclic analysis with VCCT in a 3D FEM model should be used. The model predicts heightened SERRs at nodes that stick out of the disbond front, resulting in too large disbond growth rate predictions. Another effect of this is that the disbond front remains very straight, a well known behaviour of VCCT. This may be solved by using CZM instead of VCCT as this method does not include the step stiffness but a smoother transition for each element.

6.2. Results of the sensitivity study

Firstly, a number of conclusions from previous research can be confirmed with this new model. Both the increase of the Mode II SERR ahead of the fastener and the rapid suppression of the Mode I SERR have been clearly shown.

The conclusion that two fasteners may be required to completely suppress the disbond growth has also been re-affirmed. The Mode II SERR showed an almost linear decrease behind the fastener which levels out further beyond the fastener. Considering the nature of the Paris' relation this effect might be considered strong enough to completely arrest the disbond growth as the model showed a halving of the SERR as the disbond front reached 5 [mm] behind the fastener location. This matches previous research which found a minimum non-zero Mode II SERR further behind the fastener[24].

The different experiments of the sensitivity study have been compared based on average SERR as a function of disbond length. Few differences were recorded between different fastener material stiffness, shaft radius and head radius. This was especially true for the Mode I SERR, a logical result of the force causing this opening mode being rather low compared to the fastener stiffness along the appropriate axis. This was so much so that the fastener may be considered a rigid body for the Mode I loading.

The Mode II SERR proved most dependant on the fastener head geometry, countersunk fasteners performed worse compared to the non-countersunk samples. This may not have a large effect in practice as these differences only start to occur when the SERR has already been significantly reduced, ensuring the disbond growth rate is already quite limited. This does not mean countersunk fasteners are not suitable as DAFs, especially as experimental results show the countersunk fasteners perform better due to reduced cracking of the adherends[23]. This does not contradict each other; the countersunk fastener carries less load, as a result of which the adherend does not suffer as much from fatigue.

These differences only start to occur when the countersunk section of the fastener covers a large part of the thickness of the specimen. This also explains why these differences are not mentioned by Huth[1]: in these experiments the plates were relatively thick. This more closely resembles the "half countersunk" fasteners, which indeed showed no difference with their non-countersunk counterparts. During the experiments differences in the fastener and adherend rotation have also been recorded. These rotations clearly show the shaft and adherend interact differently based on the shaft being angled or regular.

Generally, it has been shown that in thin specimen the disbond growth behaviour far away from the fastener is insensitive to fastener design. This allows for designing fasteners specifically for reducing the cracking of the adherends, which appears to be a primary feature of DAF in bonded Glare[23].

7

Recommendations

Based on the observations made in this research several recommendations can be made. These are split into three groups: verification of the results, improvement of the model and possible future experiments.

Firstly, the result can be further verified. This may be done using CZM to model the same experiments. The results are expected to be different as CZM does not have the same limitations as VCCT with regards to curved crack fronts. This should result in a closer match between the model and the validation data. The general trends and conclusions should still stay the same.

The model may be improved in a number of ways. It may be possible to implement symmetry boundary conditions along the centre plane which would drastically reduce run time. An attempt to do so has been made in this research but has been rejected due to failure of the model to converge past the static loading step. This is thought to be caused by the VCCT and the boundary condition interacting with each other.

Another possible improvement to the model would be to add an extra "through thickness" section as shown in figure 7.1. This would allow the bonding to be modelled closer to the fastener hole also allowing the behaviour near the DAF to be analysed.

Furthermore, to more accurately approach the expected disbond fronts the mesh may need to be altered. This might be done with a mesh similar to the one shown in figure 7.2. This does come with complications as VCCT requires the elements ahead of the disbond front to have the same dimensions as those behind the disbond front[102].

It has also been observed that the conclusions regarding the fastener head may vary from reality.

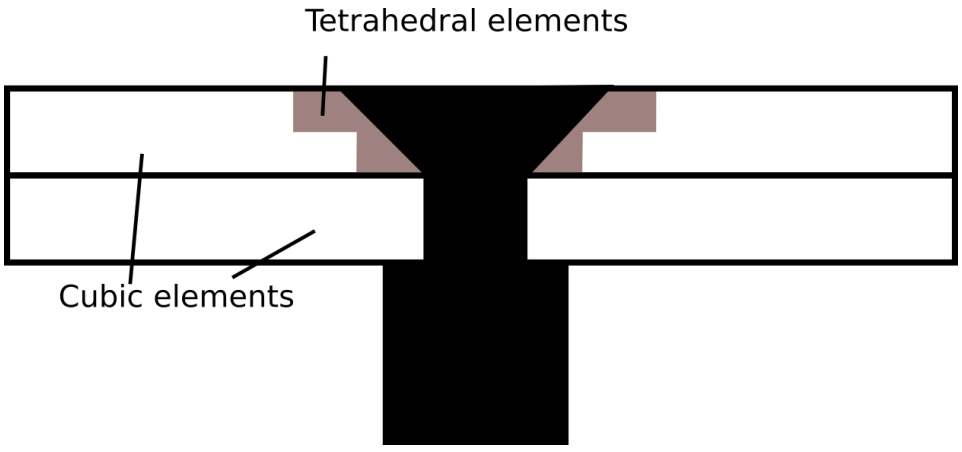

Figure 7.1: *Sectioning the area may allow for the bonded area to be modelled closer to the hole*

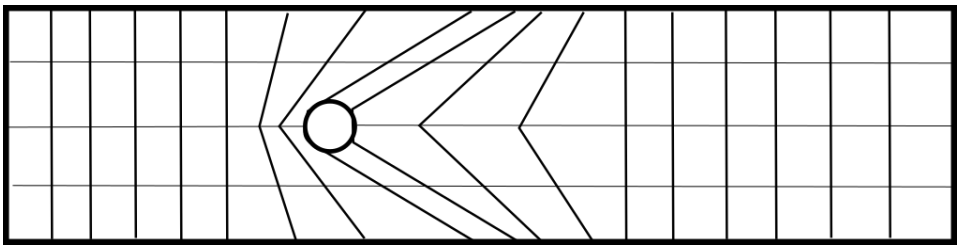

Figure 7.2: *A possible solution to fix the disbond shape predicted by VCCT could be to align the mesh with the expected disbond growth*

Zavatta[23] for instance found non countersunk fasteners resulted in higher disbond growth rates, caused by cracking of the adherend. It has also been observed that cracking in the aluminium plies occurs before full disbond arrest is achieved, Zavatta suggests this may even be a "distinctive feature of disbond arrest in bonded GLARE". This may be need to be taken into account in future work.

Furthermore, the fastener was modelled with zero clearance. It has already been shown that clearance has a significant effect on DAF effectiveness. It is expected the disbond growth characteristics remain non effected by fastener geometry, but this assumption will have to be verified.

Lastly, it may be necessary to use quasi-static loading instead of a fatigue load in order to analyse the behaviour near the fastener. This circumvents some of the damage extrapolation issues encountered with the direct cyclic approach and is considerable faster. If this is used, VCCT linear scaling should not be enabled as it causes the analysis to fail to converge. A tolerance for unstable crack propagation should be enabled and set to a relatively low value to allow the model to converge past the region near the fastener where unstable crack growth might occur.

With some questions regarding fastener design answered, it should be possible to further analyse joint design. Questions regarding allowed spacing, required number of rows and whether rows should be staggered or in-line remain. These may be answered by extending existing models.

Bibliography

[1] H. Huth, "Influence of fastener flexibility on the prediction of load transfer and fatigue life for multiple-row joints," in *Fatigue in mechanically fastened composite and metallic joints*, ASTM International, 1986.

[2] D. Bürger, *Mixed-Mode Fatigue Disbond on Metallic Bonded Joints*. PhD thesis, Delft University of Technology, 2015.

[3] R. Boyer, *Materials properties handbook: titanium alloys*. ASM Internat., 1994.

[4] *ASM handbook. Properties and selection: nonferrous alloys and special-purpose materials*. ASM, 1990.

[5] C. Y. Ho, J. M. Holt, and H. Mindlin, *Structural alloys handbook: 1996 Edition; incorporating supplements throught 1995*. Cindas/Purdue Univ., 1997.

[6] M. Bauccio *et al.*, *ASM metals reference book*. ASM international, 1993.

[7] J. Adams *et al.*, *ASM metals handbook Vol. 2: Properties and selection: Nonferrous alloys and special-purpose materials*. 1990.

[8] H. E. Boyer and E. Timothy L. Gall, *Metals Handbook*. 1985.

[9] J. M. Holt, "Handbook, structural alloys edition," *CINDAS/Purdue University, West Lafayette, IN*, 1996.

[10] A. Documentation and U. Manual, "Version 6.14," *Dassault systemes*, 2014.

[11] R. Slayton and G. Spinardi, "Radical innovation in scaling up: Boeing's dreamliner and the challenge of socio-technical transitions," *Technovation*, vol. 47, 09 2015.

[12] "Hexcel ready to fly on the a350 xwb," *Reinforced Plastics*, vol. 57, no. 3, pp. 25 – 26, 2013.

[13] J. Ekh, *Multi-Fastener Single-lap Joints in Composite Structures*. PhD thesis, KTH, School of Engineering Sciences (SCI), 2006.

[14] T. Kruse, T. Körwien, S. Heckner, and M. Geistbeck, "Bonding of CFRP primary aerospace structures - Crack stopping in composite bonded joints under fatigue," *ICCM International Conferences on Composite Materials*, vol. 2015-July, no. July, pp. 19–24, 2015.

[15] S. Stelzer, S. Ucsnik, and G. Pinter, "Strength and damage tolerance of composite-composite joints with steel and titanium through the thickness reinforcements," *Composites Part A: Applied Science and Manufacturing*, vol. 88, pp. 39–47, 2016.

[16] Temiz, S. Akpinar, M. Aydın, and E. Sancaktar, "Increasing single-lap joint strength by adherend curvature-induced residual stresses," *Journal of Adhesion Science and Technology*, vol. 27, no. 3, pp. 244–251, 2013.

[17] Q. Zeng and C. Sun, "Fatigue performance of a bonded wavy composite lap joint," *Fatigue & Fracture of Engineering Materials & Structures*, vol. 27, no. 5, pp. 413–422, 2004.

[18] S. Minakuchi, "Fiber-reinforcement-based crack arrester for composite bonded joints," in *Proceedings of The 20th International Conference on Composite Materials*, pp. 2118–4, 2015.

[19] U. Turaga and C. Sun, "Improved design for metallic and composite single-lap joints," *Journal of Aircraft*, vol. 45, no. 2, pp. 440–447, 2008.

[20] I. van Teeseling, "Towards the certification of bonded primary fiber metal laminate structures by bolted disbond arrest features," Master's thesis, Delft University of Technology, 2019.

[21] L. Richard and K. Y. Lin, "Analytical and experimental studies on delamination arrest in bolted-bonded composite structures," *58th AIAA/ASCE/AHS/ASC Structures, Structural Dynamics, and Materials Conference, 2017*, no. January, pp. 1–12, 2017.

[22] R. Hangx, "Disbond arrest in fibre metal laminates," Master's thesis, Delft University of Technology, 2017.

[23] N. Zavatta, *Crack growth in adhesively bonded joints under quasi-static and fatigue loading*. PhD thesis, Alma Mater Studiorum - Università di Bologna, April 2020.

[24] L. I. Richard and K. Lin, "Analytical and experimental studies on delamination arrest features in aircraft composite structures," in *56th AIAA/ASCE/AHS/ASC Structures, Structural Dynamics, and Materials Conference*, p. 2066, 2015.

[25] M. L. Benzeggagh and M. Kenane, "Measurement of mixed-mode delamination fracture toughness of unidirectional glass/epoxy composites with mixed-mode bending apparatus," *Composites science and technology*, vol. 56, no. 4, pp. 439–449, 1996.

[26] R. Alderliesten, "Damage tolerance of bonded aircraft structures," *International Journal of Fatigue*, vol. 31, no. 6, pp. 1024 – 1030, 2009. Damage Tolerance of Aircraft Structures.

[27] I. Floros and K. Tserpes, "Numerical simulation of quasi-static and fatigue debonding growth in adhesively bonded composite joints containing bolts as crack stoppers," *The Journal of Adhesion*, vol. 0, no. 0, pp. 1–23, 2019.

[28] I. Floros and K. Tserpes, "Fatigue crack growth characterization in adhesive cfrp joints," *Composite Structures*, vol. 207, pp. 531 – 536, 2019.

[29] E. C. CORDIS, "Boltless assembling of primary aerospace composite structures," 2016. cordis.europa.eu/project/id/314180/reporting.

[30] C. R. Nathan van 't Hof, "Project_results," February 2021.

[31] N. Cossons and B. S. Trinder, *The iron bridge: Symbol of the Industrial Revolution*. Phillimore, 2002.

[32] U.S. Department of Transportation Federal Aviation Administration (FAA), "Advisory circular - composite aircraft structure. ac 20-107b, - composite aircraft structure," 2009. www.faa.gov/regulations_policies/advisory_circulars/index.cfm/go/document.information/documentID/99693.

[33] C. H. E. Cheung, *Delamination arrestment in bonded-bolted composite structures by fasteners*. PhD thesis, University of Washington, 2016.

[34] C. H. Cheung and K. Y. Lin, "Numerical analysis of fastener delamination/disbond arrest mechanism in aircraft composite structures," *Journal of Aircraft*, vol. 49, no. 2, pp. 630–635, 2012.

[35] L. R. K.Y. Lin and C. Cheung, "Delamination/disbond arrest features in aircraft composite structures," *Ed. William E. Boeing, Department of Aeronautics and Astronautics, Seattle, WA*, vol. 98195, 2014.

[36] L. I. Richard, “Experimental and analytical study of delamination arrest by multiple fasteners in composite structures,” Master’s thesis, University of Washington, 2013.

[37] T. Kruse, T. Körwien, and R. Ruzek, “Fatigue behaviour and damage tolerant design of composite bonded joints for aerospace application,” *ECCM 2016 - Proceeding of the 17th European Conference on Composite Materials*, no. June, pp. 26–30, 2016.

[38] I. S. Floros, K. I. Tserpes, and T. L"obel, “Mode-I, mode-II and mixed-mode I+II fracture behavior of composite bonded joints: Experimental characterization and numerical simulation,” *Composites Part B: Engineering*, vol. 78, pp. 459–468, 2015.

[39] R. Sachse, A. K. Pickett, M. Käß, and P. Middendorf, “Numerical Simulation of Fatigue Crack Growth in the Adhesive Bondline of Hybrid CFRP Joints,” 2015.

[40] R. Sachse, A. Pickett, W. Adebahr, M. Klein, M. Käß, and P. Middendorf, “Experimental investigation of mechanical fasteners regarding their influence on crack growth in adhesively bonded crfp-joints subjected to fatigue loading,” in *20th International Conference on Composite Materials, ICCM20*, 2015.

[41] C. H. E. Cheung and K. Y. Lin, “Reliability of damage tolerance composite structure using fasteners as disbond arrest mechanism,” *Collection of Technical Papers - AIAA/ASME/ASCE/AHS/ASC Structures, Structural Dynamics and Materials Conference*, no. May, 2009.

[42] P. M. Gray, “Experimental and analytical study of mode ii interlaminar failure of bolted and bonded composite structures,” Master’s thesis, 2012.

[43] K. Y. Lin, L. Richard, and W. Liu, “Delamination arrest fasteners in aircraft composite structures,” *ICCM International Conferences on Composite Materials*, vol. 2013-July, pp. 1577–1580, 2013.

[44] L. Richard and K. Lin, “Arrest Features in Aircraft Composite Structures ” JAMS Technical Review,” no. January, pp. 1–10, 2016.

[45] L. I. Richard and K. Y. Lin, “Delamination arrest features in aircraft composite structures under static and fatigue loading,” *ICCM International Conferences on Composite Materials*, vol. 2017-Augus, 2017.

[46] L. I. Richard and K. Y. Lin, “Delamination arrest by fasteners in aircraft structures under static and fatigue loading,” in *2018 AIAA/ASCE/AHS/ASC Structures, Structural Dynamics, and Materials Conference*, p. 2246, 2018.

[47] B. Kim, S. Park, and D. Lee, “Fracture toughness of the nano-particle reinforced epoxy composite,” *Composite Structures*, vol. 86, no. 1-3, pp. 69–77, 2008.

[48] “Enhancement of fracture toughness of carbon fiber laminated composites using multi wall carbon nanotubes,” *Carbon*, vol. 79, no. 1, pp. 413–423, 2014.

[49] V. Mirjalili and P. Hubert, “Effect of carbon nanotube dispersion on the fracture toughness of polymers,” 2009.

[50] V. Mirjalili, M. Yourdkhani, and P. Hubert, “Dispersion stability in carbon nanotube modified polymers and its effect on the fracture toughness,” *Nanotechnology*, vol. 23, no. 31, 2012.

[51] A. Manta and K. Tserpes, “Parametric numerical simulation of impact response of carbon nanotube/polymer nanocomposites,” *Plastics, Rubber and Composites*, vol. 45, no. 4, pp. 157–165, 2016.

[52] Y. Liu, Y. Zhao, B. Sun, and C. Chen, "Understanding the toxicity of carbon nanotubes," *Accounts of chemical research*, vol. 46, no. 3, pp. 702–713, 2013.

[53] M. Ellenbecker, S. Tsai, M. Jacobs, M. Riediker, T. Peters, S. Liou, A. Avila, and S. FossHansen, "The difficulties in establishing an occupational exposure limit for carbon nanotubes," *Journal of Nanoparticle Research*, vol. 20, no. 5, p. 131, 2018.

[54] E. Koricho, A. Khomenko, and M. Haq, "Fatigue behavior of glass-bubbles modified adhesively bonded composite joints," No. VOLUME 5, pp. 181–187, 2015.

[55] A. Erkliğ, M. V. ÇAKIR, and Ö. Y. Bozkurt, "Nano clay additive effect on shear strength of gfrp joints," *Sakarya Üniversitesi Fen Bilimleri Enstitüsü Dergisi*, vol. 23, no. 6, pp. 1115–1122, 2019.

[56] S. M. R. Khalili, M. Tavakolian, and A. Sarabi, "Mechanical properties of nanoclay reinforced epoxy adhesive bonded joints made with composite materials," *Journal of Adhesion Science and Technology*, vol. 24, no. 11-12, pp. 1917–1928, 2010.

[57] Q. Meng, C. H. Wang, N. Saber, H.-C. Kuan, J. Dai, K. Friedrich, and J. Ma, "Nanosilica-toughened polymer adhesives," *Materials & Design*, vol. 61, pp. 75–86, 2014.

[58] T. Löbel, D. Holzhüter, and C. Hühne, "Disbond-stopping concepts for bonded composite joints," vol. 2016-January, 2016.

[59] T. Löbel, D. Holzhüter, M. Sinapius, and C. Hühne, "A hybrid bondline concept for bonded composite joints," *International Journal of Adhesion and Adhesives*, vol. 68, pp. 229–238, 2016.

[60] D. D. Cartié, J. M. Laffaille, I. K. Partridge, and A. J. Brunner, "Fatigue delamination behaviour of unidirectional carbon fibre/epoxy laminates reinforced by Z-Fiber® pinning," *Engineering Fracture Mechanics*, vol. 76, no. 18, pp. 2834–2845, 2009.

[61] R. Maurin, C. Baley, D. D. Cartié, and P. Davies, "Influence of through-thickness pinning on composite shear properties," *Applied Composite Materials*, vol. 19, no. 6, pp. 853–864, 2012.

[62] D. D. Cartié, G. Dell'Anno, E. Poulin, and I. K. Partridge, "3d reinforcement of stiffener-to-skin t-joints by z-pinning and tufting," *Engineering Fracture Mechanics*, vol. 73, no. 16, pp. 2532 – 2540, 2006. Fracture of Polymers, Composites and Adhesives.

[63] K. Pingkarawat and A. P. Mouritz, "Improving the mode I delamination fatigue resistance of composites using z-pins," *Composites Science and Technology*, vol. 92, pp. 70–76, 2014.

[64] J. Bartley-Cho and W. Nickerson, "Overview and status of "composite joints with inherent disbond arrest capability (cojac)" program," vol. 2019-May, 2019.

[65] S. Razavi, E. Esmaeili, M. Samari, and S. Razavi, "Stress analysis on a non-flat zigzag interface bonded joint," *The Journal of Adhesion*, vol. 94, no. 3, pp. 199–217, 2018.

[66] U. Turaga and C. Sun, "An investigation of adhesive single-lap joints with attachments," in *44th AIAA/ASME/ASCE/AHS/ASC Structures, Structural Dynamics, and Materials Conference*, p. 1957, 2003.

[67] L. Hart-Smith, "Adhesive-bonded double-lap joints. nasa cr-112235," *National Aeronautics and Space Administration*, 1973.

[68] L. Hart-Smith, "Design methodology for bonded-bolted composite joints. volume i. analysis derivations and illustrative solutions," tech. rep., Douglas Aircraft Company, McDonnell Douglas Corporation, 1982.

[69] L. J. Hart-Smith, "Bonded-bolted composite joints," *Journal of Aircraft*, vol. 22, no. 11, pp. 993–1000, 1985.

[70] G. Kelly, "Quasi-static strength and fatigue life of hybrid (bonded/bolted composite single-lap joints," *Journal of Composite Structures*, vol. 72, pp. 119–129, 2006.

[71] A. Barut and E. Madenci, "Analysis of bolted-bonded composite single-lap joints under combined in-plane and transverse loading," *Composite Structures*, vol. 88, no. 4, pp. 579–594, 2009.

[72] F. Esmaeili, M. Zehsaz, and T. N. Chakherlou, "Experimental investigations on the effects of torque tightening on the fatigue strength of double-lap simple bolted and hybrid (Bolted/Bonded) joints," *Strain*, vol. 50, no. 4, pp. 347–354, 2014.

[73] M. Samaei, M. Zehsaz, and T. Chakherlou, "Experimental and numerical study of fatigue crack growth of aluminium alloy 2024-T3 single lap simple bolted and hybrid (adhesive/bolted) joints," *Engineering Failure Analysis*, vol. 59, pp. 253–268, 2016.

[74] M. Mariam, M. Afendi, M. A. Majid, and M. Ridzuan, "Experimental study on the fatigue strength of bonded/bolted metal-fibre," in *AIP Conference Proceedings*, vol. 2030, p. 020040, AIP Publishing, 2018.

[75] G. Kelly, "Load transfer in hybrid (bonded/bolted) composite single-lap joints," *Composite Structures*, vol. 69, no. 1, pp. 35–43, 2005.

[76] M. El Zaroug, F. Kadioglu, M. Demiral, and D. Saad, "Experimental and numerical investigation into strength of bolted, bonded and hybrid single lap joints: Effects of adherend material type and thickness," *International Journal of Adhesion and Adhesives*, vol. 87, pp. 130–141, October 2018.

[77] K. P. Raju, K. Bodjona, G. H. Lim, and L. Lessard, "Improving load sharing in hybrid bonded/bolted composite joints using an interference-fit bolt," *Composite Structures*, 2016.

[78] K. Bodjona, K. Raju, G.-H. Lim, and L. Lessard, "Load sharing in single-lap bonded/bolted composite joints. part i: Model development and validation," *Composite Structures*, vol. 129, pp. 268–275, 2015.

[79] C.-T. Hoang-Ngoc and E. Paroissien, "Simulation of single-lap bonded and hybrid (bolted/bonded) joints with flexible adhesive," *International Journal of Adhesion and Adhesives*, vol. 30, no. 3, pp. 117–129, 2010.

[80] C. Bois, H. Wargnier, J.-C. Wahl, and E. Le Goff, "An analytical model for the strength prediction of hybrid (bolted/bonded) composite joints," *Composite Structures*, vol. 97, pp. 252–260, 2013.

[81] T. N. Chakherlou, M. Zehsaz, and M. Samaei, "Experimental Investigation of the Effects of Clamping Force on the Fatigue Life and Fatigue Crack Growth of Single Lap Simple Bolted and Hybrid (Bolted/Adhesive) Joints," *Transactions of the Indian Institute of Metals*, vol. 69, no. 7, pp. 1335–1341, 2016.

[82] G. Di Franco and B. Zuccarello, "Analysis and optimization of hybrid double lap aluminum-GFRP joints," *Composite Structures*, vol. 116, no. 1, pp. 682–693, 2014.

[83] F. Esmaeili, T. N. Chakherlou, and M. Zehsaz, "Investigation of bolt clamping force on the fatigue life of double lap simple bolted and hybrid (bolted/bonded) joints via experimental and numerical analysis," *Engineering Failure Analysis*, vol. 45, pp. 406–420, 2014.

[84] F. Caputo, G. Lamanna, and A. Soprano, "Effects of tolerances on the structural behavior of a bolted hybrid joint," in *Key Engineering Materials*, vol. 488, pp. 565–568, Trans Tech Publ, 2012.

[85] T. Ireman, T. Ranvik, and I. Eriksson, "On damage development in mechanically fastened composite laminates," *Composite Structures*, vol. 49, no. 2, pp. 151 – 171, 2000.

[86] P. Mallick and M. Fu, "Fatigue of hybrid(adhesive/bolted) joints in srim composites," *International Journal of Adhesion and Adhesives(UK)*, vol. 21, no. 2, pp. 145–159, 2001.

[87] Z. Emami Geiglou and T. N. Chakherlou, "Numerical and experimental investigation of the effect of the cold expansion process on the fatigue behavior of hybrid (bonded-bolted)double shear lap aluminum joints," *International Journal of Fatigue*, vol. 126, no. April, pp. 30–43, 2019.

[88] C. H. E. Cheung, P. Gray, and K. Y. Lin, "Design and optimization of an axial mode ii crack arrest specimen," in *53rd AIAA/ASME/ASCE/AHS/ASC Structures, Structural Dynamics and Materials Conference 20th AIAA/ASME/AHS Adaptive Structures Conference 14th AIAA*, p. 1892, 2012.

[89] M. Heidari-Rarani and M. Sayedain, "Finite element modeling strategies for 2d and 3d delamination propagation in composite dcb specimens using vcct, czm and xfem approaches," *Theoretical and Applied Fracture Mechanics*, vol. 103, p. 102246, 2019.

[90] L. I. Richard, *Delamination arrest features in aircraft composite structures under static and fatigue loading*. PhD thesis, University of Washington, 2017.

[91] R. L. Hendrickson, "Numerical evaluation of energy release rate at material interfaces for fatigue life predictions," Master's thesis, Utah State University, 2018.

[92] G. R. Irwin, "Analysis of stresses and strains near the end of a crack transversing a plate," *Trans. ASME, Ser. E, J. Appl. Mech.*, vol. 24, pp. 361–364, 1957.

[93] R. Krueger, "Virtual crack closure technique: history, approach, and applications," *Appl. Mech. Rev.*, vol. 57, no. 2, pp. 109–143, 2004.

[94] I. Raju and T. O'brien, "Fracture mechanics concepts, stress fields, strain energy release rates, delamination initiation and growth criteria," in *Delamination behaviour of composites*, pp. 3–27, Elsevier, 2008.

[95] A. Gliszczynski, S. Samborski, N. Wiacek, and J. Rzeczkowski, "Mode i interlaminar fracture of glass/epoxy unidirectional laminates. part ii: Numerical analysis," *Materials*, vol. 12, no. 10, p. 1604, 2019.

[96] A. W. Paris P, Gomez M, "A rational analytic theory of fatigue," *The trend in engineering*, vol. 13, pp. 9–14, 1961.

[97] P. Paris and F. Erdogan, "A critical analysis of crack propagation laws," *Basic engineering*, pp. 528–533, 1963.

[98] P. P, "The fracture mechanics approach to fatigue.," *Sagamore army materials research conference Syracuse University Press*, vol. 10, pp. 107–32, 1967.

[99] J. Jokinen, M. Kanerva, M. Wallin, and O. Saarela, "The simulation of a double cantilever beam test using the virtual crack closure technique with the cohesive zone modelling," *International Journal of Adhesion and Adhesives*, vol. 88, pp. 50 – 58, 2019.

[100] G. Mabson, "Fracture interface elements," 2003.

[101] I. Guiamatsia, J. Ankersen, G. Davies, and L. Iannucci, "Decohesion finite element with enriched basis functions for delamination," *Composites Science and Technology*, vol. 69, no. 15-16, pp. 2616–2624, 2009.

[102] K. Y. Lin, L. Richard, and C. H. E. Cheung, "Delamination/disbond arrest features in aircraft composite structures," tech. rep., Jun 2018. www.tc.faa.gov/its/worldpac/techrpt/tc18-5.pdf.

[103] A. Pirondi, G. Giuliese, F. Moroni, A. Bernasconi, and A. Jamil, "Comparative study of cohesive zone and virtual crack closure techniques for three-dimensional fatigue debonding," *Journal of Adhesion*, vol. 90, 03 2014.

[104] E. Smeets, "Development of a fatigue analysis tool using cohesive zone modelling for composite specimens," Master's thesis, Delft University of Technology, 2019. resolver.tudelft.nl/uuid:ac18b7c8-8769-4c21-837c-edde62a4b3da.

[105] R. D. Campilho, M. D. Banea, J. Neto, and L. F. da Silva, "Modelling adhesive joints with cohesive zone models: effect of the cohesive law shape of the adhesive layer," *International journal of adhesion and adhesives*, vol. 44, pp. 48–56, 2013.

[106] A. Turon, P. P. Camanho, J. Costa, and C. Dávila, "A damage model for the simulation of delamination in advanced composites under variable-mode loading," *Mechanics of materials*, vol. 38, no. 11, pp. 1072–1089, 2006.

[107] K. Tserpes and I. Floros, "Fatigue crack growth simulation in adhesively bonded composite joints," *Fatigue & Fracture of Engineering Materials & Structures*, vol. 42, no. 7, pp. 1430–1440, 2019.

[108] A. Turon, J. Costa, P. Camanho, and C. Dávila, "Simulation of delamination in composites under high-cycle fatigue," *Composites Part A: Applied Science and Manufacturing*, vol. 38, no. 11, pp. 2270 – 2282, 2007.

[109] P. W. Harper and S. R. Hallett, "A fatigue degradation law for cohesive interface elements–development and application to composite materials," *International Journal of Fatigue*, vol. 32, no. 11, pp. 1774–1787, 2010.

[110] F. Moroni and A. Pirondi, "A procedure for the simulation of fatigue crack growth in adhesively bonded joints based on the cohesive zone model and different mixed-mode propagation criteria," *Engineering Fracture Mechanics*, vol. 78, no. 8, pp. 1808–1816, 2011.

[111] L. F. Kawashita and S. R. Hallett, "A crack tip tracking algorithm for cohesive interface element analysis of fatigue delamination propagation in composite materials," *International Journal of Solids and Structures*, vol. 49, no. 21, pp. 2898–2913, 2012.

[112] T. Belytschko and T. Black, "Elastic crack growth in finite elements with minimal remeshing," *International journal for numerical methods in engineering*, vol. 45, no. 5, pp. 601–620, 1999.

[113] J. A. Pascoe, R. C. Alderliesten, and R. Benedictus, "Methods for the prediction of fatigue delamination growth in composites and adhesive bonds–a critical review," *Engineering Fracture Mechanics*, vol. 112, pp. 72–96, 2013.

[114] M. v. T. René Alderliesten, S. van der Zwaag, *Fatigue Crack Propagation and Delamination Growth in Glare*. PhD thesis, Delft University of Technology, 2005.

[115] "Hi-lok™fasteners (hi lok™)." jet-tek.com/product-specialties/hi-lok-fasteners-hi-lok/ Retrieved 29 October 2020.

[116] I. van Teeseling, "Tudelft$_m sc_t hesis_i vt$," 2018.

[117] Y.-H. Lai, M. D. Rakestraw, and D. A. Dillard, "The cracked lap shear specimen revisited—a closed form solution," *International Journal of Solids and Structures*, vol. 33, no. 12, pp. 1725–1743, 1996.

[118] G. Fernlund and J. Spelt, "Failure load prediction of structural adhesive joints: Part 1: Analytical method," *International Journal of Adhesion and Adhesives*, vol. 11, no. 4, pp. 213–220, 1991.

[119] A. E647-00, "Standard test method for measurement of fatigue crack growth rates," 2004.

[120] B. Egan, C. McCarthy, M. McCarthy, and R. Frizzell, "Stress analysis of single-bolt, single-lap, countersunk composite joints with variable bolt-hole clearance," *Composite Structures*, vol. 94, no. 3, pp. 1038 – 1051, 2012.

[121] A. Turon, P. Camanho, J. Costa, and C. Dávila, "A damage model for the simulation of delamination in advanced composites under variable-mode loading," *Mechanics of Materials*, vol. 38, pp. 1072–1089, 11 2006.

[122] E. Bruun, C. H. Cheung, P. Gray, and K. Y. Lin, "Design and experimental validation of a mixed-mode crack arrest specimen," in *53rd AIAA/ASME/ASCE/AHS/ASC Structures, Structural Dynamics and Materials Conference 20th AIAA/ASME/AHS Adaptive Structures Conference 14th AIAA*, p. 1696, 2012.

A

Comparing VCCT to CZM

In modelling hybrid joints two methods are used in to analyse the disbond growth in fatigue: VCCT and CZM. In choosing what method to use to model the disbond growth in hybrid joints a comparison was done which consisted out of a literature study, described in section A.1, and a comparison study , which can be found in section A.2

A.1. Comparing VCCT to CZM

VCCT and CZM are both analysis methods which can be used to model disbond growth in fatigue. The exact workings of which are described in the literature review 2.4. When choosing which method to use a number of points are of importance. Firstly is the question of accuracy and computational time. In the next sections these will be compared more in depth.

Another question is the difficulty to implement. Currently Abaqus does not have a ready made implementation to model fatigue using CZM. Different user defined subroutines are implemented by several authors in order to incorporate fatigue behaviour into the cohesive zone model[104]. In contrast to this, modelling fatigue using VCCT fracture criterion has already been implemented in Abaqus.

Another difference between the two methods is the complexity. VCCT is a relatively straightforward method, which makes it attractive to use[99]. In practice it only requires two constants to implement the Paris relation, these constants are available for the FM94 adhesive. This means modelling with VCCT can be done using material data alone without any estimated or guessed parameters. CZM on the other hand allows for a large number of parameters to be altered. The shape of the TSL can be changed almost infinitely[22], although most commonly the bi-linear TSL from[121] is used[104]. Furthermore, the number of elements across the width of the processing zone needs to be about 3 to 5[104]. Some researchers also implement a fatigue parameter that adds yet another degree of freedom[27]. This means the CZM will almost definitely require some form of calibration. An effect of this is that the final result of validation might not prove the model to be accurate as it might be the result of a curve fitting exercise.

Another important feature to consider is that VCCT allows the different crack opening modes to be compared. This is not possible using CZM[99]. This can be especially important when analysing the behaviour of the joint. When trying to predict fatigue life this feature becomes much less meaningful.

In other aspects CZM outperforms VCCT. One example of this is the improved possibilities to predict crack nucleation which for VCCT is implemented in Abaqus using an adjusted Paris relation[10]. Using CZM stress concentrations are used to predict fracture[99]. In this project the time to crack nucleation is not considered and so this feature is not taken into consideration.

Furthermore, VCCT uses a step stiffness which can result in large differences in crack growth

when the SERR is dependent on the disbonded area. In contrast, CZM the bond state defines the stiffness of the cell, possibly allowing for courser meshes. On option to partially remove this error is to compare crack growth rate to crack length rather than number of cycles.

Another issue is that VCCT follows mesh lines, resulting in straight disbond fronts even when curved disbond fronts are expected. CZM does not face these issues and can thus more closely match the validation data. As the mechanically fastened DAFs are known to result in strongly curved disbond fronts, this may be an important feature to consider.

A.2. Comparison study

To compare computational time between VCCT and CZM it was decided to do a comparative study on a MMB specimen. This was chosen as an analytical solution exists for the SERR[119]. This allows for the development of an analytical model which can be used to evaluate the accuracy of the FEM models.

The specimen consists out of two plates connected to a loader, as shown in figure A.1. For the adhesive the same material properties are taken as those for the SLS model. The adherends are modelled as aluminium with a Young's modulus of 73.1 [GPa]. The test was conducted at a displacement of 10 [mm] and load ratio of 0.1. Only the first 10 [mm] of disbond growth were analysed.

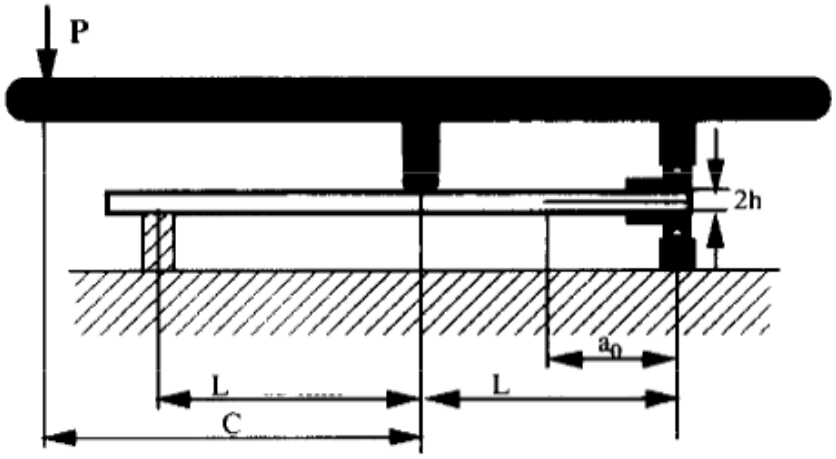

Figure A.1: *Setup of the MMB test, adjusted from[25]*

A.2.1. FEM model

Two models were used for comparison. The CZM model[1]. The VCCT model consists out of three components: two adherends and a loader, and is very similar to the model used to analyse the hybrid joints.

Both the adherends were created using 3D extrusions. The loader was modelled using a discrete rigid body. At the tip the loader and top adherend are connected using a tie constraint while at the centre a normal interaction is used. The tie constraint only works for course enough meshes as the

[1] Implemented by Eva Smeets, based on the work from Turon et al[108]

it tends to be applied to multiple rows of nodes when finer meshes are used. This causes the loading to be altered.

The bottom adherend is pin constrained at both ends, with one end allowed to move horizontally. The adherends are extended slightly beyond the constrained nodes, as shown in figure A.2. This is done to improve convergence.

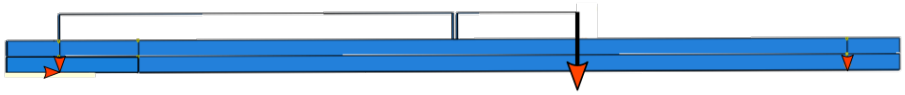

Figure A.2: *Boundary conditions are applied to allow the nodes to move horizontally. The specimen is extended beyond the constrained nodes to aid convergence, the vertical displacement of the loader is applied using a boundary constraint*

The same VCCT criterion is used as the one the hybrid joint. The disbond growth rate is also computed using the same interpolation method used for the hybrid joint, as described in section 3.3. The only difference is that the number of points used for interpolation is reduced from seven to five. This was done to allow for a larger number of measurements in the courser meshes, which otherwise would result in one or two data points only.

The CZM model used cohesive elements to model the disbond growth. The load introduction was done using coupling constraints.

A.2.2. Analytical model

An analytical solution to compute the SERR is available[119]. As the specimen was set up for the driving force to be pure Mode II, the Paris relation[97] can be directly used to compute the disbond growth rate.

Firstly the force required to reach a given displacement is computed using equation A.1.

$$P = \sqrt{\frac{\frac{4}{3}G_c b^2 E_{11} h^3 L^2}{(3c-l)^2(a+h\chi)^2) + \frac{3}{4}(a+0.42h\chi)^2}} \tag{A.1}$$

Using this the SERR is calculated using equations A.2[2] and A.3. Because L is three times C the specimen is under pure Mode II loading. Here χ is computed using equation A.4, with Γ as defined in equation A.5.

$$G_I = \frac{12P^2(3C-L)^2}{16b^2h^3E_{1f}}(a+\chi h)^2 \tag{A.2}$$

$$G_{II} = \frac{9P^2(C+L)^2}{16b^2h^3E_{1f}}(a+0.42\chi h)^2 \tag{A.3}$$

$$\chi = \sqrt{\frac{E_{11}}{11G_{13}}\left[3-2\left(\frac{\Gamma}{1+\Gamma}\right)^2\right]} \tag{A.4}$$

$$\Gamma = 1.18\frac{\sqrt{E_{11}E_{22}}}{G_{13}} \tag{A.5}$$

[2]The mass of the system is not modelled and is thus be neglected.

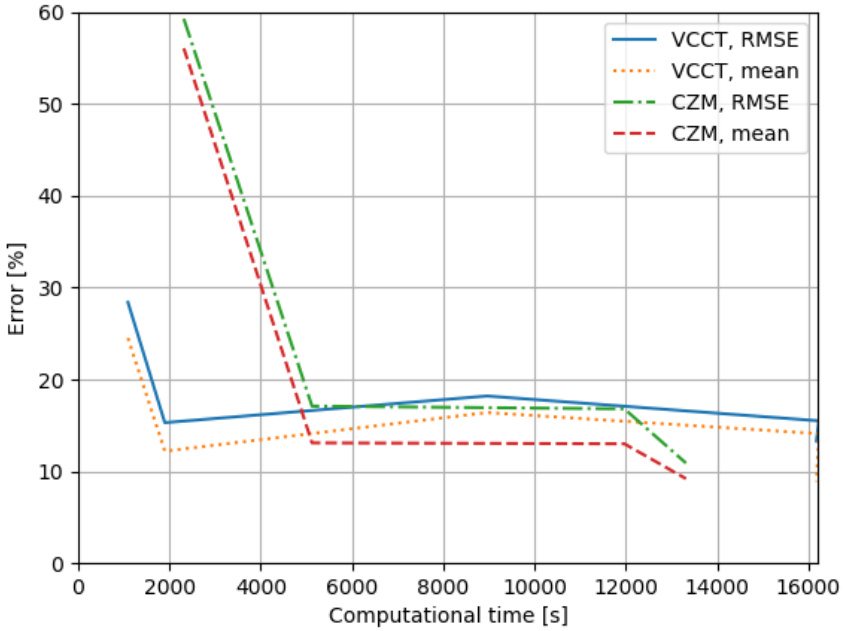

Figure A.3: *The mean and root mean squared errors in disbond growth rate for different computational times*

Lastly, the disbond growth rate is computed using equation A.6.

$$\frac{dA}{dN} = c(G_{II_{max}} - G_{II_{min}})^n \tag{A.6}$$

A.2.3. Results

The analytical and experimental results are compared using equation A.7. The accuracy for each run is summarised into one value by averaging the errors for all the data points. These results are then compared to the computational time as shown in figure A.3.

$$\epsilon = \frac{da/dN_{experimental} - da/dN_{analytical}}{da/dN_{analytical}} \tag{A.7}$$

A.2.4. Discussion and Conclusions

Obviously the method used to find an average error in disbond growth rate is highly limited in its usefulness. One example of this is the fact that the number of measurements is dependent on mesh size. Furthermore, the method for calculating disbond growth rate is dependent on the crack length versus number of cycles which has already been established to be inaccurate due to the increase in SERR with increased crack length and the step stiffness associated with VCCT.

Nevertheless it appears VCCT is capable of predicting disbond fatigue growth relatively accurate at a lower computational cost. When more computational time is available CZM is able to converge faster too a smaller error. Similar conclusions are found in literature[89]. Other researchers found CZM did run 2 to 15 times faster[103], but they focused solely on disbond length versus cycles which introduces errors when analysing VCCT as described before.

In conclusion it was chosen to use VCCT for three reasons. Most important is the ability to

compare different opening modes. Second is the reduced number of material parameters required, allowing for validation without requiring calibration. Lastly, due to the reduced computational cost a larger number of experiments may be run using VCCT which may add value to the sensitivity study.

B

Details Model Definition

During the development of the models, some technical issues were encountered. This appendix includes the most important issues and how they were solved.

B.1. Bonding interaction

The most important feature in the analysis is the bonding interaction. The definition of this needs to be done in a specific manner otherwise the analysis will fail in a number of possible different ways.

The interaction was defined using a surface to surface contact between the lap and strap. The settings used for interaction can be foun in table B.1, other than which the standard settings are used which include the BK law for mixed mode behaviour. The critical energy release rates and exponent do not matter for the fatigue analysis as long as they are sufficiently greater than the maximum value reached during the initial static loading step. These parameters are not used in the direct cyclic step.

The definition requires a couple of specific steps. Firstly, a crack feature has to be added. This can be found under special → crack → create. The crack should be of the "debond with VCCT" type, with a debonding step force. A ramp force would allow for the SERR to be less mesh dependant but this has not yet been implemented for fatigue loading. Furthermore, the option "limit bonding to slave nodes in subset", found under the "bonding" tab in the interaction property, should be enabled. This should limit the bonding to a subsection of the intersection of the master and slave surface.

This interaction can only include the fracture contact property. If another property is added, for instance a normal interaction, this second interaction seems to be ignored completely. This should instead be done using a separate interaction.

Lastly, the definition of the crack properties in fatigue has to be done by altering the keywords. First, the first part of the debonding definition in the static step has to be copied to the bottom of the direct cyclic step. This will look something like:

> *Debond, slave=part-1.surface_1, master=part-2.surface_2, debonding force=STEP, frequency=1

Table B.1: *Settings for the interaction of the bonded surface*

Discretization method	Node to surface
Sliding formulation	Small sliding
Degree of smoothing for master surface	2.0
Clearance	Uniform value across slave surface: 1e-8
Bonding	Limit bonding to slave nodes in subset enabled

Table B.2: *Relevance of fracture criteria[10]*

Factor	Description	Value
tol	Fracture tolerance	Seems to have no effect
c_1	Constant multiplier for delamination initiation	Not applicable
c_2	Exponent in delamination initiation	Not applicable
c_3	Constant multiplier for crack delamination growth	0.000702
c_4	Exponent in delamination growth	3.85
r_1	Ratio between G_{thresh} and G_c below which no crack propagation occurs	standard set at 0.01, in the experiments reduced to 0
r_2	Ratio between G_{pl} and G_c above which the disbond growth rate will be greatly accelerated	standard set at 0.85, in the experiments increased to 1
G_{cI}	Critical strain energy release rate for opening mode I	Not applicable
G_{cII}	Critical strain energy release rate for opening mode II	Not applicable
G_{cIII}	Critical strain energy release rate for opening mode III	Not applicable
η	Exponent of the BK law	Not applicable

Next, the fracture criterion has to be added, this has the format:

*FRACTURE CRITERION, TYPE=fatigue,MIXED MODE BEHAVIOR=BK, TOLERANCE=tol
c_1,c_2,c_3,c_4,r_1,r_2,G_{cI},G_{cII} G_{cIII},n

The meaning of each of these values can be found in table B.2. The critical strain energy release rates are not of importance as the experiments never showed growth outside of the Paris regime. Similarly r_1 and r_2 which limit the Paris region are set to 0 and 1 respectively for the same reason. Lastly, η is set to 1, again the value does not matter as it is only used to find the critical SERR.

B.2. Mesh sensitivity

VCCT is very sensitive to the meshing in a number of ways. Most importantly the disbond front will follow the grid lines. It also appears VCCT is very dependant on mesh size[89, 90]. As a result of this mesh convergence can be troublesome[23].

In the mesh convergence study it has become clear that the aspect ratio of the elements is also of importance. This is related to the requirement that element lengths in front of and behind the crack tip are of equal length[33]. In both the MMB and SLS specimen non-cubic elements resulted in a complete absence of mesh convergence. Similar results were found by Zavatta[23]. The solution is to only use cubic elements in all experiments.

B.3. Boundary conditions and constraints

Applying multiple constraints, boundary conditions or interactions to the same node some of these may be ignored. This had some implications for the model definition.

Firstly, while the model shows a clear symmetry along the lengthwise axis, the entire problem had to be modelled. The bonded nodes that were present at the symmetry line caused numerous

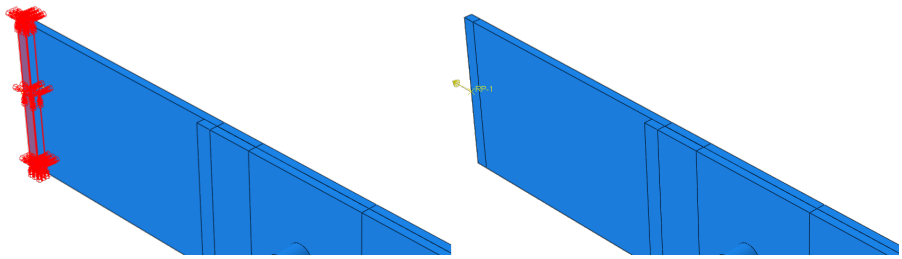

Figure B.1: *The application of boundary conditions are seperated from constraints*

issues that were deemed too difficult to resolve.

Furthermore, the load was applied at the clamped edge on a single reference point and was distributed over the entire face using a tie constraint. Originally the boundary conditions caused by the edge being clamped were also applied to this face. Interestingly enough, the boundary conditions seemed to be ignored by the solver when a constraint was already applied at these nodes. The solution was to extend the specimen and apply the boundary conditions at the original location with the loads were introduced on the specimen face. The exact configuration of which can be seen in figure B.1.

B.4. Step definition

The simulation consists out of two distinct steps: a static step and a direct cyclic step. The static step is included as it is required to enable the VCCT fracture mechanics and define the fastener pre-load. The direct cyclic step is used to model the fatigue damage.

The direct cyclic step simulates one loading cycle and attempts to find the transient response[10]. It does this by computing the response a number of iterations. Using the data from these a truncated Fourier series is created that describes a displacement function for all time steps. As a result of this, artefacts such as the ones shown in figure B.2 start showing up when few iterations are used with many Fourier terms. As no clearance is modelled the problem is linear and the solution only needs to carry one Fourier term to describe all the displacements perfectly, as shown in figure B.3[1].

An attempt was made to only model the first half of the loading cycle in order to reduce the computational cost. While the analysis will run the final solutions will not work. The reason for this is that the Fourier series requires the start and end values to be the same, requiring a full cycle to be simulated.

[1] This actually shows two Fourier terms, but Abaqus does not consider the offset from the x-axis a Fourier term

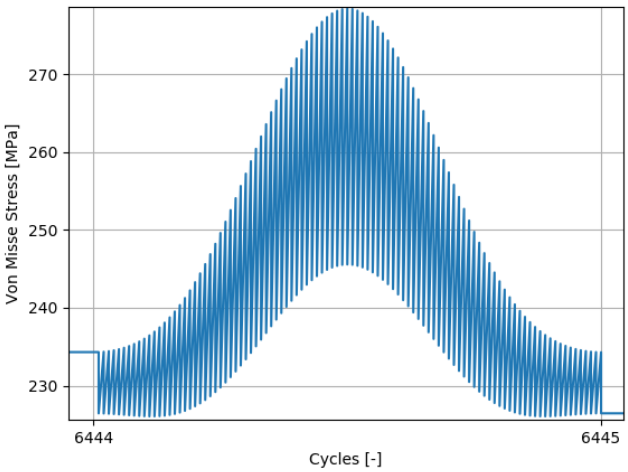

Figure B.2: *A large number of Fourier terms can lead to artefacts, indicating over fitting of the data*

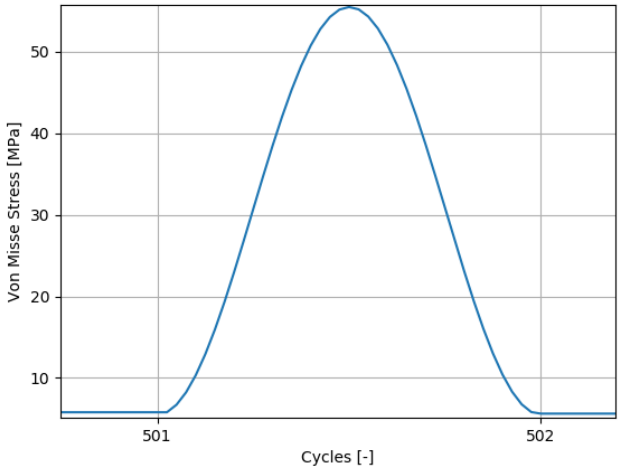

Figure B.3: *Using only one Fourier term, the model response is accurate and does not show the presence of artefacts*

C

Convergence

The convergence study regarding the mesh and time step settings covered three aspects: the number of iterations, the time increment size and the element size. The number of iterations was checked separately after which the time increment and mesh size convergence study were done together as the minimum time step might be related to the mesh size.

Results, shown in figure C.1, clearly show convergence is reached with two iterations. Furthermore, a minimum increment size of 0.05, or 5% of one load cycle, was fine enough for all mesh sizes, as can be seen in figure C.2.

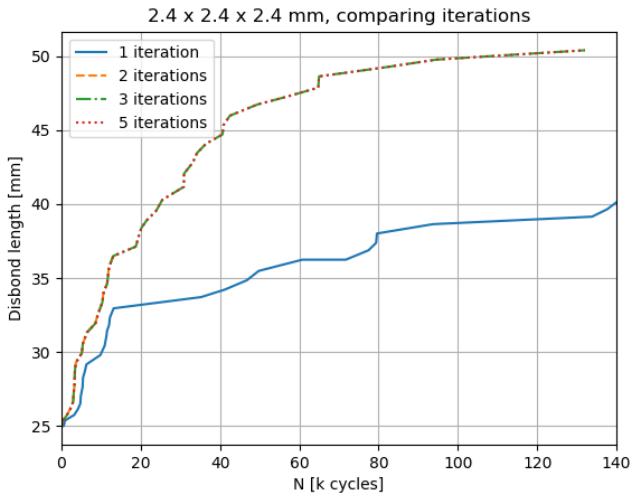

Figure C.1: *The time step converges with two iterations*

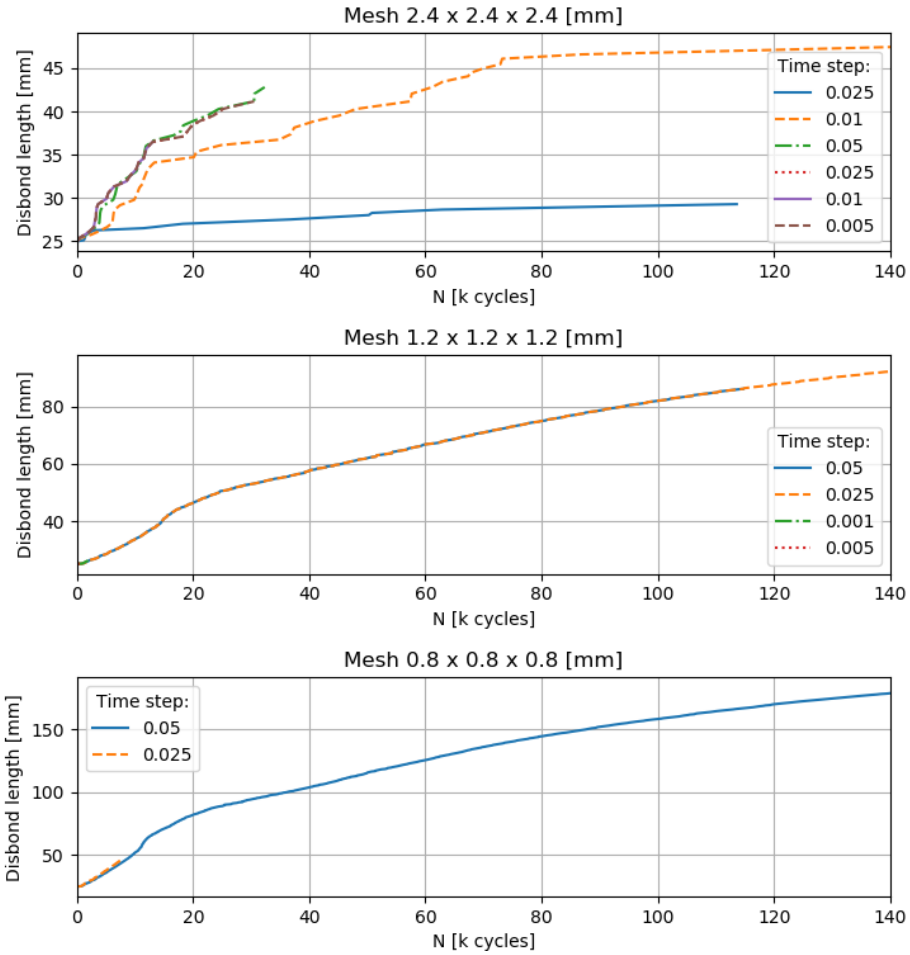

Figure C.2: *The convergence study for increment size, done for every mesh*

The mesh convergence compared the disbond growth rate vs the crack length for different mesh sizes, as shown in figure C.3. It shows that before reaching the fastener, the disbond growth rate is at most 16% larger for the mesh with elements of size 0.8 [mm] as compared to the mesh of elements of size 1.2 [mm]. This however translates to a difference of about 4% at most in the SERR. This is confirmed when comparing the average SERR between the two meshes as seen in figure C.4. This error was deemed small enough for the intended purposes.

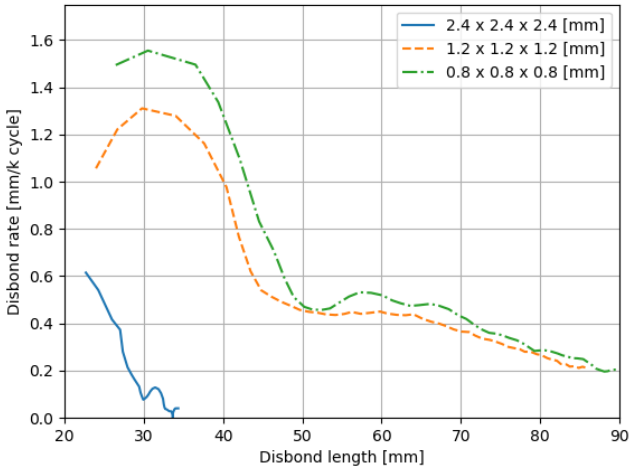

Figure C.3: *The disbond growth rate for different meshes*

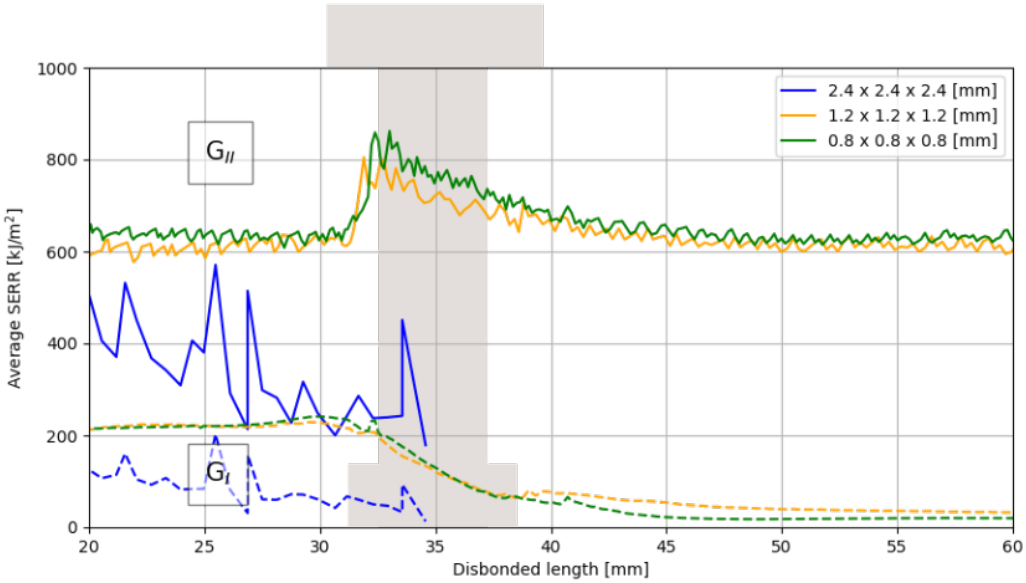

Figure C.4: *The average SERR versus crack length for different mesh sizes*

This convergence study was done on a slightly different model than the final model used for the sensitivity analysis. The plies had been rotated by 45^o causing the longitudinal stiffness to be significantly lower. One test was done with the updated settings to verify the previous conclusion, the results of which are shown in figure C.5. The mesh with elements of size of 1.2 [mm] is still considered fine enough.

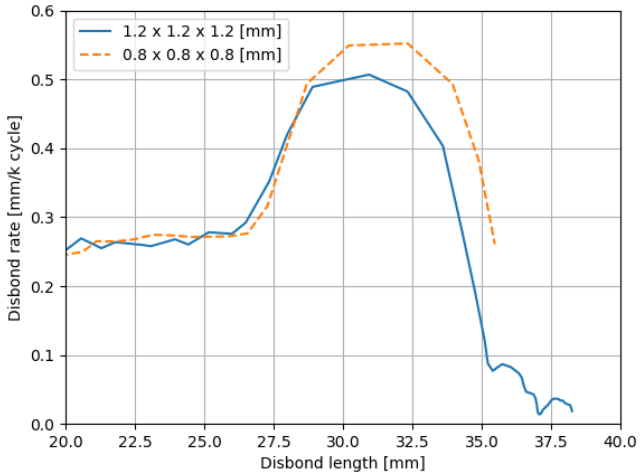

Figure C.5: *The disbond growth rate for different meshes with the updated model*

D

Verification

Apart from an array of sanity checks, a number of verification steps were taken. The effects of the assumed fastener pre-load and neglected friction are discussed in section D.1.

D.1. Modelling assumptions

Three assumptions were essential to the construction of the model: the fatigue of the adherend was neglected, the fastener pre-load was assumed and friction is neglected. A sensitivity study is done to check the effect of the last two of these assumptions. The question regarding the effect of adherend fatigue is out of the research scope.

The fastener preload was reported to be 7767 [N] by van Teeseling[20], but differed quite significantly between experiments. The error introduced by this assumption was analysed using two models. Firstly the adhesive was modelled up to the fastener hole. Increasing the fastener pre-load resulted in an increase in Mode I SERR, as can be seen in figure D.1. No such correlation was found for the Mode II SERR, where changing the fastener load had little to no effect.

At higher fastener loads even larger SERRs were observed, causing the model to predict unrealistic disbond growth rates. It is unclear what caused this behaviour but it is thought to be related to damage extrapolation. As the behaviour of this model was not entirely understood it was not used for further analysis.

The strong increase in Mode I SERR ahead of the fastener is mirrored by the results from van Teeseling. In modelling a clamped DAF he found Mode I SERR peaked in front of the clamp when increasing the applied load. This was said to be due to "geometric non-linear behaviour of the CLS specimen" and a similar explanation might explain the behaviour seen here. The fact that these effects were not observed in the second set of models indicates they may only be of effect in close proximity to the fastener. In contrast to this, the model that had a non-bonded region about the fastener hole did not show this behaviour. Both the Mode I and Mode II SERR were not affected by the fastener clamping force, shown in figure D.2. This is unexpected as typically the fastener pre-load has a large effect on the disbond arresting capabilities. This might be due to a combination of features such as a lack of friction, tight fit and an inflexible fastener.

Friction was only applied at the location around the fastener hole. This was done because the friction and VCCT fracture criterion seemed to interact, causing unexpected behaviour. It can still be of some use in evaluating the effect this assumption has on the results as this is the region where most of the clamping and thus most of the friction would occur.

Interestingly enough, the results show there is little to no difference in comparison to the base model, as can be seen in figure D.3. This suggests that friction has little effect on the results and can be safely neglected. This is unexpected as previous research did stress the importance of friction[102]. It is unclear what causes this indifference.

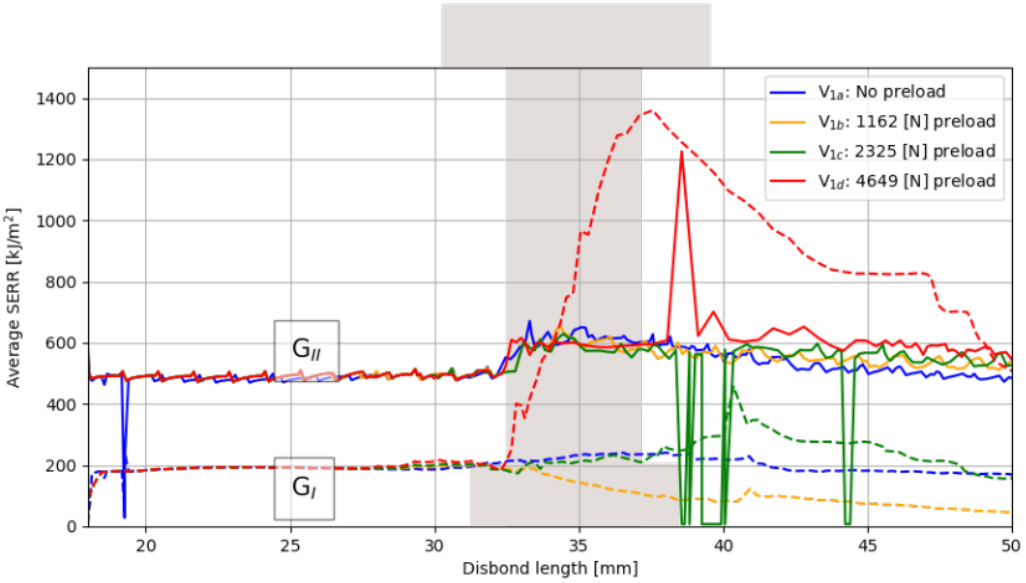

Figure D.1: *Close to the fastener the SERR is strongly dependant on the fastener pre-load*

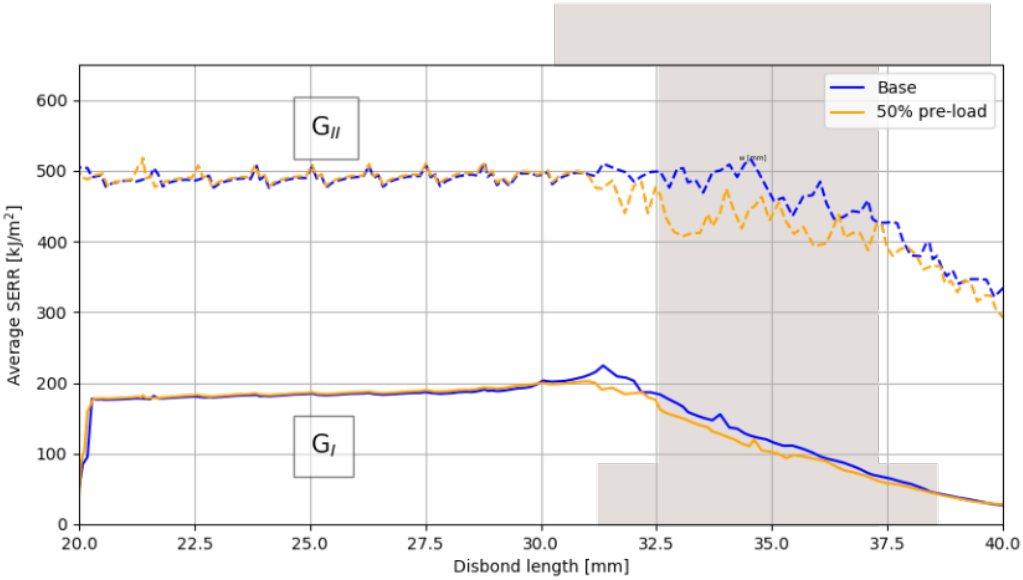

Figure D.2: *Far away from the fastener the SERR is independent of the fastener pre-load*

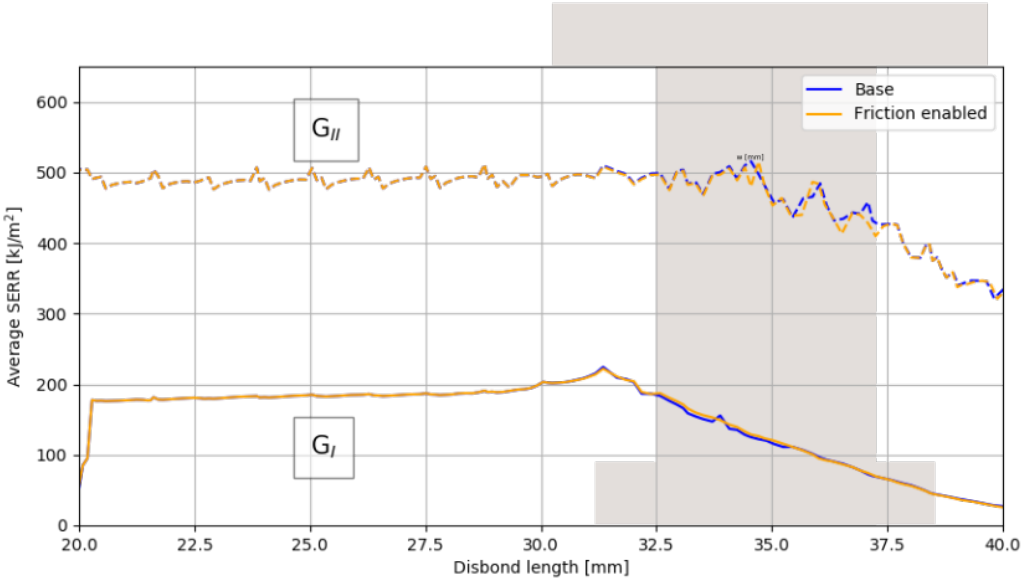

Figure D.3: *Comparing the SERR versus crack length with and without friction enabled about the fastener hole*

D.2. Comparison to previous research

As a final form of verification results are compared to those from previous research. First, results for a clamped model are compared to the 2D model developed by van Teeseling[20]. Next, comparisons are made to results reported by Zavatta[23] who presented different SERR distributions. Finally a comparison is made with the work by Richard and Lin[24] who analysed the quasi-static properties of a hybrid joint.

In his work van Teeseling[20] modelled a 2D specimen with a clamp as a DAF and computed the SERR for both Mode I and Mode II. Comparing these results as done in figure D.4 shows there are a number of prominent differences. Firstly, the difference between the predicted SERR is about 30% for Mode I and 10% for Mode II. It is unclear what exactly is the cause of this discrepancy. Another difference can be seen in the Mode II behaviour at the clamp. For the analysis done by van Teeseling this increases behind the clamp, caused by misalignment between the clamping surfaces.

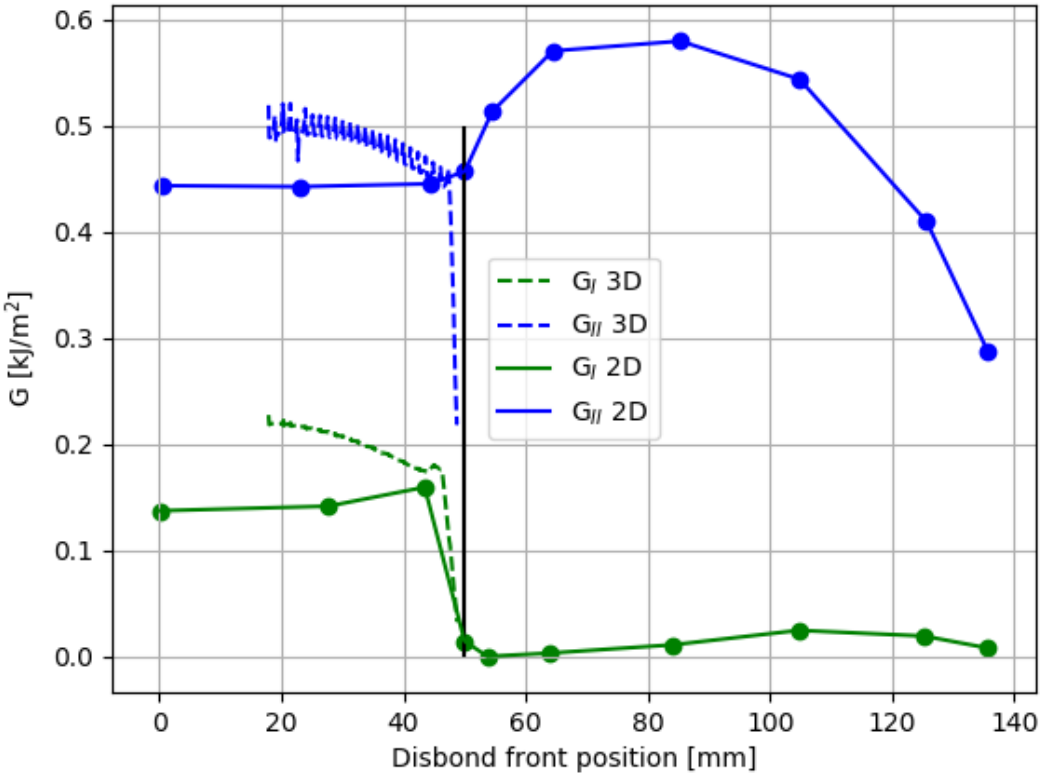

Figure D.4: *Comparison to the results from the 2D model used by van Teeseling[20]*

There are also a number of similarities. For instance, the SERR ahead of the clamp is relatively constant for both analyses. Furthermore the Mode I behaviour close to the the clamp is very similar in that it reduces to zero over a small region.

Zavatta[23] analysed the effect of the fastener on the SERR by comparing the SERR with the disbond front at different positions. With the experiments conducted in this thesis it is impossible to have the disbond front at the exact same positions. Not only because the disbond front follows a different growth shape, but also because the elements have a size of 1.2 [mm], which is too large to match the positions of 2.30, 1.30 and 0.75 [mm] as used by Zavatta.

The SERR was measured in four positions chosen to be the closest to those analysed by Zavatta, shown in figure D.5. This was done at a pre-load of 1165 [N] as the higher loads failed to return sensible results. The model with the fully bonded area was used to allow the disbond front to reach all the way up to the hole, ensuring a fairer comparison.

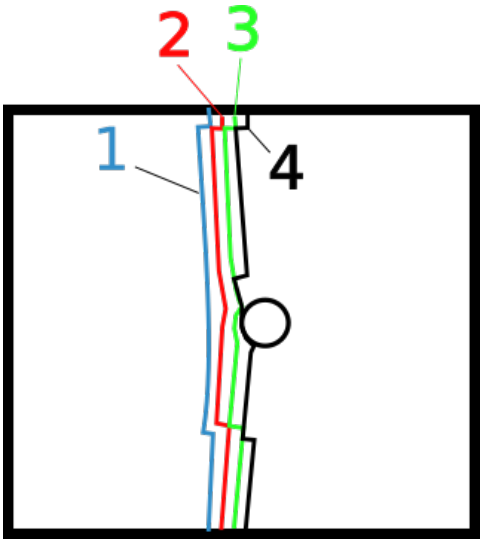

Figure D.5: *The four positions at which the cross-width SERR was measured*

The results in figure D.6 show a similar behaviour as those observed by Zavatta. Most clearly are the peak for the Mode II and Mode III loading at the fastener when the disbond front approaches the hole. Most of the smaller details, such as the increased Mode III SERR at the edges, are also visible in these results.

The suppression of the Mode I driving force is most visible at position 3. Although at the centre the Mode I SERR is reduced to close to zero as expected, no such suppression is visible further away from the fastener. This is likely due to the lack of warp in the disbond front. Other large differences, such as the peak in the Mode III SERR are likely caused by the non-straight disbond front, causing stress concentrations at the corners.

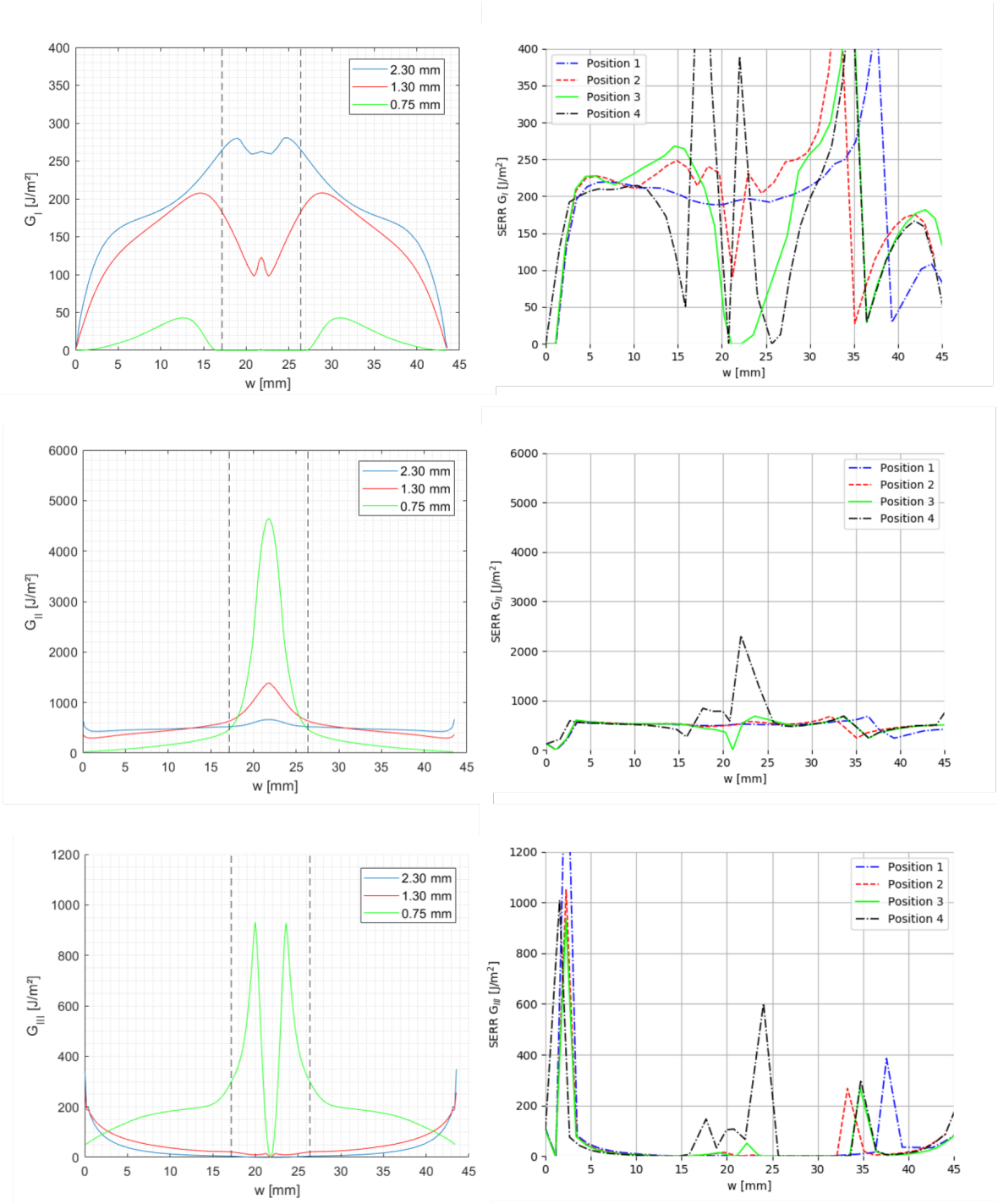

Figure D.6: *Distribution of the SERR along the specimen width*

Lastly the results are compared to those reported by Richard and Lin[24]. In addition, an extra experiment was done with quasi-static loading. This is done because this more closely resembles the experiments conducted by Richard and Lin. It has the added benefit that the disbond could be simulated further than the original fatigue analysis which failed due to issues described in section 5.1.

In order to make a fair comparison, the different experiments are compared by the normalised SERRs. These divide the computed SERR by the analytically predicted SERR with no DAF. The re-

sults are shown in figure D.7. While a number of differences can be seen, the general behaviour of these joints seems to be the same.

One difference is the peak in Mode I loading which is not recorded by Richard and Lin. This is the result of the quasi-static analysis they used. When the average SERR should increase this does not happen, instead unstable crack propagation occurs and the average SERR stays constant. Because of the unstable crack propagation the applied load does not change and the increase in SERR is not recorded.

The general trend in the Mode I SERR is the same but only reaches zero after passing beyond the fastener. This is a result of one model being 2D and the other 3D. Close to the fastener, the Mode I suppression will happen sooner than further away. Another difference is the peak in Mode II loading which was not recorded by the new model. This is due to the region close to the fastener not being modelled as bonded, causing the Mode II spike to go by unnoticed.

The experiments from Richard and Lin showed the Mode II loading was not completely suppressed, even when the disbond had passed far beyond the DAF. The fatigue analysis failed before reaching this disbond length. The quasi-static model did show similar behaviour. This is in accordance with previous findings from Cheung [122] who found a single fastener may not be enough to consistently suppress disbond growth.

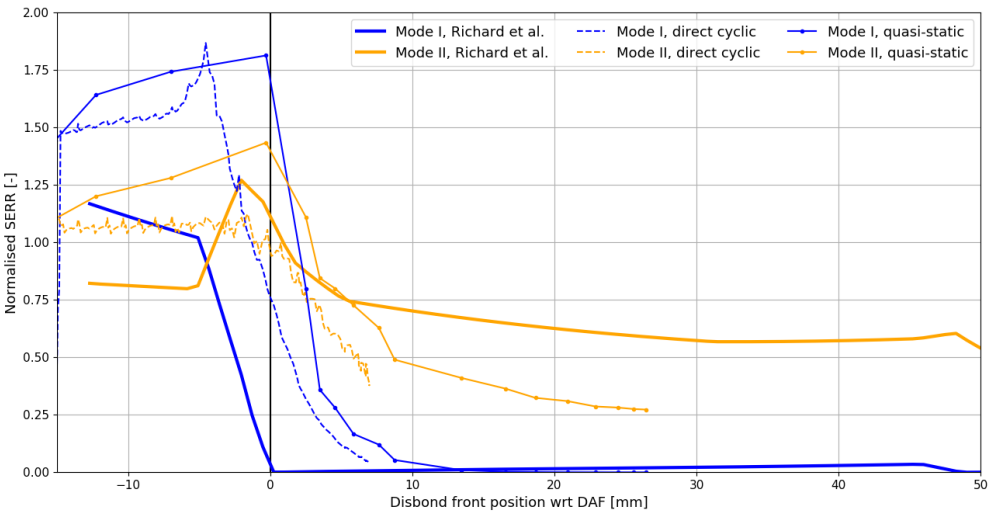

Figure D.7: *Normalised SERRs, the results are compared to those reported by Richard et al. [24]*

Even though the experiments are different in a number of ways, the behaviour of the SERR remains similar. Also, the results all seem to be in accordance with those found by the model used in this thesis. This suggests the model is adequate.